11-7-2015

Experimental Investigation of the Effect of Key Variables on the Static Strength of Aluminum Alloy Structural Adhesive Joints

Francesco Vincenzo Amoruso
University of Windsor

Experimental Investigation of the Effect of Key Variables on the Static Strength of Aluminum Alloy Structural Adhesive Joints

By

Francesco Vincenzo Amoruso

A Thesis
Submitted to the Faculty of Graduate Studies
through the Department of Mechanical, Automotive & Materials Engineering
in Partial Fulfillment of the Requirements for
the Degree of Master of Applied Science
at the University of Windsor

Windsor, Ontario, Canada

2015

Experimental Investigation of the Effect of Key Variables on the Static Strength of Aluminum Alloy Structural Adhesive Joints

by

Francesco Vincenzo Amoruso

APPROVED BY:

_____

R. Barron

Department of Mathematics & Statistics

_____

V. Stoilov

Department of Mechanical, Automotive & Materials Engineering

_____

R. Riahi, Advisor

Department of Mechanical, Automotive & Materials Engineering

August, 19 2015

DECLARATION OF ORIGINALITY

I hereby certify that I am the sole author of this thesis and that no part of this thesis has been published or submitted for publication.

I certify that, to the best of my knowledge, my thesis does not infringe upon anyone's copyright nor violate any proprietary rights and that any ideas, techniques, quotations, or any other material from the work of other people included in my thesis, published or otherwise, are fully acknowledged in accordance with the standard referencing practices. Furthermore, to the extent that I have included copyrighted material that surpasses the bounds of fair dealing within the meaning of the Canada Copyright Act, I certify that I have obtained a written permission from the copyright owner(s) to include such material(s) in my thesis and have included copies of such copyright clearances to my appendix.

I declare that this is a true copy of my thesis, including any final revisions, as approved by my thesis committee and the Graduate Studies office, and that this thesis has not been submitted for a higher degree to any other University or Institution.

ABSTRACT

Fuel economy targets are pushing car makers to develop several strategies in order to reduce the weight of the vehicles. Within this scenario adhesive bonding is nowadays a widespread technology that represents a joining technique aiming to replace or to combine fastening for lightweight construction of car bodies and multi-material design.

In this work an experimental investigation into the static strength of aluminum alloy structural adhesive lap joints is carried out by varying factors influencing the bonding behaviour of the joint. The impact of surface roughness, geometrical control factors (adherend thickness and adhesive thickness) and test conditions (test temperature and test speed) is evaluated.

The outcomes derived from the tensile tests are analyzed in terms of load, elongation and energy at failure. Finally a failure mode analysis is conducted in order to either verify or explain the results obtained.

DEDICATION

To my parents, Irma and Francesco
and my sister Vincenza

ACKNOWLEDGEMENTS

This thesis is the final outcome of a two year Double Degree Master program that was possible only thanks to the collaboration and organization efforts of two universities, University of Windsor and Politecnico di Torino, and a leading group in the automotive sector, Fiat Chrysler Automobiles.

Therefore I would like to express my deepest appreciation to the persons representing the aforementioned institutions who played a very important role in coordinating this program, Dr. Andrzej Sobiesiak from University of Windsor, Prof. Giovanni Belingardi from Politecnico di Torino, Edoardo Rabino from FCA Italy and Mohammed Malik from FCA Canada.

I wish to acknowledge my industrial advisor Mr. Kurt Damphousse who provided me with the material for the research. I also express my gratitude to Keith Mensing from Dow, Andy, Matt and Gali from University of Windsor, for their willingness in help me throughout the experimental part of the project.

I offer my sincere gratitude to my academic advisor Dr. Reza Riahi, who supervised my activities and offered his support throughout my thesis project, while allowing me to make my own choices.

I further want to thank my Advisors from Politecnico di Torino, Prof. Giovanni Belingardi and Prof. Massimo Rossetto, together with Giovanni Monfrino from Fiat Group Automobiles, for their important support and suggestions.

I am profoundly thankful to my parents; they have always morally supported me and economically sustained me throughout my studies. Moreover, without their education, I would never have achieved my academic successes.

A huge “thank you” goes to my big sister, Vincenza. She always encouraged me during this year, being a constant reference point.

Finally, special thanks goes to my colleagues, housemates and friends who shared with me this unique experience, Biagio, Fabio, Ivan and Sergio.

TABLE OF CONTENTS

LIST OF TABLES

LIST OF FIGURES

LIST OF APPENDICES

LIST OF ABBREVIATIONS

MPGe	Miles per gallon equivalent
EPA	US Environment Protection Agency
RSW	Resistant spot welding
SPR	Self-piercing riveting
RT	Room temperature
SLJ	Single lap joint
DLJ	Double lap joint
EAA	European aluminum association
FCA	Fiat Chrysler Automobiles
BSR	Best surface roughness
BAT	Best adhesive thickness
C.O.V	Coefficient of variance
PTFE	Polytetrafluoroethylene
NVH	Noise/vibration/harshness
CO_2	Carbon dioxide

NOMENCLATURE

F	Tensile test loading
Δx	Minimum interlock in a riveted joint
Δt	Minimum sheet thickness in a riveted joint
Δ	Solubility parameter
R_a	Average surface roughness
T	Temperature
Ta	Adhesive thickness
t_1	1.3 mm adherend thickness
t_2	2.1 mm adherend thickness
Θ	Contact angle
σ_x	Normal stress in x direction
σ_y	Normal stress in y direction(peel)
τ_{xy}	Shear stress in the adhesive layer
T_g	Glass transition temperature
F_y	Aluminum adherends yielding load
F_s	Lap shear joint failure load
b	Overlap area width length
l	Specimens length

1. INTRODUCTION

Nowadays the automotive scenario resembles the current economic and environmental situation. As a greenhouse gas, CO_2 is the main gas responsible for global climate change and tight CO_2 emissions control is resulting in legal requirements aimed to considerably reduce the average fleet consumption to meet the expectations coming out from this increasing global concern.

Combustion of fossil fuels is among the most influential human activities giving rise to CO_2 emission for both developed and developing countries.

In Figure 1-1 it is shown how the combustion of fossil fuels such gasoline and diesel involved in transportation for people and goods account for 31% of total US CO_2 emissions, representing the second largest source of it.

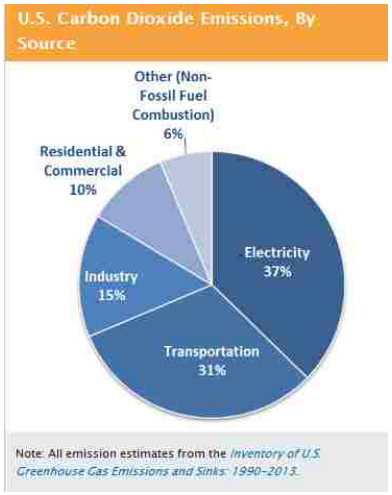

Figure 1-1: US CO_2 emission sources [1]

Therefore, together with the environmental impact (greenhouse effect), the increased fuel prices and worries about fossil fuels availability for the future are the main economic issues promoting this CO_2 reduction trend towards low emission vehicles.

A quantitative impact of these requirements is shown in Figure 1-2 for the trend of fuel efficiency regulations for both passenger cars and light duty vehicles adopted by most of the main North American car manufacturers.

According to the US EPA regulations, the target is to raise the average fuel economy from 33MPGe (actual value with regards to model year 2015) up to 54.5MPGe (23.2 km/l) for model year 2025.

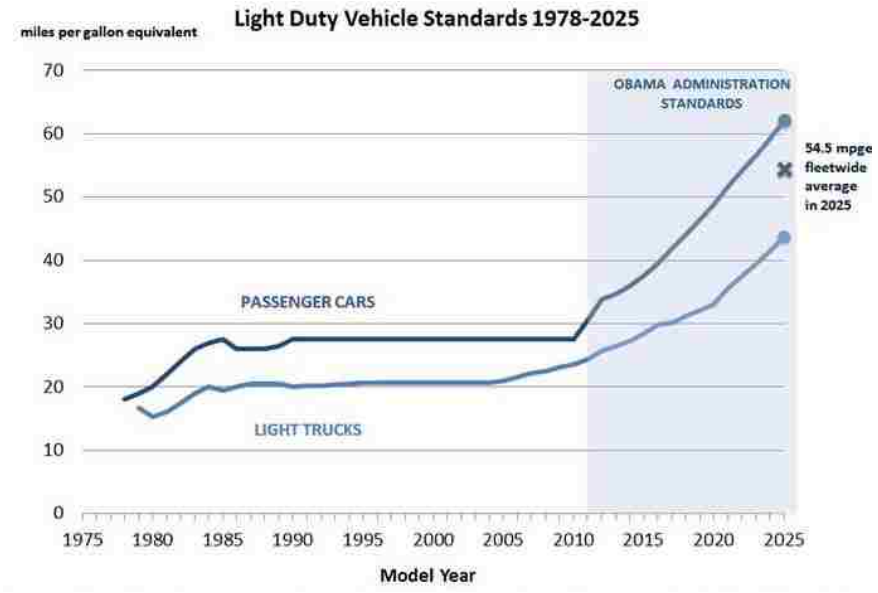

Figure 1-2 : Fuel economy standard for both passenger and light duty vehicles from MY 1978-2025 [2]

It should be mentioned that miles per gallon equivalent (MPGe) is the common fuel efficiency measure adopted for plug-in electric vehicles, alternative fuel, and gasoline driven vehicles. As an example, the energy consumed by an electric vehicle per mile can be easily converted in MPGe through the following relationship: 33.7KWh/mile= 1MPGe [3].

In order to meet fuel economy requirements, emerging technologies have been developed by car makers such as the following:

- Weight reduction
- Engine strategies
- Traffic management
- Driving attitude
- Aerodynamics

Indeed, according to different studies, a 10% mass reduction leads to fuel savings between 1.9% and 3.2% in gasoline engines and between 2.6% and 3.4% in diesel engines; these values refer to not re-sized powertrains. Instead, in the case of re-sizing

to match the lower vehicle weight, fuel saving would be more conspicuous than that shown. [4]

With regards to weight reduction, car manufacturer focus is placed on either to increase the fuel economy of a vehicle or to reduce both the shipping weight and the portability of the device. Thus, in the weight reduction framework, researchers have developed their attention in research of new materials such as aluminum alloys, composite materials and high-strength steels in order to substitute conventional mild steels.

This material conversion process has brought the attention of OEM's also towards new kind of joining techniques. In fact, the resistance spot welding process (RSW), used mainly for joining steel blanks for body-in-white applications, has some issues when aluminum material is concerned. Indeed, the thermal and electrical properties of aluminum and the presence of a highly insulating oxide layer are not particularly suitable for the welding process. Therefore, self-piercing riveting (SPR) and adhesive bonding process have found greater importance in the last 50 years to either replace or combine with RSW. The former, in the same manner of RSW, leads to localized loads on the joint area but has more ability to join aluminum to aluminum and aluminum to other materials. On the other hand, adhesive bonding represents the most versatile solution. Mix material design can be deeply realized by means of this process which allows joining components with great differences in electrical and thermal properties or in ductility. Moreover, one of the main advantages provided by adhesive bonding is the uniform stress distribution over the joint area. This helps to reduce localized stress concentration, increase both static and fatigue strength of the joint and provide good joints stiffness properties. All these factors are crucial for the targets like NVH, torsional rigidity and weight savings required by the automotive structures.

1.1. Thesis organization

The remainder of thesis is organized in the chapters listed below:

- CHAPTER 2: summarizes the literature review performed by the author. It provides theoretical background in order to explain the physics behind the adhesion phenomena and in addition a brief description of aluminum joining techniques is given. Moreover, comparative studies performed by other authors on the adhesion influencing factors are mentioned.
- CHAPTER 3: deals with the methodology adopted in this research project. In particular, the experimental investigation carried out is explained in details together with the material used. The following procedures are described along with their peculiarities: adhesive application, joints assemble and fixture, adhesive curing process, tensile tests (both at room and high temperatures).
- CHAPTER 4: The outcomes derived from the experimental work described in Chapter 3 are here reported and discussed. The impact of the main investigated variables: surface roughness, adhesive thickness and adherend thickness, on the lap joints shear strength is explained and the best combination of them found. The effect of temperature and test speed, considering their influence for a polymeric material, is investigated. Fracture surface of the specimens is analyzed in order to support the achieved results.
- CHAPTER 5: The findings of the research are drawn and summarized. Some recommendations for future works are presented.

.

2. LITERATURE REVIEW

The three main joining techniques adopted to join two or more components can be classified as: welding, riveting and adhesive bonding.

Considering Al-alloy as material to be joined several issues affect the welding process. In fact, as shown in Table 1, higher currents (round three times more) and slower welding times (one third) are required with respect to steel-material based welding process. This lead to rapid electrodes wear and the need for more precisely controlled welding parameters [5].

Another drawback for the resistance spot welding of aluminum sheet metals is the presence of a natural oxide layer on the aluminum surface (Al_2O_3) which is highly insulating. The oxide layer melting temperature exceeds 2000° and therefore it should be removed chemically or mechanically before the welding process.

Table 1: RSW parameters for 1.0+1.0 mild steel and aluminium sheets [5]

Material	Welding current [kA]	Welding time [periods for 50 Hz]	Welding Force [kN]
Mild steel	11	8	2.7
Aluminium alloy 5xxx, 6xxx series	25	4	2.5

The above considerations are the basis why aluminum is increasingly being bonded adhesively. [6]

In the following section focus will be placed upon the most common aluminum alloy joining techniques: self-piercing riveting and adhesive bonding.

2.1. Self-piercing riveting

Self-piercing riveting (SPR) is a cold sheet metal forming process adopted to join two or more sheets of material. This form of fastening has been spreading in the automotive field in the last 20 years due to stricter environmental concerns. This has forced OEM's to place an emphasis on emerging technologies to reduce weight and maximize fuel economy. Researchers have devoted considerable time and resources into new material development such as aluminum alloys and composite materials in order to substitute for steel. Figure 2-1 displays the main steps in the SPR process.

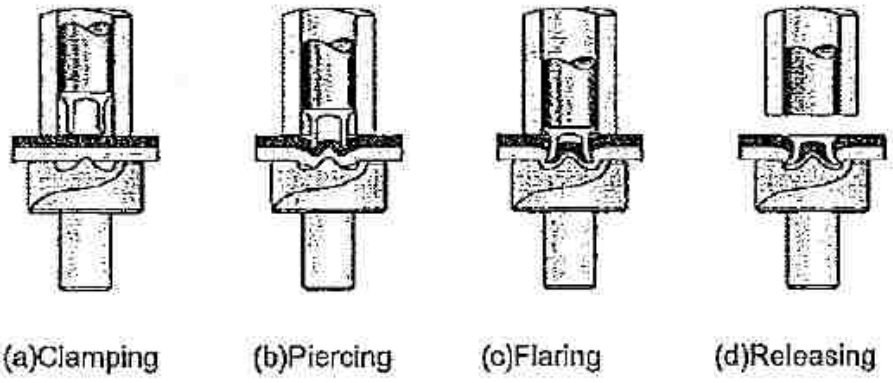

Figure 2-1: Schematic representation of the SPR process steps [7] [8]

This self-piercing riveting process could be summarized in four steps [7]

- Clamping: A blank holder presses the two sheets against the die
- Piercing: The punch pushes the rivet, piercing the top sheet and into the bottom sheet
- Flaring: The lower sheet material flows into the die and the rivet legs start flaring forming a mechanical interlock between the two substrates
- Releasing: The release of the punch, once it has reached the predetermined value of force or stroke, leads to the final configuration of the joint.

There are several control parameters affecting the design of the riveted joint which may be divided into relevant groups: geometrical factors, material factors, and technological factors. [8]

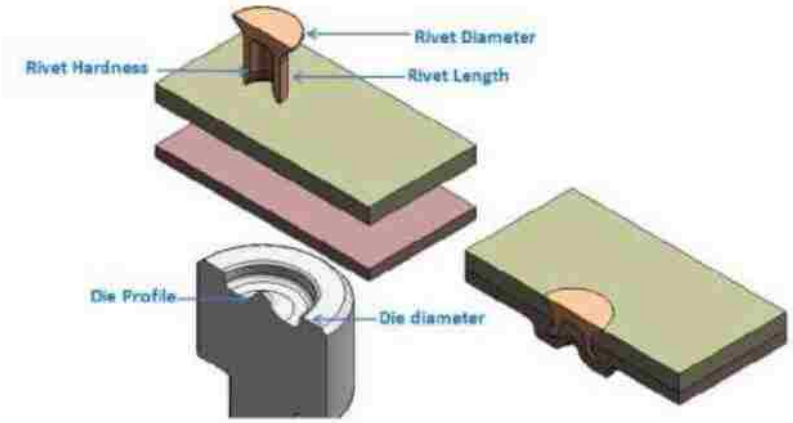

Figure 2-2: Self-piercing riveting geometrical parameters [8]

- Geometrical factors as illustrated in Figure 2-2:

  - *Rivet Length*: Selection must be tailored to the stack realization. As a rule of thumb, the rivet length should be 3mm longer than the total stack thickness. More attention should be applied when considering a stack oriented in an asymmetrical configuration.
  - *Rivet Diameter*: Common diameter dimensions employed for structural and non-structural joints range between 3mm and 5mm.
  - *Die Profile and Diameter*: Die diameter must be selected according to rivet length. In particular, the volume of the die should match the volume of the rivet. The die profile is related to the material properties which define the specific deformation process: a lower ductility requires a shallower die profile.

- Material factors:

  - *Rivet Hardness*: Hardness must be chosen according to the substrate material. The rivet must be harder than the substrate material and selected on the basis of the rivet length: the longer the rivet, the higher the rivet hardness required.

Mallick et al. [9] investigated the behaviour of the SPR joint by varying parameters such as: sheet thickness (1mm and 2mm), rivet diameter (3mm and 5mm), rivet length (4mm and 5mm for 1-mm thick substrates, 6mmm and 6.5mm for 2-mm thick substrates), rivet hardness (normalized, 410 Hv and 480 Hv), and die tip height (0, 0.025 mm and 0.050mm).

Table 2: Self-piercing riveting geometrical parameter variation matrix [9]

Source	Percent of Contribution
Die tip height	58.61%
Sheet thickness	6.35%
Rivet diameter	0.45%
Rivet Length	8.87%
Rivet Hardness	4.53%
Rivet Coating	4.46%
Error	18.72%
Total	100%

From Table 2, it can be seen that die and rivet geometry are major influences on static strength. These parameters were found to be less prevalent with regards to fatigue joint analysis. Authors attributed this behaviour to the fact that fatigue failure in the jointed specimens occurred in the substrate and not at the rivet location.

2.2. Adhesive bonding

Adhesive bonding is a joining technique in which a chemical agent (usually polymeric-based class of material), the *adhesive*, bonds together two substrates made of similar or dissimilar material acting effectively like a "bridge" between them. In order to get the *adherents* to stick together, surface attachment forces are developed through them and the *adhesive.* These forces come into being from several origins such as chemical, mechanical or electrostatic.

A first *adhesives* classification originates from their manifestations in mainly*: structural adhesive bonding* and *nonstructural adhesive bonding* [10].

In *structural adhesive bonding* the adhesive transmits forces between the two substrates developing the strength of the joint capable of bearing loads, either *adherents* go through high stresses up to yielding or the *adhesive* fails. Considering automotive applications some authors [11] defined *structural adhesive bonding* as " a durable and stiff joint between high strength, stiff parts suitable for crash relevant areas". The concept of durability is related to full service time of the vehicle while the stiffness is expressed in terms of numbers by the Young's moduli of the adhesives and the substrate materials to be bonded which respectively range on order of 10E3 MPa and 10E5 MPa. On the other hand, *nonstructural adhesive bonding* is suitable for application which implicates holding lightweight material together without bearing high loads. Primary goals pursued by *nonstructural bonding* fall in sealing functions, thermal and/or electrical insulation, NVH (noise/vibration/harshness) performance improvement by damping vibration and exerting soundproofing action. In this project, emphasis will be placed on detail considerations concerning *structural adhesive bonding.*

2.2.1. Adhesive bonding advantages and disadvantages

The adhesive bonding results as a key factor for automotive car manufacturers provide several benefits summarized as follow [10] [11] [12] [13] [14] [15]

- Multi-material design approach
- Weight savings
- Uniform stress distribution over joint area
- High fatigue strength
- NVH improvement
- Sealing against moisture ingress

Multi-material design: nowadays widespread in several engineering applications which involve conjunction between traditional materials such steel and innovative or lightweight material such composites, aluminum and magnesium based alloys or high-strength steels. Multi-material design approach brings to formation of hybrid structures by means of mechanical joining techniques, adhesive bonding or a combination of both. In this field the *adhesives*, being electrical insulating and acting as a barrier to the *adherends* mixing, prevent galvanic corrosion issues usually encountered in joining dissimilar metals which occupy a different place in the

electrochemical series. Requirements about the compatibility of the chosen *adhesive* with the mating *adherends* have still to be fulfilled.

Table 3: List of adhesive bonding advantages and disadvantages [10]

Advantages	*Disadvantages*
• High load-carrying capacity possible due to large (surface) area bonding	• Sensitivity to peel or cleavage versus pure tension or shear
• Minimal stress concentration due to load-spreading over bond area	• Extremely complicated stress analysis required for critical applications
• Suitability to very thin as well as thick adherends	• Requires careful joint (adherend) surface preparation
• Causes little or no change to the chemistry or structure of adherends	• Requires rigid process control
• Suitability for joining similar or dissimilar materials	• Sometimes very limited working times
• Seals against many environments	• Curing times can be long
• Insulates against electricity or heat	• Direct inspection is not possible; NDE methods are needed
• Minimizes or prevents galvanic corrosion between dissimilar materials	• Repair of defective joints is virtually impossible
• Damps vibrations and shock loads	• Upper service temperature is very limited, especially for organic types
• Resists fatigue and imparts damage tolerance (with compliant adhesives)	• Life of joints is sensitive to the environment
• Attractive strength-to-weight ratio	• Sensitivity to attack by some solvents
• Provides smooth contours	• Many adhesives (especially natural types) are subject to attack by bacteria, molds, rodents, vermin, etc.
• Can be faster and cheaper than mechanical fastening or welding	

.

Uniform stress distribution and large area of contact: *Adhesives* are characterized by a continuous bond line which distributes the applied stresses over the entire surface area faced by the mating parts. In fact, in contrast with welding and riveting techniques (mechanical joints) in which localized stresses on single contact points likely cause development of severe stress concentration zones (Figure 2-3), adhesive bonding prevents their onset by reducing the peak stress levels, determining a uniform stress spectrum and improving the *fatigue resistance* of the joint.

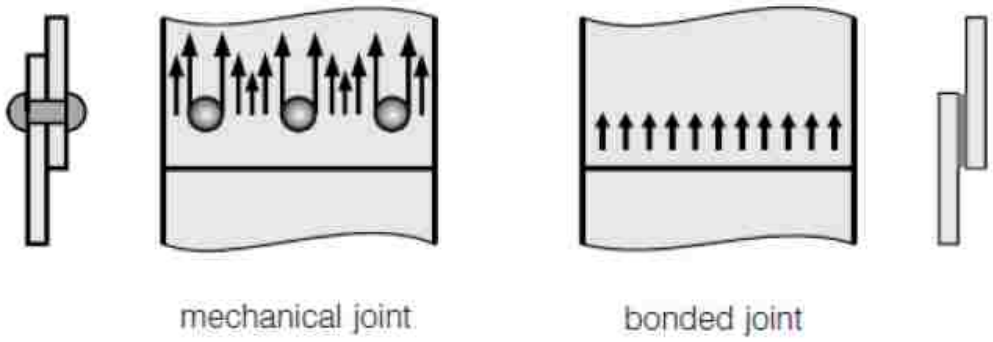

Figure 2-3: Schematic of stress distribtuon for mechanical joint (RSW,SPR) and bonded joint [14]

Moreover, considering the aforementioned fastening methods, the need for holes removes resistant material capable of withstanding the load and this builds differences in load baring capability along the loaded joint area as it shown in Figure 2-4.
Table 3 shows a list of advantages and drawbacks for adhesive bonding joints.

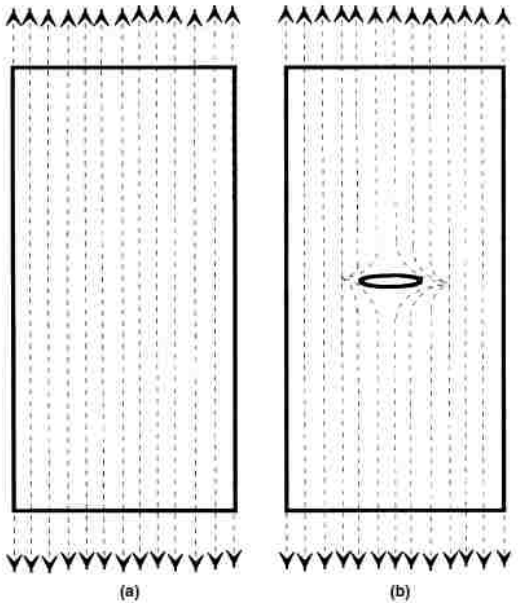

Figure 2-4: Schematic of stress distribution for a uniformly loaded structure without (a) and with the presence of holes or defects (b) [10]

Uniform stress distribution provides the following benefits: [14]
-static and dynamic strength of the joint
-increased stiffness of the vehicle structure
The higher body stiffness is related to modes of vibration associated to higher values of resonance frequency which allow better NVH and handling characteristics together with noise damping. The increase of vehicle body structures stiffness is shown, for instance, in some application (Figure 2-5) where large panels of thin gauge material are stiffened more properly through bonded joints than with respect to conventional mechanical joints. The bonded stiffeners, in fact, thanks to their large area of contact with respect to the latter ones result in less amount of unstiffened area.
Uniform stress distribution in the bonded joints provides in addition the possibility to use light materials exploiting the full and uniform utilization of their mechanical performances which are not affected by the adhesive attached.
This along with the ability of joining dissimilar material results in large *Weight savings.* Indeed, is claimed that by using 1 kilogram of adhesive, vehicle weight decreases of 25 kilograms [16].

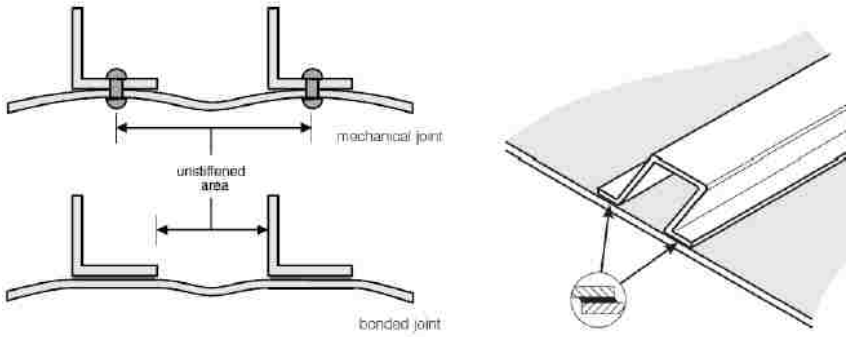

Figure 2-5: Schematic of large panels of thin gauge materials stiffened with mechanical joint and bonded joint [14]

Large area of contact typical of adhesive bonding it's also a joint design parameter which can be aided by change its geometry configuration or by acting on the surface adherends topography. Considering single lap joints (slj), many authors showed the relation be1tween the lap shear strength and the overlap area which represents the area of contact in this case. In particular, as shown in Figure 2-6, increasing the length of the overlap the strength increases by decreasing amount while shear strength increases linearly with the increase of overlap width.

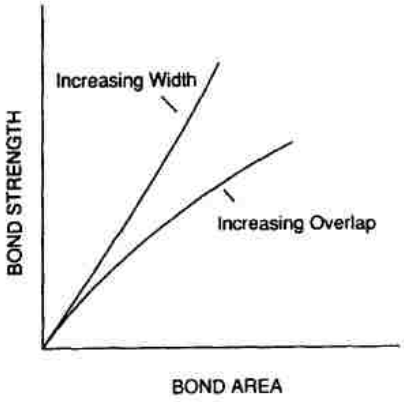

Figure 2-6: Illustration of dependance of bond strenght versus bond area [17]

Another interesting feature in comparison with riveting and welding is the nature of the joint that being an attachment to a surface does not introduce mechanical or thermal defects in the mated substrates which are otherwise responsible for weakening zones around the localized area of contact. For *adhesive bonding, sealing* performed basically by nonstructural adhesive bonding manifestations is another important function. Environmental factors that can affect the durability of the joint

such as moisture and debris ingress show their impact limited by the continuous bond which act like a barrier against external attack by liquid or gases.

Moreover the aesthetic of the final assembly is also improved by adhesive bonding with respect to the conventional joining techniques. This is due to the absence of weld seams, rivet heads or any other surface modifications caused by the joining method. Smooth surfaces are therefore achieved and benefits provided mainly for applications in aerospace sector where the smoothness of exteriors reduce drag resistance and determines uniform behaviour of the exposed structures to the air. Precise glue metering and fillet control is still required to ensure gap filling and a "clean" appearance of the assembly. Limitation related to *adhesive bonding* as a joining technique:

- Proper surface preparation needed
- Curing process
- Wettability issue
- Environmental conditions
- Loading mode dependent behaviour
- Recycling issues
- Joint geometry dependent behaviour

Some of these factors will be clarified throughout the remainder of the thesis. In particular, the surface preparation influence will be explained in 2.3.1. Both advantages and disadvantages of adhesive bonding as a joining technique are summarized in Table 3.

2.2.2. Adhesion and cohesion

Adhesion is a complex phenomenon and is therefore difficult to ascribe a precise description of the mechanism to it. Instead of a single theory which explains all the physiological and chemical sources guiding interactions between the adhesive and its respective adherends, is common to say that several "rationalizations" of adhesion phenomena are suitable for explaining each of them. These "rationalizations" come out form experimental observations which are rationalized and used to build several adhesion theories. The usefulness of these different adhesion theories is not aimed to give an exact explanation of the adhesion mechanism but is practically helpful in

order to make strength prediction of adhesive bonds by considering the joint's geometry and operating environment. In particular, adhesion theories found their application in certain circumstances, but none are universally applicable. Starting from a chemically-based approach for adhesive bonding, a first classification of the mechanisms governing the joints formation is related to:

- Existing forces between adhesives and adherends
- Energy states of material bodies description

In fact, understanding the forces exchanged in the adhesion physical phenomena along with the description of the initial and final energy belonging to the faced substrates material through the adhesive is fundamental in any nature phenomena description. Bond strength is the result of two main forces:

- adhesion forces
- cohesive forces

Adhesion forces concern the interaction taking place in the area of contact adhesive/substrates (adhesion zone) leading to hold two materials together at their surfaces. *Cohesive forces* are built within the polymer's molecules of the adhesive itself determining its internal strength. It can be stated that adhesion forces are established between two different materials while cohesive forces arise inside the bulk of a single material. The adhesion and cohesive aspects of an adhesive joint are depicted in Figure 2-7. The overall strength of an adhesive joint is controlled by a combination of the adhesion strength and the cohesive strength of the materials, along with design and geometry of the joint. As in a chain, the weakest link in a bonded joint determines its failure load. Therefore, for an optimally designed adhesive joint, the adhesion and cohesion aspects should be balanced, so that neither factor dominates the mechanical performance of the joint.

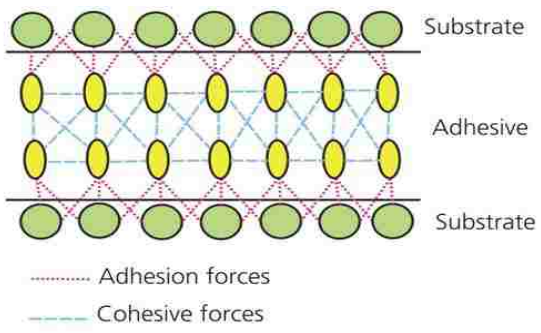

Figure 2-7: Schematic representation of adhesion and cohesive forces acting in adhesive bonds [18]

Figure 2-8 shows the bond cross section as subdivided in different layers in which the aforementioned interactions are present. Cohesive forces are present in the cohesion zone, an adhesive section zone in which the experienced behaviour is determined by its physical and chemical nominal properties as expressed in data sheet of the material.

Adhesion forces embrace both adhesion zone in the surface of substrate in contact with adhesive and transition zone which encloses adhesive state close to the substrate surface. Adhesion to the surface of substrates leads to alteration in structure and composition of the adhesive with respect to the one present in the cohesion zone.

Transition zone acts as a bridge between the pure nominal properties of adhesive in the cohesion zone and the modified properties associated to the adhesion zone. In this zone both composition and macroscopic properties of the adhesive go along a continuous change. Thickness values of this 'bridge' layer range in the order of few nanometers up to millimeters depending on the nature of both adhesive and substrates and according to the adhesive curing conditions selected. Bonded joint behaviour is affected by the extension of the transition zone especially when its thickness is higher compared to adhesive thickness owned by the cohesion zone.

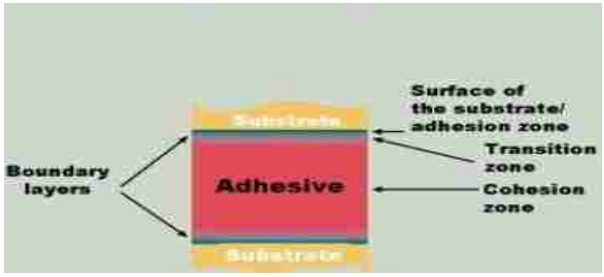

Figure 2-8: Schematic of the bond cross section [18]

Forces exploited in adhesive bonding arise at different levels mainly:

- Interatomic level
- Intermolecular level

The former originate from the need of material atoms to reach a stable electronic configuration represented by a full outermost electron shell for each atom. In order to reach this stable electronic configuration, "ionic bonding" comes out from the direct exchange of electrons, between different atoms, which leads to opposite charged ions

formation. Balance of attractive and repulsive forces along with a minimization of the potential energy associated to the collection of ions are responsible for the bond.

Besides the direct exchange of electrons between two different atoms, intimate sharing of electrons give rise to covalent bonding within the molecules formed. Another type of intimate sharing of electrons occurring in metals is the metallic bonding which is combined to delocalization of electrons in the material. Intermolecular bonding instead is established between the previous formed individual molecules or aggregates in order to produce more extended molecules. Forces involved in this further bonding can be broadly grouped as primary and secondary forces according to their relative bond energy. In particular primary forces act as short range interactions and own high bond energy conversely weaker secondary forces come out from long range interactions.

Therefore primary forces belong to ionic, covalent and metallic bonding while most common secondary forces are "van der Waal's forces". With regards to "van der Waal's forces", interaction and attraction occurs between either permanent or induced dipoles and are named respectively as "dipole-dipole" and "dipole-induced dipole" interactions. The general expression of van der Waal's forces, for one mole of gas , is given by

$$\left(p + \frac{a}{V^2}\right)(V - b) = RT \qquad \textbf{(2.1)}$$

where p is the gas pressure, V volume, T absolute temperature, R gas constant, and a and b are constants characteristic for each gas. In particular, a is a measure of intermolecular attraction.

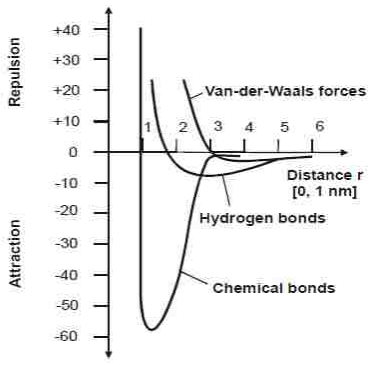

Figure 2-9: Secondary forces curves of potential energy against the distance r [19]

Moreover, Table 4 shows the average energy expressed in KJ/mol and its specific expression with regards to the several types of van der Waal's forces. Finally a comparison between both primary and secondary forces developed either at interface or within the bulk of a material in a bonded joint is illustrated.

Table 4: Secondary forces values of the potential energies as causes for adhesion [19]

Type of van-der-Waals forces	Average energy	Range
Orientation forces Dipole-dipole (Keesom forces	24 kJ / mol	$E = \frac{2\mu^4}{3k\,Tr^6}$
Induction forces Dipole-induced dipole (Debye forces)	15-20 kJ / mol	$E = \frac{2\alpha \cdot \mu^2}{r^6}$
Dispersion forces (London forces)	5-10 kJ / mol	$E = \frac{3h\nu_e \cdot \alpha}{4r^6}$
Hydrogen bridging bonds	40-50 kJ / mol	$E = e^{-Kr}$

Indeed for what concerns these forces, Table 5 shows a quantitative analysis on the bond energy expressed in Kj/mol together with a brief description of their trend while Figure 2-9 shows their relative curves as function of the distance r. The relative extent of one the above stated forces determines the bonded joint strength, nevertheless the accurate determination of their influence on both adhesive and cohesive strength is difficult.

Figure 2-10: Interatomic forces leading to the surface tension of a liquid [20]

Considering now an energy view perfective, the aforementioned forces act also between two or more materials surfaces and are called" surface forces". In particular

as far as the bulk of the material is concerned, each atom is surrounded by neighboring atoms, thus interatomic forces are developed and a stable state is achieved with a net force equal to zero. On the other side, atoms present on the surfaces are subjected to an unbalance of forces as illustrated in Figure 2-10 In order to counteract this unbalance, atoms tend to be further apart creating force acting on the plane of the surface which defines the surface tension. Lastly, the surface tension leads to the surface energy of a material which characterizes its adhesion properties.

In general indeed, to enable good adhesion properties (good wetting), liquid surface energy (related to the adhesive) has to be lower than the solid substrate surface energy. This situation is associated to low contact angle values. It should be mentioned that, considering two surfaces in contact (liquid interaction with a solid), the contact angle is defined as the angle the tangent to the surface makes with the solid surface. The relation between liquid, vapor and solid interfacial tension and the contact angle comes out from the Young's equation as.

$$\gamma_{lv}\, cos\theta = \gamma_{sv} - \gamma_{sl} \qquad \textbf{(2.2)}$$

where γ_{lv} is the liquid-vapor interfacial tension or surface tension , γ_{sv} is the solid-vapor interfacial tension, γ_{sl} is the solid-liquid interfacial tension and θ the contact angle.

Table 5: Primary and secondary forces bond energy values and description of the bonds [17]

Type of force	Source of force	Bond energy (KJ/mol)	Description
Primary or Short Range Forces	Covalent forces	60–700	Diamond or cross-linked polymers. Highly directional.
	Ionic or electrostatic	600–1000	Crystals. Less directional than covalent.
	Metallic	100–350	Forces in welded joints.
Secondary or van der Waals Forces	Dispersion	0.1–40	Arise from interactions between temporary dipoles. Accounts for 75–100% of molecular cohesion. Forces fall off as the 6th power of the distance.
	Polar	4–20	Arise from the interactions of permanent dipoles. Decrease with the 3rd power of the distance.
	Hydrogen bonding	Up to 40	Results from sharing of proton between two atoms possessing loan pairs of electrons. Longer range than most polar and dispersion bonds.

Adhesion and cohesive forces are strictly related to the failure modes existing in an adhesive joint; adhesive failure and cohesive failure.

- Cohesive failure can happen both inside the adhesive and the substrate. Figure 2-11 a) shows the joint separation though the bulk of the adhesive with visible layers of adhesive left on both the adherend surfaces, conversely in Figure 2-11b) the failure occurs in the bulk of substrate material. The above failures refer respectively to cohesive failure as is normally defined and cohesive failure inside the adhrerend which is rarely encountered and is named also as "coherent failure of substrate".

- Adhesive failure as depicted in Figure 2-11 c) is defined as a failure initiated either at the interface adhesive/substrate or at a boundary layer which is located in proximity of this interface.

- "Mixed mode" failure is the most common failure mechanism for joints in service or during testing coming out from a mixing of the aforementioned failures modes. Figure 2-11d) represents regions in which visible adhesive layers are still present on both the adherends but this does not take place all along the substrate surfaces. This failure is usually expressed as a percentage of cohesive or adhesive modes.

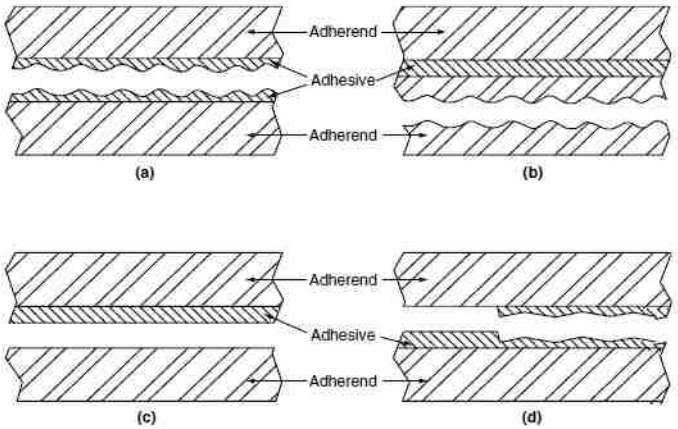

Figure 2-11: Adhesive bonds failures; a) cohesive failure inside the adhesive, b) cohesive failure inside the adherend, c) apparent adhesive failure, d) mixed mode failure [10]

The investigation of the failure mode gives insights about the bond quality produced.
A more detailed theory concerning failure mode for adhesive joints is expressed by Bikerman's theory' and is based on the following statement: "Failure occurs where and when the local stress exceeds the local strength. This can happen in an adherend, a boundary layer, or in the adhesive " [21]. It comes out that properly made bonds will experience cohesive failure mode (or 100% cohesive according to *mixed mode* failure definition)either inside the adhesive or the substrate, conversely pure adhesive failure occurring at the interface adhesive/adherents is highly improbable and indicates an inadequate surface preparation [10] [21].
In particular Bikerman claims that failures which are supposed to happen at adhesive/adherents contact area take actually place either in the adhesive near to the interface or, due to the presence of a boundary layer, close to the interface itself according to the following reasons:

- Adherents contamination
- Air trapped inside the bond
- Weakly attached oxide layer

Several proofs about the improbability of adhesive failure can be considered. As an illustration, probability reasoning can be used by analyzing cracks propagation in the system constituted by adhesive and adherends as depicted in Figure 2-12. Atoms belonging to adherends or adhesives are represented respectively with white and black circles. Assuming stresses applied normally to main plane of phase boundary different crack propagation paths can arise, once local stress exceeds local strength, at some specific points initiating the failure process.
Figure 2-12 shows on left side the crack propagating from a point located at interface adhesive/adherends towards the right.
The subsequent paths can be followed by the crack with the same probability:

- between two atoms of the substrate
- between an atom of the substrate and one of the adhesive
- between two atoms of adhesive

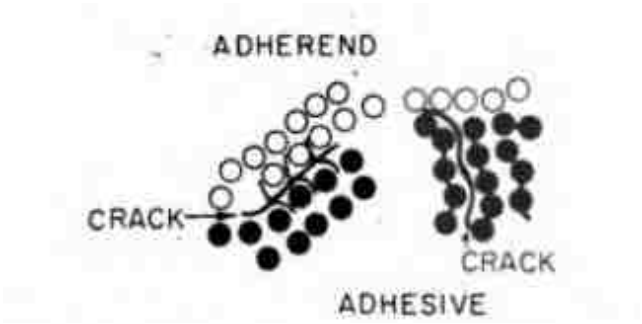

Figure 2-12: Schematic of crack progragation in a system constituted by an adhesive and an adherend [21]

This leads to have a probability of 1/3rd for an interfacial crack to be originated along the phase boundary for two atoms, one of the substrate and the other one of the adhesive. For three atoms long crack case the probability becomes $(1/3)^2$ in which the power term 2 can be expressed as n, for n+1=3. By using mathematical induction and extending the same concept over a generalized n+1 atoms case, the probability to have a pure interfacial failure is $(1/3)^n$. This probability is really low leading to values about 1/59000 for n equal to 10 by considering crack path developed along 11 atoms.
Calculation refinements have to be performed concerning the three dimensional state of the crack propagation, specific adhesive molecular structures and relative intermolecular forces intensity developed between similar or dissimilar materials.
All of them together bring the above calculated probability of interfacial detachment to even lower values. As already mentioned adhesive failures and cohesive failure are usually present in a mixed mode. A way to look both adhesive and cohesive failure together can be founded through the surface attachment theory of joint strength. This theory attributes the adhesive joint strength and its corresponding mode of failure to the degree of interfacial surface attachment. The latter is influenced by boundary layer effects, wetting considerations and other phenomena. Adhesion behavior in function of the degree of interfacial surface attachment is summarized in three different states as shown in Figure 2-13

- Boundary failure(a)
- Transition region (b)
- Cohesive plateau region (c)

a) Boundary failure region (Figure 2-13 region (B)) is characterized by values of adhesive joint strength lower than cohesive strength of the bulk adhesive material. Failures happen at adhesive/substrate interface where mechanical and physical forces responsible of the bond strength at the interface are weaker than interatomic and intermolecular forces which keep the bulk of adhesive material together.
b) Transition region (Figure 2-13 region (B/C)) is identified with a mixed type of failure which is developed according to an increase of tenacity of surface attachment. In fact, in this region, the degree of surface attachment affects substantially the adhesive strength of the joint as shown by the curve slope which reaches a considerable value.
c) Cohesive plateau region (Figure 2-13 region (C)) is the last region of the curve experienced by the adhesive strength with respect to the tenacity of surface attachment.

Once reached a critical value along the horizontal coordinate, defined as saturation value of degree of surface attachment, an opposite relation between the interfacial and the cohesive strength comes out with respect to the one before stated in the boundary region. Failure becomes total *cohesive failure* and the strength of the adhesive joints stop growing reaching a plateau value. Under these conditions further increase in tenacity of surface attachment does not provide any increase in the mechanical strength of the adhesive joint.

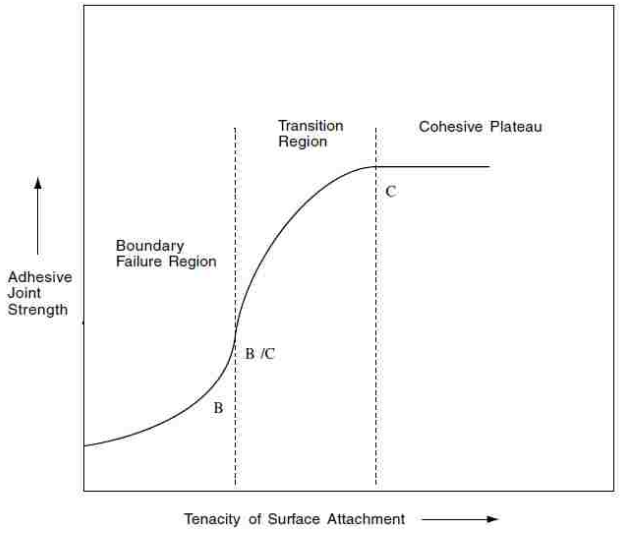

Figure 2-13: Schematic diagram of interfacial states encountered in adhesion [22]

2.2.3. Theories of Adhesion

As already mentioned in 2.2.2, several adhesion theories have been formulated. In the following section, a brief description is given for the most common theories based on mechanisms linked to [10] [15] [17] [19] [22] [23] [24] [25]:

- Adsorption
- Mechanical interlocking
- Diffusion
- Electrostatic
- Weak-boundary layers.

Figure 2-14 illustrates schematic of adhesion 'rationalizations' and its causes. These latter range from mechanical anchoring of adhesive on substrate surface profile, diffusion between compatible polymer chains, double layer contact charging at the interface, interaction of polar functional groups, hydrogen bonds or chemical cross links reactions. Table 6 shows scale of action experienced in the interaction adhesive/substrates according to the different mechanisms. Molecular and atomic interaction level takes always place at the phase boundary, nevertheless further factors of interest in the mentioned theories belong to either microscopic level, such as the contact surface of the adhesive and the adherend in the mechanical anchoring theory , or macroscopic level as the surface charge in the electrostatic theory.

Table 6: List ofadhesion theories and of their scale of action [22]

Traditional	Recent	Scale of Action
Mechanical interlocking	Mechanical interlocking	Microscopic
Electrostatic	Electrostatic	Macroscopic
Diffusion	Diffusion	Molecular
Adsorption/surface reaction	Wettability	Molecular
	Chemical bonding	Atomic
	Acid–base	Molecular
	Weak boundary layer	Molecular

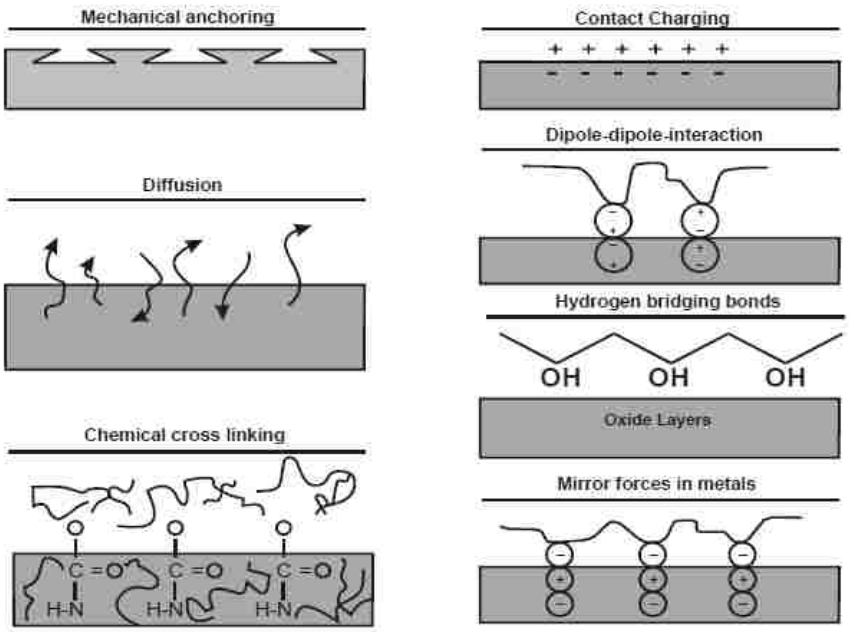

Figure 2-14: Physical and chemical causes for adhesion in adhesive bonds [22]

2.2.3.1. Adsorption theory

The adsorption theory along with mechanical interlocking theory represents the most widely applicable theory to explain adhesion phenomena; in particular adsorption theory contribution takes place for all adhesive bonds being intimate contact between molecules always present. Two main steps trigger the basis of this theory:

- Wetting phenomenon
- Existence of interfacial forces adhesive/adherends

Firstly, intimate molecular contact is established between adhesive and substrate resulting in the development of surface forces at the interface. The process which leads to a continuous contact adhesive/adherends and subsequent interfacial forces is called "wetting". Intimate contact can be expressed for the respective surfaces involved in range of few angstroms in distance. For this latter, to be happen, adhesive spreading over the surface has to be spontaneous in order to maximize the interfacial contact. Good wetting (Figure 2-15(a))is experienced when the adhesive spreading onto the substrate surface allows the adhesive to fill properly valleys and crevices

present in the surface itself; conversely poor wetting (Figure 2-15(b)) is usually associated to a flawed interface in the adhesive bonds where adhesive bridges over the valleys formed by these crevices. Flaws such as voids, contaminants or weak boundary materials provide magnification of applied loads at the periphery of flaws inducing its propagation and lowering the overall theoretical strength of the bonded joint. It comes out that in order to achieve good wetting and intimate contact of the adhesive with the surface, the goal is to eliminate or minimize the interfacial flaws.

The degree of wetting is related to contact angle phenomena which define balance which occur between surface energy/surface tension of liquid-solid interface versus the liquid-vapor and solid-vapor interfaces it replaces [10]. Once wetting has been established at the interface adhesive/adherend, permanent adhesion occurs in the second step through physical or chemical adsorption of the adhesive molecules onto the substrate which arise from the development of molecular attraction forces. In particular, many authors [15] [17] state that existence of secondary forces (Van der Wall's forces) across the atoms/molecules of the interface are sufficient enough to provide the strength of the bond. Despite the fact that secondary forces are acknowledged as the major contributor to adsorption mechanism, some considerations should be applied when considering in service joints strength which shows the need for the presence of primary bonds.

For instance, secondary forces result to be inadequate to provide good adhesion in case of presence of medium such as water (liquid or vapor) at the interface. Hydrolysis mechanism takes place displacing the adhesive from substrate to which is attached lowering the initial high surface energy of substrate itself due to the absorption of water. Thus, primary bonds less susceptible to hydrolysis phenomena aid maintaining good strength of the bond. Adsorption is also influenced by kinetic concepts linked to the adhesive change of phase from liquid (l) to solid(s) after its application to the substrate; wetting equilibrium has to be recognized and it can be achieved both before (liquid adhesive phase) or after (solid adhesive phase) adhesive set. This leads to different equilibrium conditions according to the adhesive phase considered being the surface energy of the solid phase different from the one of liquid phase.

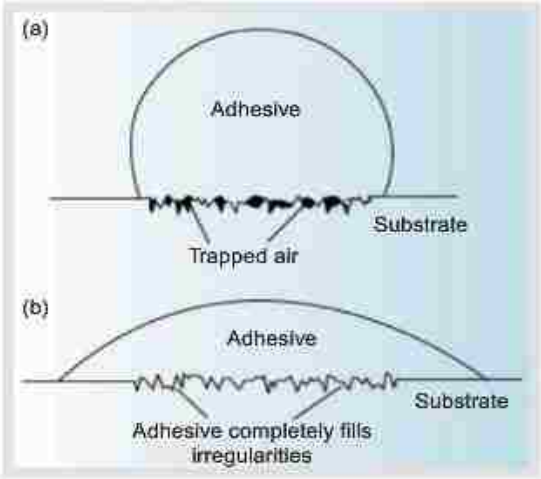

Figure 2-15: Schematic of good or poor wetting of an adhesive over a substrate material [22]

2.2.3.2. Mechanical interlocking

Mechanical theory of adhesion according to Mc-Bain and Hopkins can be explained with the following statement: "a good joint must result whenever a strong continuous-film of partly-embedded adhesive is formed in situ". Moreover the mechanical adhesion, being defined on intimate contact adhesive/substrate, relies also on interaction forces described in the adsorption theory in 2.2.3.1. Mechanically theory is based on the ability of adhesives to:

- Displace trapped air at interface prior adhesive's hardening process has been achieved
- Enter substrate surface irregularities of microscopic extent such as pores, cavities, and other asperities (e.g., peaks and valleys, crevices etc.)

This theory finds application mainly for adhesive bonds with many porous substrate materials such as: wood, porous ceramics (e.g., stones, bricks, cement, and concrete), textiles, unglazed porcelain and even many metals that have a tenacious and porous native oxide or tarnish layer etc. As an example, mechanical adhesion of a thermoplastic adhesive to wood has been investigated in [15]. A scanning electron

microscopy was used in order to detect pores dimensions (in order of pm) and the features of adhesive which have been result to be conformed to the ones of the wood. Adhesive penetration in pores of different sizes showed varying depth penetration with the larger size pores subjected to lower values of penetration depth.

Interlocking extent is affected by the following factors:

- Substrate porosity pattern
- Adhesive viscosity property
- Bonding pressure and duration

Generally indeed, good adhesion is provided when concerning surface with a micro-morphology and adhesives with a low enough viscosity to completely fill the substrate surface features. A related concept to mechanical adhesion is the roughening of a surface. Extensive studies in literature can be founded which link surface roughness to strength of the bond through experimental investigation; more details will be provided in 2.3.1.1. Figure 2-16 and Figure 2-17 provide a schematic comparison of interface structure whether either a normal plane interface is considered for a smooth adherend surface or a tortuous interface path is produced by roughening methods applied to the substrates. This helps a better understanding of the mechanism and to draw some relevant criteria for good adhesion. In fact, analyzing the interface behavior for the two aforementioned cases, it comes out that surface roughness aids in adhesive bonding due to the following reasons:

- Increase of energy necessary for the de-bonding in order to overcome plastic deformations of either adhesive or the adherend. In fact, for smooth interface the crack initiated at the edge of the specimen propagates along the interface itself which acts a stress concentrator. On the other side, rough interfaces induce crack propagations to deviate direction from the plane junction depicted in Figure 2-16. Thus, some detours can go either into the adhesive or in the substrate with the subsequent plastic deformations of the respective materials.
- Interlocking effect enhanced by plastic deformation phenomena which act as energy absorbing mechanisms improving bond strength. As can been shown in Figure 2-17: Crack propagation along a rough surface interface between an adhesive and an adherend , the existence of ‘lock and key’ sites comes out

from the path followed by the adhesive which can fill completely pores present on the surface. These sites do not allow an easy separation of the adhesive from the adherend, with the former induced in plastic deformation in order to move out from the pores which have previously filled.

- increase of physical area of contact; smooth surfaces lead to produce the minimum possible area of contact that when considering rectangular bodies is represented as a plane in Figure 2-16: Crack propagation along a smooth surface interface between an adhesive /adherend conversely surface area increases dramatically once we consider rough surface as depicted in Figure 2-17. Moreover, as expressed in 2.2.3.1 interactions developed at interface act as major contributor to adhesion and their magnitude is scaled as the area of contact. Thus, the increase of the actual area of contact allows increasing substantially the total energy of surface interaction with subsequent improved adhesion.

Other factors responsible for increase of bond strength by roughening methods are given below [10] [22]:

- Mechanical anchoring
- Cleanness of surface providing its better wettability
- Change of surface physical and chemical properties leading to a high reactive surface

The theory stating that abraded surfaces allow adhesives to create stronger bond than smooth surfaces do is not universally applicable. In fact, some controversial results in experiments conducted in literature relate the increase of surface roughness either to the lowering of the joint strength or differences in joints strength within experimental scatter of the data. Explanations of these results are usually associated to poor wetting of a rough surface by viscous adhesive, voids formation at the interface and stress concentration points arising due to presence of asperities. Roughening methods are usually realized though mechanical abrading and pretreatment methods applied to substrate surfaces. With regards to surface pretreatment methods the main technological reason is usually aimed to increase the durability of the bonded joint. For instance, anodization for aluminum surfaces makes bonded joint less susceptible to humid environment impact on the strength of joint .As far as aviation context is

concerned, this outcome assumes a substantial importance. Then, pretreatment methods eventually can results in increase the adhesion.

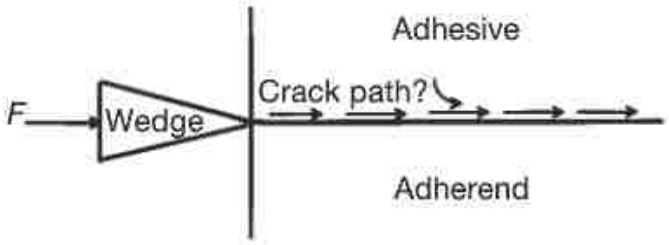

Figure 2-16: Crack propagation along a smooth surface interface between an adhesive /adherend [24]

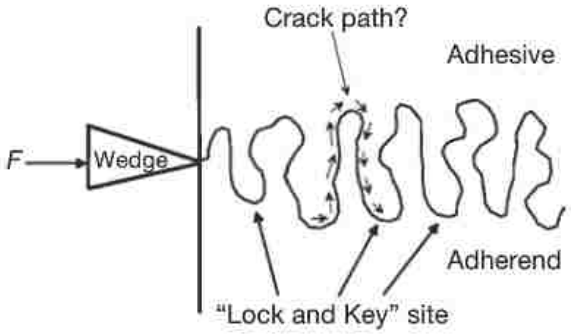

Figure 2-17: Crack propagation along a rough surface interface between an adhesive and an adherend [24]

2.2.3.3. Diffusion theory of adhesion

The first Diffusion theory concepts were introduced by Voyutski [26] in his works in the mid of 19th. Voyutski's theory is based on inter-diffusion occurring between molecules of two parts which leads the initial boundary to be removed ad depicted in Figure 2-18.Thus, Interface adhesive/adherend changes his nominal characteristic not separating anymore adhesive and substrates properties but enabling a gradual change of the respective materials properties one into the other. The interface usually acts as a discontinuity representing a substantial mismatch between the properties of the two faced materials, here stress concentrations regions are generally developed. Instead, for a diffusive adhesive bond, the interface is not proper a true interface (is instead called interphase with typically thickness in rage of 1-100 nm) and stress concentration planes along with discontinuity of adhesive/substrate physical

properties are indeed avoided. With regards to polymers in contact, Voyutski conducted studies analyzing the following factors influencing adhesion such as: time, temperature, pressure, molecular weight, polarity and crosslinking [26]. He concluded that adhesion between polymers in contact is strictly related to diffusion phenomena concerning polymeric chains. Diffusion can be classified as: slow when is developed between solid state adhesive and adherends and fast when considering liquid state adhesive (e.g., melted or thinned with a solvent). It should be pointed out here that diffusion mechanism is not broadly accepted for all polymers/polymers interaction between adhesives and substrates. Generally indeed, particular requirements are needed to guarantee proper inter-diffusion between polymers:

- Polymers have to be capable of movement; feature usually associated to polymer's temperature higher than glass transition temperature and to entanglement of polymers due to entropy concepts.
- Polymers long chains have to be compatible in terms of diffusion and miscibility one in the other in order to form a solution

These requirements are fulfilled in relatively limited number of cases; in particular diffusion mechanism is mostly accepted for pairs of same polymer (Autohesion mechanism) and when considering mutual solubility of very similar polymers.

Theory of solubility stated by Hildebrand [27] allows better understanding of criteria behind mutual solubility of materials. In the following, this section is focused on parameter basis of this theory and equation which regulate solubility of material and therefore good adhesion. Equations ((2.3) (2.4)) relate the following variables E_{coh}, δ.

$$CED = \frac{E_{coh}}{V} \tag{2.3}$$

$$\delta = \sqrt{\frac{E_{coh}}{V}} \tag{2.4}$$

E_{coh} expressed in (2.5) is defined as *the cohesive energy* of a material which is: "the amount of energy necessary to take all of the atoms or molecules in a mole of material and separate them to an infinite distance" [24]

$$E_{coh} = \Delta H_{vap} - RT \quad \textbf{(2.5)}$$

where ΔH_{vap} is the enthalpy of vaporization, R the gas constant and T the absolute temperature. The solubility parameter δ is linked to E_{coh} through (2.4), while the power square of δ represents the cohesive energy density CED. In order to predict a good adhesion phenomenon, the expression of the Gibbs free energy of mixing (both sign and magnitude) is a suitable criterion to detect spontaneous formation of a solution enhanced by good solubility of the materials participating to the diffusive bond. Generally indeed, negative values and high magnitude value of the Gibbs free energy of mixing is associated to spontaneous formation of the solution.

The expression of Gibbs free energy of mixing is given in equation (2.6) where ΔH_{sol} is the solution enthalpy variation, ΔS_{sol} the entropy variation of solution and T the absolute temperature

$$\Delta G_{mix} = \Delta H_{sol} - T\Delta S_{sol} \quad \textbf{(2.6)}$$

$$\Delta H_{sol} = \varphi_1 \varphi_2 (\delta_1 - \delta_2)^2 \quad \textbf{(2.7)}$$

The enthalpy variation ΔH_{sol} is given by (2.7), where δ_1 , δ_2 represent the solubility parameters of the adhesive and substrate, while φ_1 , φ_2 their respective mole fraction components. The above expression comes out from the assumption that the solution is not subjected to any specific chemical interaction; in this condition solution enthalpy variation values are positive or equal to zero. By considering polymeric materials, which have high molecular weight, ΔS_{sol} values are usually small. In fact, being the polymer configurational states limited in number, the system disorder when two materials are mixed is low. According to the two above observations summarized as either positive or zero ΔH_{sol} and low ΔS_{sol} values, solution concerning high molecular weight polymers show rarely spontaneous Gibbs free energy of formation as can be clearly understood from (2.6). In order to reach most negative possible values of ΔG_{mix} , condition associated to good adhesion, most negatives values of ΔH_{sol} are needed. This, according to the aforementioned assumptions, means: ΔH_{sol} =0 and therefore δ_1 =δ_2, hence criteria for good adhesion fall in same solubility parameter between adhesive and adherends. As an example, Figure 2-19 shows

schematically in a diagram some results of experiments conducted by Iyengar and Erickson [28] relating adhesive bond strength and solubility parameter for a variety of adhesives bonded to PET which is the polymer substrate adopted for the experimental investigation. PET solubility parameter is 10.3 while adhesive with known different solubility parameters where bonded to the PET realizing peel specimens which were than tested to evaluate the differences in peel strength. In agreement with the adhesion criteria explained in this section, high values of peel strength of the joints were obtained when the solubility parameter of adhesive (e.g. δ_1) matches the adherend substrate (PET) solubility parameter (e.g. δ_2).

Moreover, as it is shown in Figure 2-19, high peel strength values are related to failure change from apparent adhesion failure to cohesion failure.

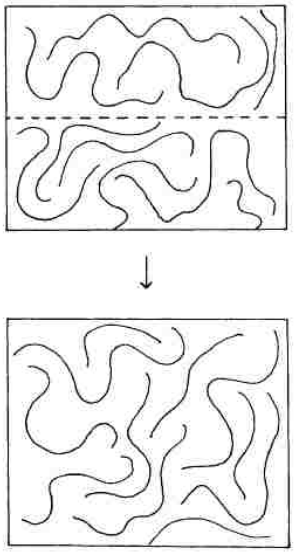

Figure 2-18: Interdiffusion between two polymeric adhesive and substrates and removement of the initial boundary [29]

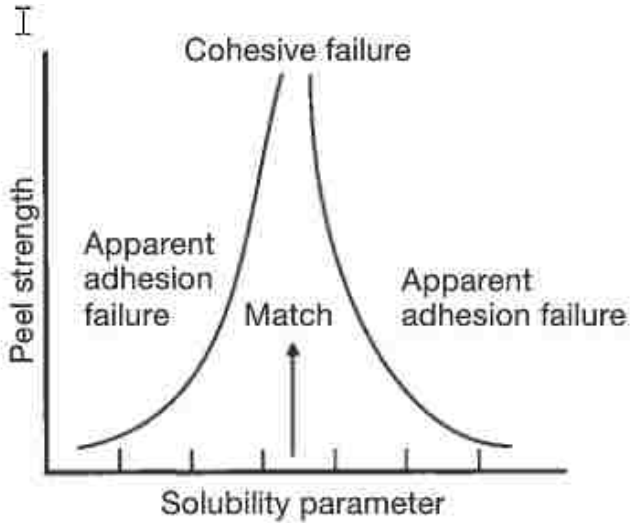

Figure 2-19: Schematic of peel strength dependance on solubility paraneter related to the adhesion of different adhesives to the PET substrate material [28]

2.2.3.4. Electrostatic theory of adhesion

The electrostatic theory resembles the interface adhesive/adherend as a plate of a condenser across which charge transfer occurs. Major contribution to the electrostatic theory was given by Derjaguin [30] based both on its analytical explanation and experiments. Figure 2-20 illustrates the interface as a double layer of opposite charges where an electropositive material donates charge to an electronegative material. Derjauguin's theory states that he force necessary to overcome couloumbic forces developed at the interface, and to allow separation of the charges surfaces, accounts for the strength of the adhesive bond.

$$W_B = 2\pi {\sigma_o}^2 h_B \qquad \textbf{(2.8)}$$

$$V^2 = \frac{8\,\pi E_C\, p\;\; h}{p} \qquad \textbf{(2.9)}$$

According to equations (2.8) and (2.9), the aforementioned theory assumes that energy stored in the capacitor E_C, which resembles the interface of the materials in contact, is equal to the work necessary to break the adhesive bond W_B. Nevertheless, this assumption does not take in account plastic deformations associated to either the

adhesive or the adherends, considering their behavior completely elastic. Therefore, the prediction of the peeling strength which comes out from this theory accounts, as energy dissipating factor, only the interfacial energy and is not suitable for most cases of adhesive bonds. In fact, as it was many times pointed out in this section; plastic deformation is the mainly factor associated to the work needed to break an adhesive bond. Despite the drawback of this theory, experimental studies performed by several authors support the fact that electric phenomena can be associated to adhesion. Firstly, electrical discharges can be noticed when considering the peeling of an adhesive from a substrate. Then, other evidences come out from the strict relation between electrical manifestations and adhesion founded out as for instance: either emission of light or of charged/neutral particles once the bond is opened in a vacuum etc.

It should be mentioned that the theory finds particular interest when the materials in contact own substantial differences in electronegativity.

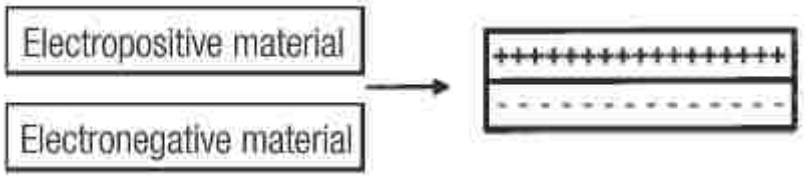

Figure 2-20: Schematic of the interface adhesive/substrate as an electrical condenser with a double layer of opposite charges [24]

2.2.3.5. Weak boundary layers

As already discussed in 2.2.2, Bikermann [21] proposed that properly made adhesive bonds fail cohesively either in the adhesive or the adherend; conversely actual adhesion failure occurring at the interface adhesive/adherend is highly improbable. Generally indeed failure goes through a weak boundary layer at the interface shown in Figure 2-21. Weak boundary layer can be defined as a layer made of foreign material located between the adhesive and the adherend very near to the interface; weak attachment of this layer on the bonding surface is recognized.

The principal weak boundary layers sources can be classified as:

- Presence of weakly attached metal oxide to their base metals causing failure to occur cohesively within the oxide.

- Poor cleanliness with subsequent adherends contamination by oil, grease or water adsorption which lowers dramatically durability strength of the joint
- Air trapped at the interface which is not properly displaced from the adhesive prior to fill the substrate surface features.

In order to eliminate or prevent formation of any weak boundary layer, attention should be taken during the following phases leading to the formation of the bonded joint: surface preparation, adhesive storage and application, curing process and in service period. Thus criteria for good adhesion deriving from the adhesion theory discussed in this section is defined as the demand for proper surface preparation allowing either to remove or modify weak boundary layers, with the latter suitable to make the weak layer cohesively strong.

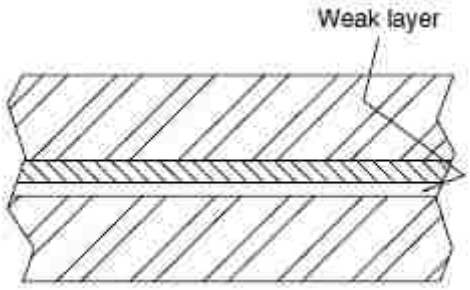

Figure 2-21: Weak boundary layer close to the interface adhesive/adherend [23]

2.3. Lap shear joint static strength factors

The single lap joint (SLJ) is the easier configuration used in order to predict the strength and the durability of the adhesive bonded joints and it's therefore the most studied in literature [17]. Nevertheless, the production of a bonded joint is affected by many factors which make its design complex, namely:

- Substrate surface preparation
- Geometrical parameters
- Environmental conditions

In fact, as illustrated in Table 7 , an improper adherend preparation and severe operating environment are among the major causes of premature failures in adhesive bonds. Other main causes fall in incompatibility between adhesive and the adherends

and improper steps during the process leading to lap joint production. Hence a deep investigation of the aforementioned factors is crucial and, as will be shown in the following paragraphs, it acquired remarkable reasons of interest for many authors.

Table 7: Major causes of premature failures in adhesive bonds [10]

Adhesive is not compatible to adherend(s), leading to:
- failure of the adhesive to wet the adherend surface(s)
- adverse chemical reactions at the bonding interface(s)
Improper adherend preparation, leading to:
- incomplete wetting of the adherend by the adhesive
- void entrapment or gas (porosity) formation at bonding interface(s)
- weak boundary layers (e.g., oxides, tarnish, reaction zones) at bonding interface(s)
Internal stresses:
- arising from adhesive shrinkage
- arising from differential C.T.E.s between adherend and adhesive
Out-of-plane peel or cleavage loading arising from improper joint design
Processing errors:
- arising from improper adherend surface preparation
- arising from improper adhesive application (e.g. working time exceeded)
- arising from improper curing or setting
Operating environment leads to degradation of the adhesive or adhesive-adherend interface(s)

2.3.1. Substrate surface preparation

Within this paragraph, the treatment of substrate surfaces prior to adhesive bonding is considered with focus on metals surface preparation, in particular on aluminum which is the material investigated in this work. The surface preparation is affected by two variables: surface cleanliness and surface roughness; the both will be described in the following paragraph through experimental studies collected from literature. Treatment applied to substrate surfaces have to be chosen according to the required bonding performance and the service condition experienced from the bonded joint, thus a sort of "fit-for purpose" surface preparation has to be pursued. Regardless of the treatment applied to surface, the generally outcomes provided are the following:

- Creation of bonding conditions with repeatable and consistent bond quality aimed at a production environment in order to obtain a predictable chemistry and morphology of the surface bonded.
- Usually improvement of wetting and adhesion properties between adhesive and adherends
- Improvement of the durability of the bonded joints

In Figure 2-22 a general scheme of procedure adopted for metal substrate surface treatment is given. First step is the degreasing phase, aimed to clean the surface removing contaminant, oils etc.; then rinse is effectuated both before and after the treatment to remove substances left from previous stages which can act as either stress concentrator points or as weak boundary layers ,lastly drying step is important to prevent water caused corrosion for some metals.

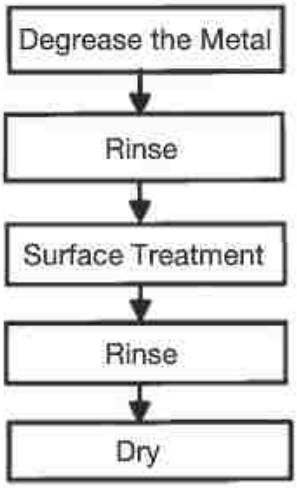

Figure 2-22: General procedure of susbtrate surface preparation for metals [24]

Generally, the three main categories of surface treatment techniques adopted are the following:

- Mechanical :grit blasting and abrasion
- Chemical treatments: degreasing, etching
- Energetic treatments :plasmas, corona discharges flame and lasers

Considering aluminum as adherend surface, this leads to a formation of a natural oxide layer and to absorption of contamination due to its high surface energy. Thus, in order to obtain a strong bonding, joint pretreatment of aluminum substrate is required. Several methods could be performed such as:

- Degreasing
- anodizing
- mechanical abrasion
- etching

- Multistage pretreatment embracing combination of the above methods

Degreasing can be used either as a stand-alone treatment or as a first stage for the subsequent treatments on the surface. Three main types of degreasing are realized by means of the following procedures: immersion/wiping techniques, vapor degreasing and ultrasonic cleaning. Organic solvent are mainly used such as: isopropyl alcohol, acetone, methyl ethyl ketone, perchloroethylene, trichloroethylene, or 1,1,1 trichloroethane. Safety issues and concerns about environmental are claiming for a preferable use of alkaline cleaning or detergents degreasing. Anodization consists in an electrochemical process; hence an electrochemical cell is realized where the anode is represented by the aluminum, while the cathode is generally the container in which the reaction occurs. Anodizing procedures fall in:

- Direct current (DC) anodic oxidation in chromic, phosphoric, or sulfuric acid electrolytes (CAA, PAA or SAA)
- Alternating current (AC) anodic oxidation producing thin surface oxide structures showing less usefulness of previous degreasing treatments but owning higher current density providing some drawbacks with respect to the previous procedure.

The main outcome of anodization is the production of a porous surface oxide as the one depicted in Figure 2-23 which aids joint adhesion and environmental resistance.

Etching consists in surface preparation realized by means of specific chemical treatments. The effects of the aforementioned treatments are summarized in Table 8.

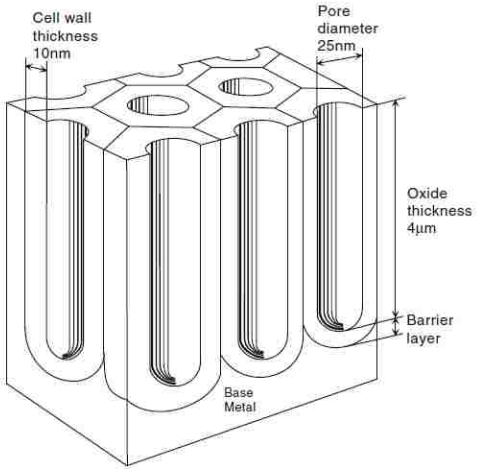

Figure 2-23: Porous surface oxide deriving from anodization of aluminum surfaces [24]

Table 8: List of main surface preparation methods and their effects for metals and plastics materials [23]

Substrate	Treatment Method	Effect of Treatment
Metals	Degreasing	Cleaning of the surface
Metals	Grit blast	Loose material (weak boundary) removal from the surface and increase in contact surface area
Metals	Acid etch/liquid pickling	Surface oxidation
Metals	Anodizing	Surface oxidation
Plastics	Corona treatment	Weak boundary layer removal and surface oxidation
Plastics	Flame treatment	Weak boundary layer removal and surface oxidation
Plastics	Chemical etching	Weak boundary layer removal and surface oxidation

2.3.1.1. Effect of surface cleanliness and surface roughness

Many experimental studies have been carried out in order to assess the influence of the surface preparation methods for the prediction of bonded joints stress-state under either static or fatigue loading condition. This paragraph is focused on literature studies concerning single lap joints in relation to surface preparation applied on their bonded surfaces. Surface cleanliness is used to remove or enhance weak boundary layers due to presence of: oil, moisture, weak oxide layers; the goal is to expose the adhered surfaces directly to the adhesive through physical and mechanical process.
Moreover, surface cleanliness allows raising surface free energy of solid conferring good wetting properties. On the other side, surface roughness as already mentioned in 2.2.3.2 provides the intimate contact needed for the adhesive to bond successfully with the adherend surfaces thanks to interlocking effect and to the increase of bonding area of contact. As far as surface cleanliness is concerned, significant works were performed by many authors to investigate the effect of contamination on the adhesion between adhesives and contaminated surfaces. Particular interest regards the automotive industry where the widely spread lubricated surfaces require desirable levels of adhesion to structural and non-structural adhesives applied. Minford in his studies [31] assessed the effect of lubricants as contaminants for both bonded and spot welded aluminum substrates. Material investigated were 2035 T4 Al, and a one part hot-curing epoxide, while the control of surface contamination was obtained varying

the concentration of an emulsified forming lubricant in which substrate surfaces were immersed. Both durability and environmental ageing condition were tested, the former by exposing either the joint to 52° and 100% relative humidity or subjecting joints to a 3,5% salt fog for 16h in a 24h-cycle, the latter by exposing joints to either humidity or salt-spray conditions for up to 180 days. Durability test showed that up to 0.82 mg/cm^2 (concentration of oil) , no significant loss in strength was noticeable; conversely from 0.95mg/cm^2 lap shear strength decreased from 10 MPA to 6MPA and failure mode changed from 90% cohesive failure mode in 60% cohesive failure mode and 40% apparent adhesive failure mode. Similar results, showing loss in shear strength were found also for environmental aged joints.

Pereira et al. [32] have carried out adhesion studies between a two component high strength epoxy and aluminum substrates. Firstly, surfaces were all cleaned to eliminate surface contaminations. Then, in order to optimize shear strength of the joints five different surface treatment were investigated, namely: sodium dichromate–sulphuric acid etch CSA , abrasive polishing AP, acetone cleaning by solvent wiping SW, caustic etch CE, and Tucker's reagent etch TR. According to Figure 2-24, which relates the failure load [kN] to the specific surface treatment, the study revealed that worse results were obtained for SW, CE while CSA, AP improved the adhesion. In particular, the chemical treatment results as the best treatment producing the higher surface activation energy. An analogous study effect was conducted by Da Silva et. al [33] who analyzed the adhesion between metal substrates and epoxy adhesives. In this case the surface treatments compared were mechanical treatment (p), and two types of chemical conversion coating (A1, A2). In this case, results of experiments indicated that the surface treatment has negligible effect on the bond strength.

Although the chemical treatments usually result the one providing higher bond performances, mechanical abrasion treatment is widely adopted in industries being easy to implement and a cost-effective solution. The latter determines the surface roughness of the adherends which in turns influences the bond strength.

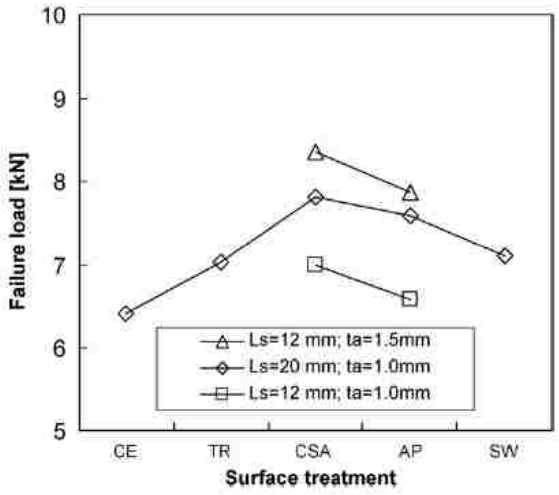

Figure 2-24: Failure load evolution over surface treatment [32]

As far as surface roughness is concerned, Uheara et.al studied adhesion of epoxy bonded carbon steel specimens. The studies revealed that, concerning tensile strength, an optimum value of surface roughness R exists while the impact of the same on the peeling strength is almost negligible. On the other side, as depicted in Figure 2-25 the shear strength-surface roughness curve lies between the aforementioned strength curves [34].

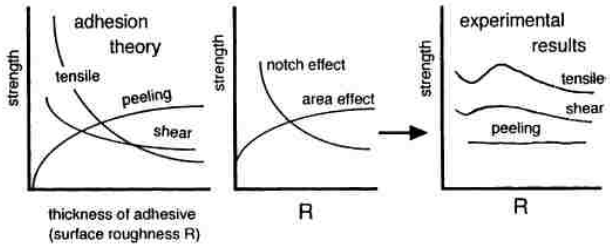

Figure 2-25: Qualitative illustration of bonding strength as combination of three factors: adhesion theory, increase of effective area of contact, notch effect [34]

The author suggested that a sort a tradeoff, coming from a combination of free factors namely: area of contact, notch effect and adhesion theory, is responsible of the joint strength behavior. In fact, according to the adhesion theory and following an analogy between the thickness of adherend and the surface roughness, the tensile strength is proportional to $1/R^2$, the shear strength to 1/R and peel strength is proportional to $t^{0.25}$. Moreover, increasing R there is an increase in effective contact area

adhesive/adherends but also higher possibility of void formation, stress concentration (notch effect) and lower wettability adhesive/adherends.

The presence of an optimum value for surface roughness was detected also by Borsellino et al. [35]. The author concluded that the increase of joint strength with surface roughness was noticeable until an 'optimal' topography of surface has been reached. Moreover, in [35] the author studied the effect of different adhesive through wettability analysis and considerations related to the specific adhesive/adherend interaction. In particular, four different adhesives were analyzed and the main differences were shown between an epoxy EPO and a vinylester resin VE, whom contact angle trend as function of surface roughness is illustrated in Figure 2-26. In fact, the two adhesive show an opposite trend with the increase of surface roughness leading to higher achieved wettability for VE resin, which features lower contact angles. On the other side, the presence of an oxide layer M_gO on the substrate surfaces affected in a different way the adhesive attached .Therefore, due to the negative impact of the oxide layer on the VE resin, the latter achieved similar bond strength than EPO adhesive albeit the mentioned differences in wettability.

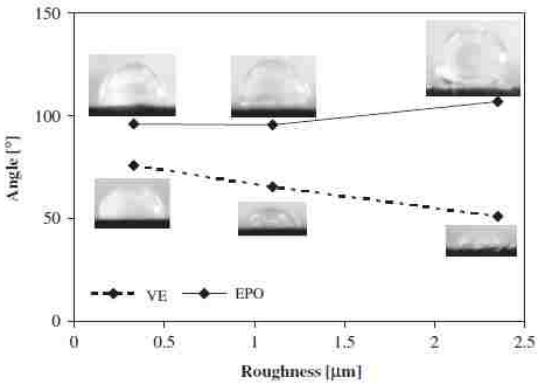

Figure 2-26: Contact angle evolution over surface roughness for two typical adhesives: EPO (epoxy), VE (vinyester resin) [35]

In another research, Spiaggiari et al. [36] investigated, in addition to different adhesives, the effect of mechanical treatment combined with different adherends materials and joint geometry configurations. The substrates materials compared were aluminum and steels and the joint geometries: single lap joint (SLJ) and double lap joint (DLJ). The test results illustrated in Figure 2-27 revealed that the average shear

failure stress [MPa] is almost constant under DLJ configuration for different mechanical treatments applied. Therefore, DLJ geometry provides a more stable joint behavior than SLJ. On the other side, steel adherends SLJ achieved higher average shear failure stresses than aluminum and an opposite trend was found for DLJ. Moreover, taking in account both the two geometry configuration, steel adherend performed always better than aluminum.

Finally, from the aforementioned studies we can conclude that, if exist, the critical roughness value promoting best value of strength is function of the following parameters [37]:

- Nature of adherends/adhesive and their interaction
- Joint geometry and applied stress

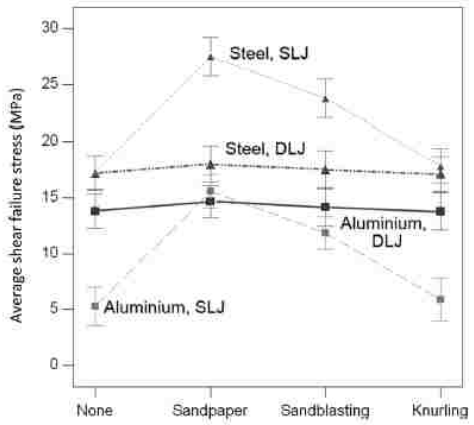

Figure 2-27: Influence of joint geometry and adherend material into the average shear strength [36]

2.3.2. Geometrical control factors

As already mentioned in 2.2.1, adhesive bonds strength is substantially affected by the joint geometry and its loading mode applied. Generally indeed, adhesives are able to withstand better specific loading modes than others. Here is reported, in decreasing order of preference, a list of the typical applied loads in adhesive bonds:

- Compression
- Shear
- Tension
- Cleavage
- Peel

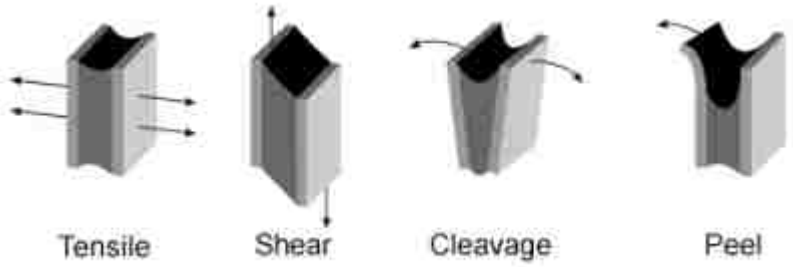

Figure 2-28: Typical applied loads in adhesive bonded joints [38]

Therefore, within this section, a brief illustration of the general stress-state to which the single lap bonded joint is subjected is given. In fact, as will be explained through some literature studies, the joint geometry and direction of loading impacts on the distribution and the types of stresses developed across the joint and hence on its strength. As far as single lap bonded joint is concerned, the mixed state of stresses experienced from the joint comes out from a combination of shearing and peeling modes. In fact, as illustrated in Figure 2-29, the load indicated with F is no collinear and it produces a bending moment leading to a rotation of the joint. This exposes the adhesive layer to both shear stresses τ_{xy} parallel to the bonded area and tensile stresses (peeling stresses) σ_y perpendicular to it. Moreover, the adherends are similarly exposed to both tension and bending. In addition, some degree of peel or cleavage load can be induced in the joint due to either possible adherends bending or joint asymmetries [10].

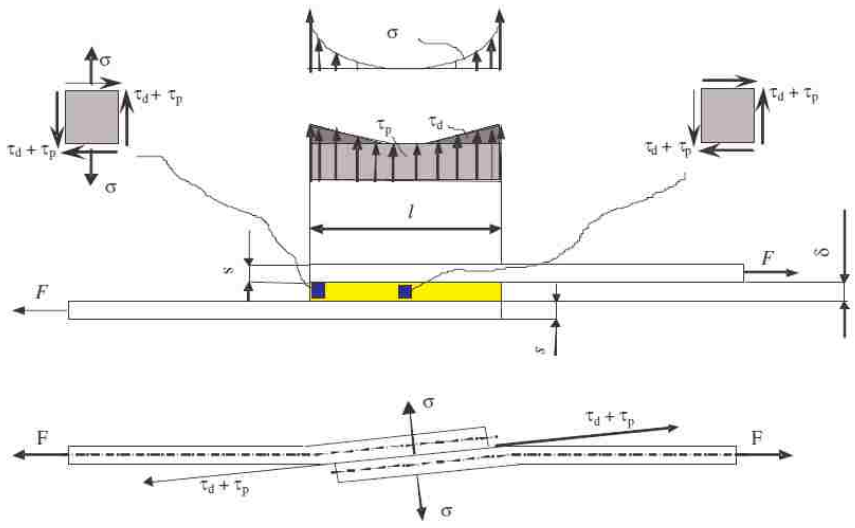

Figure 2-29: Single lap joint distribution of shear and peel stresses along the overlap area [39]

For sake of clarity, the single lap joint geometry is defined by the overlap length and overlap width, which identify the bonded area distributing the load, and by the adherend and adhesive thickness. All throughout this project, the overlap length and width were kept constant. Therefore, emphasis is placed on the adherend and adhesive thickness.

2.3.2.1. Adherend thickness

Adherend thickness was studied by De Morais et al. [40] who conducted single-lap shear tests for epoxy adhesive bonded stainless-steels joints. The results revealed that the apparent shear strength of single lap joints increased with adherend thickness.
They concluded that the increase of shear strength is correlated to a decrease of stress concentration on the joint ends due to higher bending stiffness and joint rigidity provided by thicker adherends. Similar trend were founded by Pereira et al. [32] and da Silva et al. [41]. The former investigated aluminum alloy adherends in which an increase of thickness from 1.0 mm to 1.5mm, for the same substrate surface treatment, showed 18% increase of failure load; the latter, instead, investigated steel substrates which revealed an almost linear increase of failure load with the adherend thickness. Similar additional considerations to the increase of joint rigidity were done by both the two authors considering the impact of the adherend thickness on the substrate material yielding. In fact, as can be seen in Figure 2-30, Pereira et al. [32] showed that thicker specimens leads to an the increase in the global rigidity of the system which in turns affects two parameters: rotation of specimen in the overlap region (ϑ) and the load corresponding to the initiation of substrate material yielding. Therefore, by increasing the adhrend thickness, the rotation angle of the joint decreases even for low loads and moreover the plastic yielding of the material occurs at higher loads as indicated by the arrows in the graph. It should be pointed out that the onset of adherends plastic deformation can be easily recognized by the change of slope of rotation angle versus load curve for each substrate thickness considered. Similar conclusions were stated from da Silva et al. [41].
A mathematical interpretation of the increase of bending strength of the adherends material can been provided by the methodology proposed by Adams to predict the failure load of a lap joint as function of the plastic deformation of adherends [29].

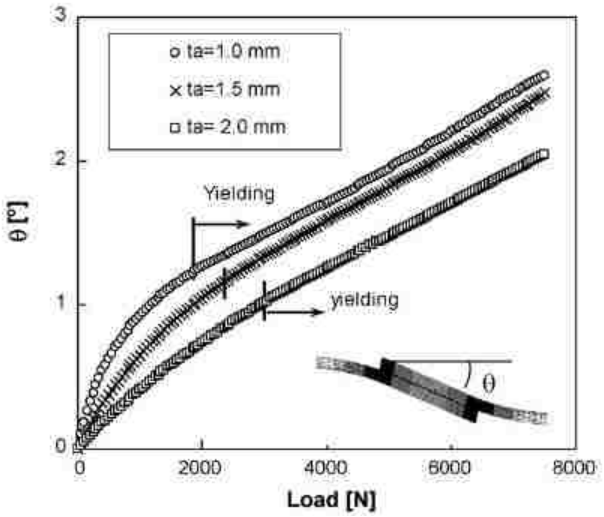

Figure 2-30: Specimens rotation angle as function of the load for different adherend thickness values [32]

First, by considering a beam under elastic deformation, subjected to a bending moment M, the maximum stress σ_s is at the inner adherend surface and expressed by equation (2.10) . Here, b represents the overlap width length and t the adherend thicknees and this notation will be kept throughout this explanation. The expression of the bending moment M at the edges of the joint overlap in equation (2.11) is provided by the theory of Goland and Reissener. Here the parameter k represents the bending moment factor which decreases (from unity) with the increase of rotation angle of the joint due to the tensile load applied.

$$\sigma_s = 6\frac{M}{bt^2} \quad \textbf{(2.10)}$$

$$M = \frac{kPt}{2} \quad \textbf{(2.11)}$$

Adherends, as already mentioned in this section, are also subjected to tensile load P which causes tensile stresses σ_t reported in (2.13). Therefore, the maximum surface stress σ_m is found as summation of σ_s and σ_t (equation (2.14))

$$\sigma_s = 3\frac{kP}{bt} \quad \textbf{(2.12)}$$

$$\sigma_t = \frac{P}{bt} \quad \textbf{(2.13)}$$

$$\sigma_m = \sigma_s + \sigma_t = \text{P (1+3k)/ bt} \quad \textbf{(2.14)}$$

$$P_{max} = \frac{\sigma_y bt}{1 + 3k} \quad \textbf{(2.15)}$$

$$P_{max} = \sigma_y bt \quad \textbf{(2.16)}$$

Thus by matching, in equation (2.14), $\sigma_m \, to \, \sigma_y$ (yield adherend strength), P eventually results in P_{max} which is described by equation(2.15).

P_{max} is therefore defined as the maximum load for which the adherends material starts to yield.

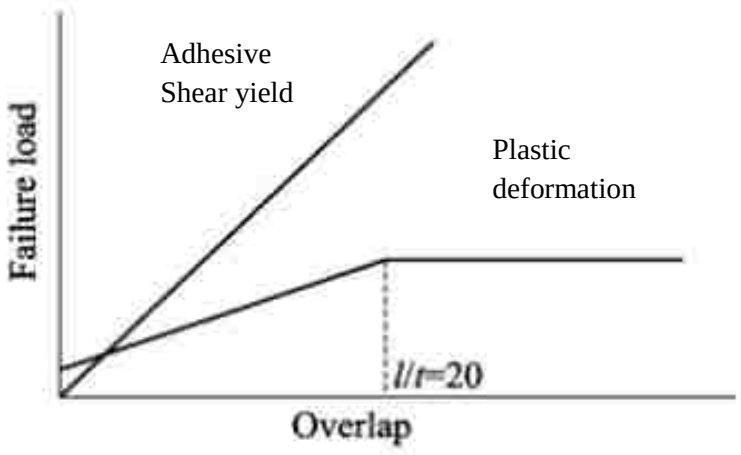

Figure 2-31: Prediction of failure load as function of plastic deformation or either the adhesive or the adherend [29].

Moreover, Adams stated that for cases in which the joints length is much higher than the adherend thickness, in particular for l/t >20, P_{max} expression is the one in (2.16).

This simplified expression shows a linear relation between the maximum load corresponding to the start of substrate material yielding and the adherend thickness as confirmed by the previously mentioned studies of da Silva et al. [41]. It should be mentioned that the explained methodology works properly when considering substrate material which are subjected to plastic deformation as consequence of the tensile load applied. For instance, it is suitable for ductile adherends such as aluminum alloys and mild steels. Finally, another aspect to take in account, together with the increase of

flexural rigidity of adherends, is the increase of bending moment. In fact, due to the load offset for single lap joint in tension, an increase of adherend thickness raises the distance between the upper adherend and the mid-thickness of the joint. As a consequence, the bending moment applied to the substrates increases and a higher stress concentration is developed at the ends of the overlap region. Gultekin et al. investigated several adherends thickness values and computed the two aforementioned parameters for each of them as reported in Table 9 [42]. The author founded an increase of lap shear strength from 1.6mm up to 4.8 mm of adherends thickness values (t_1,t_2) while from 4.8 to 6.4 mm the increase of bending moment overshadowed the benefits given by the higher system rigidity decreasing the final lap shear strength. Thus, the tests results revealed a substantial dependence of the lap shear strength on the combination of bending moment and the flexural rigidity of adherends.

Table 9: Increase of both flexural rigidity of adherends and bending moment as function of the increase of adherend thickness [42]

Sample type	$t_1 - t_2$ (thickness)	Flexural rigidity of Adherend-EI ($kNmm^2$)	Bending moment (kN mm)
Type Ia	8.0–8.0	72226.60/72226.60	65.00
Type Ib	6.4–6.4	39540.05/39540.05	53.08
Type Ic	4.8–4.8	16680.96/16680.96	46.13
Type Id	3.2–3.2	4942.50/4942.50	26.93
Type Ie	1.6–1.6	617.80/617.80	14.90

3. EXPERIMENTAL PROCEDURE AND TEST SET UP

This chapter provides an explanation of the experiments conducted in order to assess the static strength of aluminum structural adhesive joints.

3.1. Design of experiments

Firstly, by considering the factors influencing the lap shear strength joint mentioned in section 2.3, the following control factors were investigated:

- Adherend surface roughness
- Adherend thickness
- Adhesive thickness
- Effect of temperature
- Test speed

All experimental tests were performed using the lap shear geometry configuration represented in Figure 3-1.

The overlap length and adherend width length considered were kept constant and respectively equal to 25mm and 40mm.

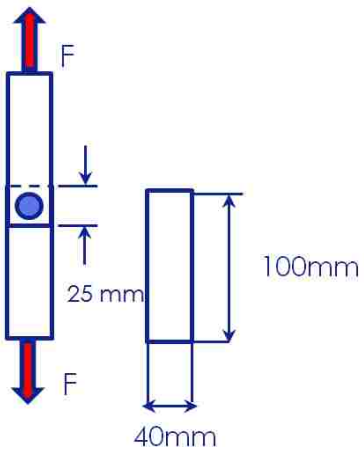

Figure 3-1: Lap joint geometry adopted in the design of experiments

A first investigation was oriented to identify the best value for the surface roughness. Hence, a full factorial design was planned according to the matrix of experiment

shown in Table 10 which states the investigated control factors along with their corresponding levels. Similarly, to identify the best value of adhesive thickness, a second full factorial design was developed as illustrated in Table 11.

Once the best values for the two aforementioned factors were determined, the effect of both temperature and of test speeds was investigated.

For sake of simplicity, in the following, best values or surface roughness and adhesive thickness will be identified respectively with the abbreviations BSR and BTA.

Table 10: Matrix of experiment variables, factors investigated: adherend thickness and surface roughness, adhesive thickness is constant for all specimens and equal to 0.25mm

Material:MS5005 –AA6016DRX			
Adherend thickness =1.3mm		Adherend thickness=2.1mm	
surface roughness[grit size]		surface roughness[grit size]	
P60 P120 P240 P320		P60 P120 P240 P320	
specimen number per condition	3	specimen number per condition	3
total specimen number	12	total specimen number	12

Table 11: Matrix of experiment variables, factors investigated: adherend thickness and adhesive thickness

Material:MS50005 –AA6016DRX			
Adherend thickness =1.3mm		Adherend thickness=2.1mm	
Adhesive thickness[mm]		Adhesive thickness[mm]	
0.11 0.34 0.74		0.11 0.34 0.74	
specimen number per condition	3	specimen number per condition	3
total specimen number	9	total specimen number	9

After the first batches of samples tested according to Table 10 and Table 11; the remaining experiments were focused on thicker specimens. They showed negligible effects for what concerns the plastic deformation of the adherends, therefore allowing a better analysis of pure adhesive shear strength performance.

The effect of test speed was verified for a specific combination of factors as listed below:

- Tensile test performed at room temperature

- Best value surface roughness (BSR)
- Best value adhesive thickness (BAT)
- Adherend thickness =2.1 mm

Test speeds analyzed are the following:

- 0.05mm/min
- 0.1mm/min
- 1mm/min
- 2mm/min
- 5mm/min
- 50mm/min
- 100mm/min

Then, test speed influence was combined with the temperature effect according to Table 12.

Table 12: Matrix of experiments, factors investigated: tensile test temperature and test speed

Material:MS50005 –AA6016DRX		
Substrate thickness =2.1mm	temperature [°C]	test speed[mm/min]
BTA	40	0.1
BSR	50	5

Each test presented in the previous tables was replicated three times under nominally identical test conditions specified.

Finally, an estimate of the fracture surface analysis was conducted in order to express the percentage of both cohesive and adhesive failure as defined in 2.2.2.

3.2. Material investigated and sample preparation

The material analyzed in this research project was provided by FCA (Fiat Chrysler Automobiles) which is the industrial partner of this research project.
The substrate's aluminum investigated in this experimental work is the aluminum alloy AA6016 DRX, belonging to the 6xxx series.

Table 13: Chemical composition AA6016 DRX (FCA standard for MS50005)

Material: MS50005 AA 6016 DRX									
Element	Al	Mn	Mg	Cr	Si	Ti	Zinc	Cu	Fe
%wt	95.3-96.6	≤ 0.25	0.2-0.8	≤ 0.2	0.5-1.5	≤ 0.15	≤ 0.15	≤ 0.25	≤ 0.35

Table 14: Mechanical properties AA6016 DRX (FCA standard for MS50005)

Material: MS50005 AA 6016 DRX		
Ultimate tensile strength [MPA]	**0.2% offset yield strength [MPA]**	**total elongation %**
175	90 to 130	23

According to the FCA standards, its nominal chemical composition and mechanical properties have to be compliant with the values reported in Table 13 and Table 14.

The adhesive adopted is the Dow Betamate1620US epoxy used mainly for body-in-white applications. It has toughening agents inside aimed to increase the energy required to fracture the joint. Thus, during an impact event the material requires more total energy to fracture the bond and peel the bond apart. The Dow Betamate1620US physical and mechanical properties are provided in Table 15 and Table 16.

Table 15: Dow Betamate1620US uncured physical properties (data provided by Dow Automotive)

Uncured physical properties Dow Betamate1620US				
Composition	**Solid content**	**Flash point**	**Young's modulus**	**Viscosity/yield stress**
Epoxy	99%	405F(205 C)	2000 MPa	50pas/800Pa

Table 16: Dow Betamate1620 cured physical properties (data provided by Dow Automotive)

Cured physical properties Dow Betamate1620US				
Specific gravity	**Elongation**	**Young's modulus**	**Tensile strength**	**Poisson's ratio**
1.21	10%	1500 MPa	29 MPa	0.378

The preparation of the samples was carried out according to the scheme of Figure 2-22 presented in section 2.3.1
Three main steps consist in: degreasing, abrading, degreasing. This sequence defines the suggested surface preparation when considering aluminum as substrate material [43].

Degreasing was realized by solvent wiping procedure. The organic solvent used was acetone which is highly used in manufacturing thanks to the following properties:

- Low toxicity
- Safer to use
- Inexpensive
- Less regulated
- Easy to obtain

First, lint-free cloths soaked in the organic solvent were used to clean the surfaces of each substrate exposed to the bonding area. Then, the threated surfaces were put to

stand for one minute to allow the complete evaporation of the solvent. Subsequently, clean hot water rinse was adopted. In order to assess the degreasing effectiveness, distilled water was spilled onto the substrate surfaces. In fact, looking at the shape of the poured water on the surfaces, a film-shape indicates a cleaned surface free from grease conversely drop-shape indicates a not proper degreased surface. The latter case suggests an additional degreasing step. Drying was accomplished by means of a drier with a stream of hot air to the surface. After degreasing, mechanical abrasion was performed manually by sanding the substrate surfaces, which take part in the bonding joint, with aluminum oxide emery cloth sandpapers. The abrasion of each work-piece was conducted until no evidence of surface gloss was visible. Four different grits sizes were selected: p60, p120, p240, p320. It should be mentioned that lower grit number results in a rougher surface preparation. Thus, as depicted in Table 18, the use of different sandpapers grit sizes allows evaluation effect of surface roughness on the joint resistance [44].

Table 17: Average roughness[µm], the reported values refer to as received surfaces and abraded surfaces with aluminum oxide emery cloth of different grit sizes (60P, 120P, 240P, 320P)

Average Roughness (Ra)		
As received	0.43	µm
320 grit	0.60	µm
240 grit	0.81	µm
120 grit	1.16	µm
60 grit	1.57	µm

The surface roughness was measured by means of an optical Wyko profiler for each treated aluminum surface with different mesh sandpaper sizes. The average roughness measurements computed from 3-points with 2.5X magnification are reported in Table 17. In order to perform the mechanical abrasion treatment, a sand scratch orientation perpendicular to the load applied in the lap shear tests was chosen. In fact, as investigated by Yan et al. [45], grinding orientation shows an effect on the bonding strength. In particular, as can be seen in Figure 3-3: Influence of sand scratch orientation on the the adhesive bond strength , the work carried out by the author showed that 90° orientation (relative to the direction of the shear load) of sand scratches results in higher bond strength with respect to both random and 45° orientation of the scratches. Figure 3-2 shows the substrate surfaces after the mechanical abrasion treatment.

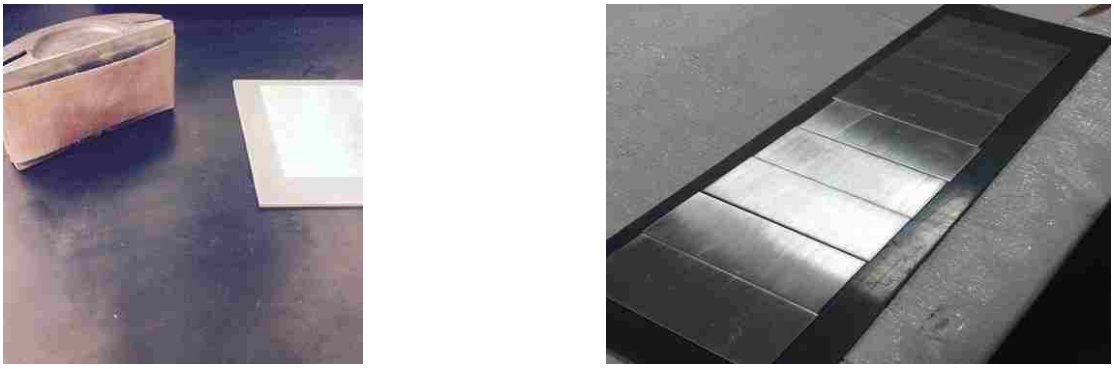

Figure 3-2: On the left abrasive tool used to manually abrase the aluminum substrate surfaces; on the right a bath of samples after the mechanical abrasion treatment was performed

Lastly, the mechanical abrasion has been followed by degreasing again in order to remove the residual particles left from the treatment.

Table 18: Abrasive grade selection proposed by Aluminum Association of America [44]

Mesh aluminum oxide grit	
Coarse finish	60-100
Medium	180-220
Fine	320-400

All along the surface preparation process, attention must be paid in the handling of the material between the subsequent phases in order to not contaminate the treated surfaces prior to bonding. Moreover, as good practice, bonding of the surfaces has to be performed after the completion of the aforementioned treatments.

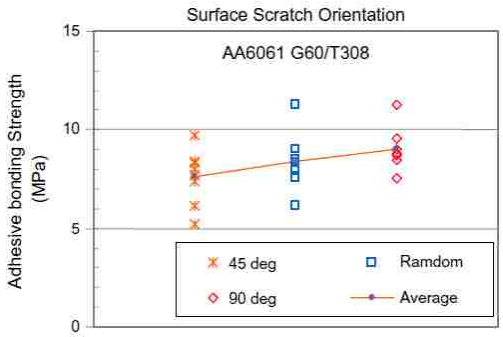

Figure 3-3: Influence of sand scratch orientation on the the adhesive bond strength [45]

3.3. Lap joint production

This paragraph gives the description of the procedure adopted to construct the single lap joints (slj) specimens used to gather information about the shear strength according to the standard ASTM D1002.
According to Figure 3-4, the dimensions of prepared adherends plates are the following:

- a = 40 mm
- b = 100 mm
- s = 1.3 mm or 2.1 mm
- l = 25 mm

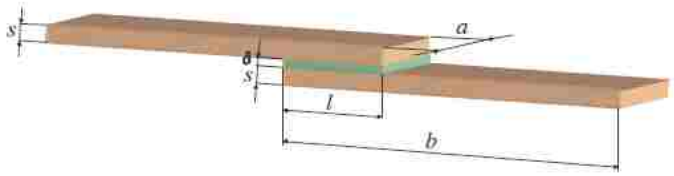

Figure 3-4: Schematic of the single lap joint analyzed

The procedure consists of the following steps:

- Adhesive application
- Assemble and fixture of the joint
- Adhesive curing process

Adhesive application is affected by the form of the adhesive. Despite of liquid form adhesives, which easily flow covering the bonded area of the joint, paste adhesives as the one here analyzed require special care.
In particular, according to the manufacturer instructions, an easier dispense of the DowBetamate1620 is realized by pre-warming the adhesive cartridge (on the left in Figure 3-5) in the range of temperature (20°-65°) which guarantees adhesive dispensing consistency. In this work, after some trials, a reasonable dispensing nozzle temperature of 35°C was chosen. The adhesive was applied to the substrate surfaces

by means of a dispensing gun with the tip perpendicular to the work-piece and by following the scheme shown on the right of Figure 3-5 in order to avoid air entrapment.

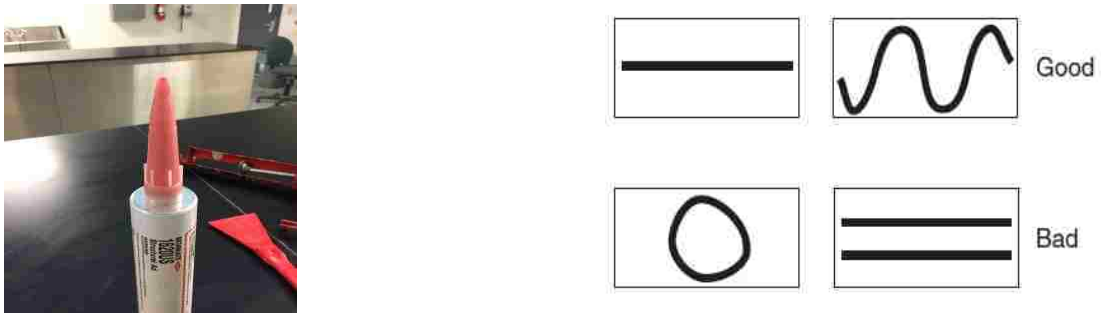

Figure 3-5: On the left Dow betamate1620US adhesive cartridge, on the right an illustration of adhesive application methods

As explained by da Silva et al. [46] single lap joint bonding presents some issues for the correct measure of adhesive properties which is affected by the control of the following main geometrical aspects:

- Overlap length
- Adhesive thickness
- Adhesive spew fillets
- Joined parts alignment

The control of these factors is crucial in the joint assemble and fixture steps.

Overlap length measurement was realized by means of a caliper to establish the specified adherends bonding area. In order to control the *adhesive thickness*, and thus keep the substrates at constant distance, microspheres glass beads of precise diameter acting as spacers were uniformly distributed onto the adhesive as illustrated on the left of Figure 3-6. After applying the glue on the two flat adhererends, the parts were mated together progressively by rotation as shown on the right of Figure 3-6 in order to reduce the number of voids formation.

Care was taken to remove any extra glue squeezed out from the sides of the overlap area after the manual assemble of the joint. This aids in prevent *adhesive spew-fillets* formation.

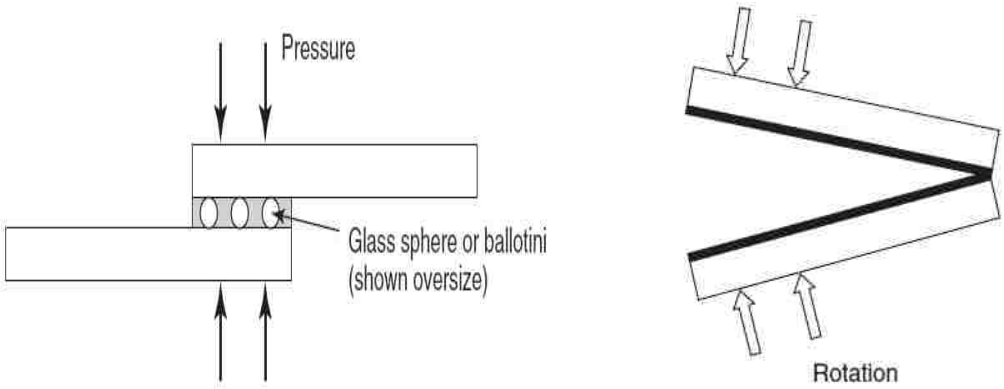

Figure 3-6: Microspheres glass beads adopted to control the bondline thickness (left); rotation movement used to mate the two adherends parts (right)

Hence, the two mated parts were clamped together using a traditional fixture method. C-clamps were used to maintain the prior achieved configuration all along the subsequent phases avoiding any possible movement of the samples. *Correct alignment* of the substrates was realized by using some reference blocks held against the adherends. Attention was paid to maintain the joint alignment even after the handling of the material needed to move the joint into the oven for the curing process. In addition, thin Teflon (PTFE) films were put in the area of contact between the C-clamps and the aluminum substrate surfaces to prevent their attachment after the adhesive curing in the oven has occurred.

Moreover, in order to minimize bending stresses during the testing, and to ensure symmetric loading of the joint, tab ends of the same material and thickness of the substrates were bonded to both ends of the specimens. It should be pointed out that another function performed by these plates is to protect the specimens against local damages caused by the gripping of the testing machine. In the left of Figure 3-7 we can see the machine used to cut the tab ends from the original aluminum coupons (100mm x 40mm). Two set of tab ends (rectangular shape)were produced for both the aluminum thickness (1.3mm, 2.1mm) with dimensions 40 mm x 25 mm x 1.3 mm(or 2.1 mm). In the right of Figure 3-7 it can be seen the joints after assemble and fixture steps.

Figure 3-7: Cutting machine used for produce the tab ends (left); Lap single joints clamped prior to the adhesive curing phase (right)

The last step of the lap joint production conceives the adhesive curing which is a chemical process necessary to change the adhesive state from liquid to solid enhancing its bearing capabilities. The one-part epoxy adhesive investigated in this work solidifies and crosslinks under a heat-curing process.

Adhesive curing temperature and time were selected according to technical data sheet provided by the adhesive manufacturer respectively as 180°C and 30 min.

With regards to automotive industry, it should be mentioned that the aforementioned curing parameters are suitable to simulate the car paint baking process allowing adhesive to set in this phase of the assembly line.

Figure 3-8: PTL-MMB01 oven adopted to cure the specimens at 180° for 30 min.

For each prepared joint, curing process was performed inside an oven, depicted in Figure 3-8 under constant pressure applied through clamps to the joint areas subjected

to adhesive bonding (overlap length and both ends of specimens). The bonded joints were then allowed to cool down uniformly until reaching room temperature to avoid possible residual thermal stresses. Finally they were stored in a dessicator for at least 24 hours prior to testing to prevent moisture ingress, which can degrade the adhesive joint strength.

It should be mentioned that for the selection of a suitable and repeatable method to fixture the joints a trials and error procedure has been followed.

In the following a description of one of them is given. For instance, a former fixture was designed and implemented as illustrated in Figure 3-.

Figure 3-9: First trial fixture implemented for the single lap joint

The design aim of this fixture was to better control the previously discussed main geometrical aspects. In fact, by means of this fixture, the substrates are kept in place and their correct alignment is provided by their allocated space properly machined according to the width and the length of the specimens as illustrated in Figure 3- (b).

Moreover, in order to allow the fixture's capability of containing two specimens, a specific cross sectional shape (H-shape as illustrated in Figure 3- (*a*)) was designed. This feature results in decreasing the curing time needed for specimen enabling two specimens to be cured at the same time. In addition the clamping pressure is here applied uniformly all along the specimen area though the application of a top plate (shown in Figure 3- (c)) provided with threads to which bolts are fastened and tightened. Then, C-clamps were placed in the ends of the fixture to better clamp the tab ends bonded to the joints. For sake of material availability, steel was chosen to realize the boding equipment. On the other side, it should be pointed out that it is

recommended, for the fixture, to adopt the same material of the substrates to reduce the residual thermal stresses.

The control of adhesive thickness was accurately performed through mechanical shims placed inside the fixture. Shims were produced in precise dimensions according to desired bondline thicknesses mentioned in 3.1. Before the application of the adhesive, urethane release agent was sprayed onto both the metallic parts of the fixture, in contact with the specimens, and the mechanical shims.

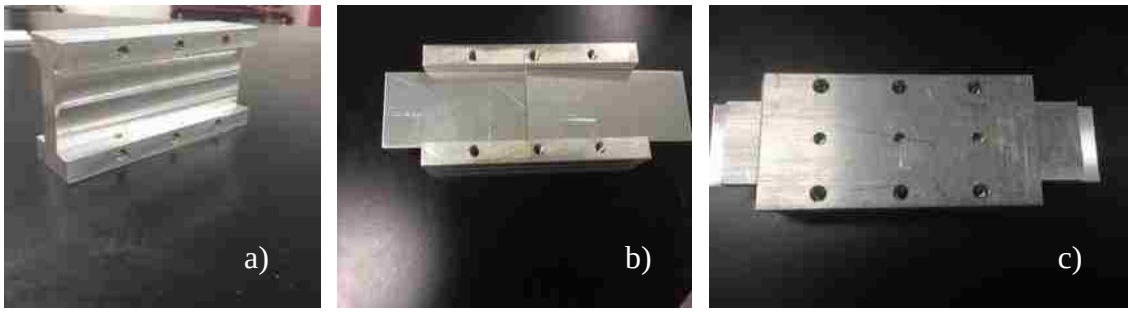

Figure 3-10: On the left a) view of the H-cross sectional shape of the fixture; in the center b) adherends are kept aligned inside the fixture; On the right c) top plate provided with threads to which attached bolts provide the required pressure to fixture the samples

Some problems arise after the production and testing of the first batch of joints. In fact, the aforementioned curing time and temperature resulted as not proper for this application. Moreover, lap shear testing revealed an apparent adhesive failure from the fracture of the specimens leading to low failures load.

A possible explanation of the latter result comes out from the mold release type and application method adopted which might be not suitable for this bonding procedure.

In fact, an unexpected interaction between the mold release and the adhesive has occurred during the curing phase. With regards to the different response to the curing temperature and time applied, substantial heat transfer through the metallic parts surrounding the specimens is claimed to be the motivation. A more detail analysis, through thermocouples in contact with specimens, should then be applied to evaluate the proper curing variables. This, in fact, would guarantee a uniform sample heating up to the adhesive solidification.

3.4. Lap shear tests

3.4.1. Lap shear test at room temperature

The static shear strength was obtained using an MTS 150KN load frame electromechanical universal testing machine illustrated in Figure 3-.

Figure 3-11: Tensile machine for test at room temperature

This machine is provided with pneumatic interchangeable serrated wedges grips for testing either flat or rounded specimens. In this work, flat face grips with capacity of 150KN and specimen range 0-9mm was adopted.

To ensure repeatability of the tests and correct alignment of the specimens throughout the duration of the test, the latter were positioned in the jaws of the grips and constrained by properly dimensioned metal spacers. Then, the grips were manually tightened to prevent specimen slippage during testing.

A software program connected to the tensile machine (MTS TW Elite) was used to create a customized template which enables the lap shear testing once control parameters regarding specimen geometry and specific test variables have been entered.

The aforementioned parameters considered are the following:

- Specimen thickness
- Cross-head speed ratio
- Data acquisition rate

Specimen geometry thickness was checked before each test run by means of a digital caliper. Cross-head speed ratio was varied according to the specific test condition as mentioned in 3.1. Moreover, data acquisition rate was selected according to the test cross-head speeds; in particular higher data acquisition rate (around 50 Hz) was set for slow cross head speeds , while lower data acquisition rate (1Hz) for fast cross head speeds. Tensile tests were then performed at a selected constant cross-head speed up to final failure of the joint. In fact, the software program provides the termination of the test whenever a break is detected either inside the adherend or the adhesive.

Each time, the failed specimen was removed and another specimen was tested until completion of the designed tests in 3.1.

As previously mentioned, three specimens were tested for each analyzed condition with the aim to decrease experimental variability of results. Some more specimens than the planned ones were prepared for testing whenever previous tests reported large deviations in results. These usually derived from poor joint preparation leading to not significant outcomes which needed to be discarded.

The provided lap shear testing outputs are load, displacement and time. In order to perform data analysis, the mentioned outputs were recorded into an appropriately named file corresponding to the analyzed test condition after each test run. For sake of results consistency, the load of the tensile machine was verified every time once the device was started and in addition, for each test run, all the output variables were initiated assigning to them a zero signal. Figure 3- shows fractured specimens after testing in the tensile machine.

Finally, an attempt for the load bearing capability assessment of the structural adhesive joint was realized by creating another customized template named as load and dwell test. Once detecting the maximum value of failure load from the previous tests, performed on the thicker specimens, the final load for the dwell tension test was set as 80% of the maximum load detected.

Figure 3-12: Fractured specimens after the tensile tests

The main features of the last implemented template are represented in Figure 3-.
Each loop activity comprises two control variables: set load and dwell time. It should be pointed out that the dwell time is defined as the time allowed for the extension of the specimens during the phase in which the load is maintained at a specified constant level (set load).
The test was performed at constant cross-head speed of 0.1 mm/min. Several attempts were conducted to select reasonable values for the set load and dwell time of both the 1-loop activities in order to maintain the specimens at the previously mentioned final constant load.
In fact by implementing just one loop activity, the specimens are not able to maintain the set load during the dwell time due to stress relaxation behavior of the material related to its viscous-elastic properties. On the other side ,due to lack of knowledge about possibly a compensation factor which has to be specified for the tensile machine, the test carried out did not allow to maintain a constant load as it is shown in Figure 3-. The plot reported refers just to the first around 200 sec of the test. Anyway, the tests was carried out for a total dwell time of 1h: 30 min, in which the load kept decreasing and eventually reached a load around 14.5 kN. Therefore, the constant load condition did not applied as desired.

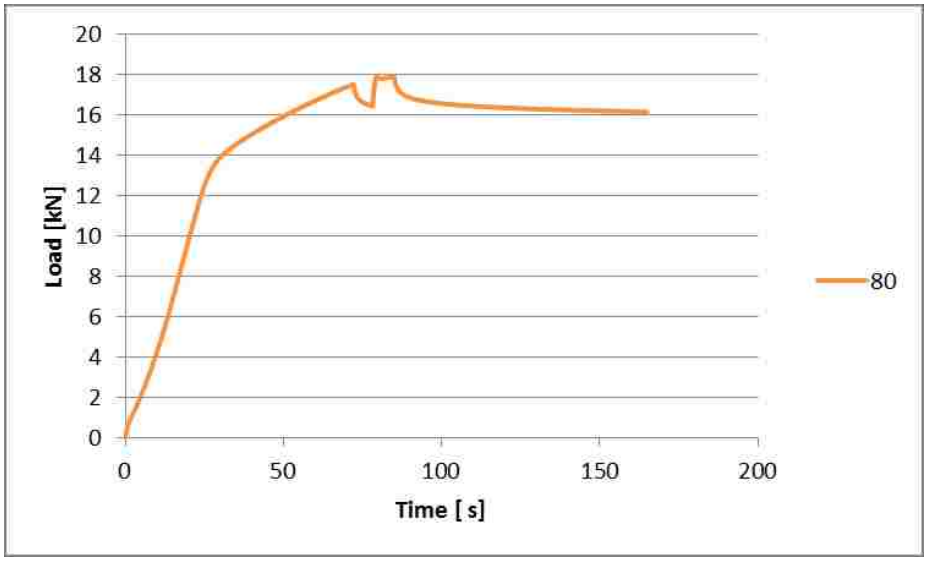

Figure 3-13: Coupon #80, attempt to realize a constant load condition for the sls joint tested at 0.1mm/min

The coupons tested did not break within the total dwell time selected and their residual deformation after test is showed in Figure 3-.

Figure 3-14: Deformed coupons after the attempts in realizing a constant load test condition

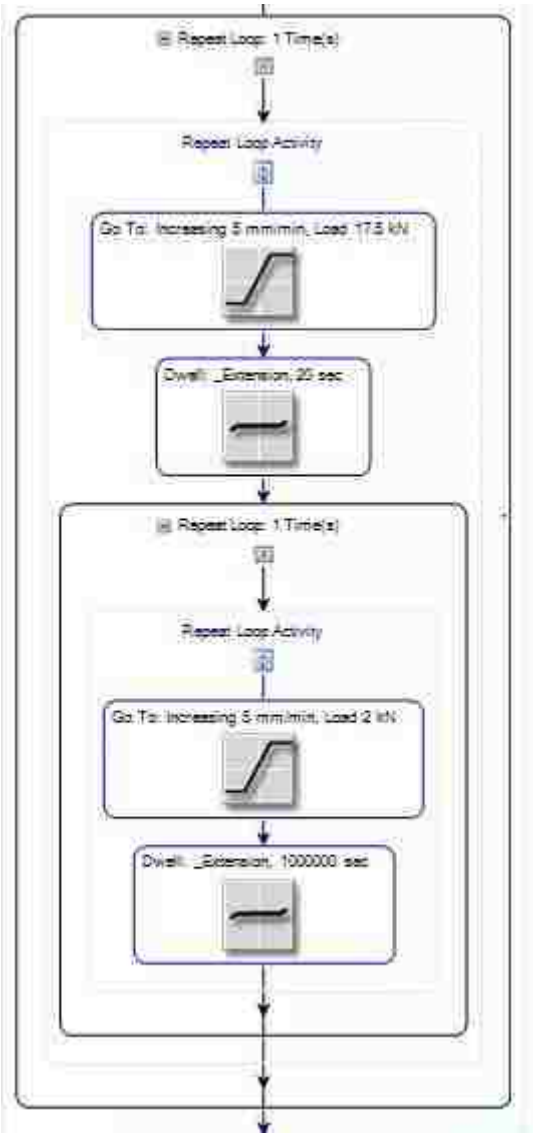

Figure 3-15: Procedure implemented in the tensile machine software program(MTS) to assess the load-bearing capability of the structural adhesive joint

3.4.2. Lap shear test at higher temperature

This section focuses on the tensile tests performed at high temperatures which require different equipment with respect to the room temperature tensile tests.

In fact, in order to perform mechanical testing of the specimens across a broad range of temperatures, the previously described tensile machine was combined with an environmental chamber (MTS) as illustrated in Figure 3-.

The temperature selected were 40° (103F) and 50° (122F) which simulate possible encountered in service condition for automotive applications.

Moreover, the chamber was installed together with a cooling system attached to its back to prevent possible damages due to machine overheating. Figure 3- shows on the right the temperature controller which clearly displays the set point and the current temperature, while on the left we can see the specimen inserted in the hydraulic grips used for these tests. Hydraulic grips are feed with special hydraulic fluids in order to withstand elevate temperatures.

Figure 3-16: Tensile machine combined with the environmental chamber to provide test at high temperatures

Before starting of the test, was important to notice that the temperature experienced by the specimens does not meet instantaneously the current temperature showed by the temperature controller. Therefore, some measurements have been conducted in order to understand the reasonable time needed for the specimen temperature to match the one of the furnace.

The use of thermocouple and a non-contact infrared thermometer as depicted in Figure 3-18 allowed the mentioned measurement to be performed

Figure 3-17: Enlarged view on the specimen inserted in the hydraulic grips of the tensile machine (left); The temperature controller showing both current and set temperatures (right)

In particular, once the temperature of furnace reached the set value and stabilized, the specimen was inserted inside the jaws of the grips as shown on the left of Figure 3-.
Only one end of the specimens was initially tightened by the grips to prevent possible material deformations due to the effect of temperature on the otherwise constrained sample. Then, by means of the previously mentioned measurement devices, the specimen temperature was continuously controlled and the time needed to the reach the set temperature was found to be 5 minutes. Thus, each test started around 5 min after the specimen was placed inside the pre-heated environmental combustion chamber and at the same time also the other end of the specimen was tightened. Similar considerations about the correctness and consistency of results made for room temperature tests applied again in this case.
The capacity of the tensile machine is 300 kN and the same customized template created for tests at room temperature, with the information related to the specimens geometry and test variables, was employed. Two cross-head speeds were investigated: 0.1 mm/minute and 5mm/min.

Figure 3-18: A non-contact infrared thermometer (left); A thermocouple (right)

4. RESULTS AND DISCUSSIONS

In this chapter the experimental results coming out from the tensile tests, performed according to the methodologies explained in chapter 3, are presented and discussed. The discussion is divided in 5 main subsections, one for each variable investigated: substrate surface roughness, adhesive thickness, adherend thickness, test temperature, test speed. Thus, from the tensile-load displacements curves obtained, for each test condition, a trend for the lap shear bond strength is generated and analyzed.

The data analysis is focused on the following quantities acquired from the tensile tests:

- Failure load
- Displacement at failure
- Energy at failure

As already mentioned in section 3.3, starting from the failure load, the lap shear strength can be easily computed according to ASTM D1002. Then, combining failure load with the displacement at failure, for each test condition, the energy at failure is evaluated. It should be mentioned that the latter represents notably interest for crash worthiness applications. The influence of investigated variables on the lap shear bond strength is then analyzed through a failure mode analysis by means of the observation of specimens surface fractures carried out as explained in section 3.

The load-displacement curves for all the tested samples for each test condition are reported in Appendix A.

4.1. Effect of surface roughness and adherend thickness

The roughness and the surface activation energy are expected to play a significant role in the adhesion process. In this section, the outcomes deriving from the experiments planned in Table of section 3.1 are presented and discussed.

The lap-shear tests were performed at constant crosshead rate of 5 mm/min until final joint failure and the data processing was accomplished with an EXCEL® spreadsheet.

The parameter selected to assess the strength of the lap shear joint is the failure load that is the peak load registered in the load displacement curve recorded from the test corresponding to load in which de-bonding process occurs.

In fact, the same single lap joint geometry was adopted for all coupons tested as described in Figure 3-1. Therefore, the failure load is related to the average shear stress, which is developed across the joint, through a constant value represented by the bonding area equal to 1000 mm^2. Hence, no difference is found in using either the failure load or average shear stress as indicator of lap shear bond strength.

The lap shear tensile tests were performed for four different values of surface roughness achieved by manual abrasion realized with different mesh sandpaper sizes, followed by wiping with acetone. For each surface roughness, the average failure load is computed from 3 tested samples and error bars are shown indicating the standard deviation of the 3 measurements. Figure 4-2 shows the obtained values of average failure load [kN] versus the surface roughness [µm].

The other manufacturing specimen parameters adopted are:

- Thickness adherend =1.3 mm
- Thickness adhesive = 0.25 mm

A similar plot was generated considering a thicker aluminum substrate stack. In fact, as can be seen in Figure 4-3, surface roughness values analyzed are the same of Figure 4-2. Adhesive thickness was kept equal to 0.25 mm while the adherend thickness tested was 2.1mm. Following this procedure, in addition to the impact of surface roughness on the adhesion process, the adherend thickness influence was taken in account.

Finally, in order to summarize the combining effect of surface roughness and adherend thickness, Figure 4-4 reports the effect of the both aforementioned factors on the single lap joint failure load.

4.1.1. Single lap joint failure load

Considering a typical single lap adhesive joint load-displacement curve, some characteristic points can be identified. The first point to be considered is related to the change of slope of the load-displacement curves which states the end of the linear

elastic part of the graph. In particular, as explained by Campilho et al. [47] , it represents the onset of plastic deformation of aluminum-alloy adherends.

As far as the onset of adherends plasticization is concerned, is should be underlined its strict correlation to both the property of the adherend material and the geometry of coupon. Therefore, as can be seen from load-displacement curves reported in Appendix A, load and elongation at this point, for each stack thickness, are subjected to low variability being the other geometry dimensions and material property equal for all the cases analyzed.

In particular, as explained in section 2.3.2.1, for aluminum thinner joint stack the adherend plasticization occurs at lower loads with respect to thicker aluminum joints stack. As an example, Figure 4-1 shows a comparison between the two adherends thickness tested in the project with shown their respective load values for which the adherends start to yield. As expected, it comes out that the 1.3mm aluminum adherends start to yields a substantial lower load level (Fy=9.88kN) with respect to the 2.1mm aluminum adherends (Fy=17.2kN). Another characteristic point of the load-displacement curve is the peak-load value which represents the adhesive yielding corresponding to the failure load of the joint. Finally the load steeply drops to zero until the final elongation of the joint has been reached.

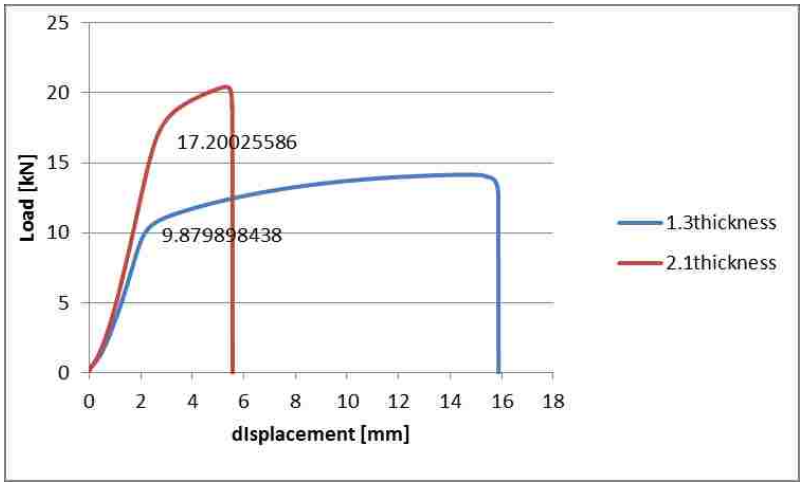

Figure 4-1: Typical load-displacements curves for 1.3mm adherend thickness and 2.1 adherend thikcnees; the numerical values reported on the graphs show their respective yielding loads.

After this whole explanation, regarding the load-displacement curve features and its characteristic points, a first analysis was conducted in order to investigate the

influence of the surface roughness on the failure load which resembles the lap shear bond strength.

In fact, after having correlated the different mesh sandpaper sizes to their produced value of roughness on the treated surface by means of an optical wiko prolifer, the average failure loads were plotted against the roughness values for both the two joint stack thickness values.

From Figure 4-2 and Figure 4-3 it can be seen that surprisingly the effect of surface roughness on the average joints failure loads shows substantial differences when considering the two different adherend thickness values.

In fact, taking in account that the surface roughness is a parameter affecting the surface of the material, the adherend thickness was not supposed to influence the failure load trend against the surface roughness but only its magnitude.

In particular, Figure 4-2 shows that the high roughness value tested (R_a =1.57μm) is the most beneficial for the adhesion process while lower roughness values show negligible differences on the failure loads behavior.

According to the literature, as already explained in section 2.3.1.1, generally the lap shear bond strength against surface roughness foresees the presence of a critical roughness value. In fact, as far as epoxy-adhesives are concerned, usually after an initial increment of strength performance related to the increase of effective contact area, the lap shear bond drops due to lower wettability between the adhesive and the adherends. Therefore, as a matter of fact, for 1.3mm aluminum adherends joints could be useful to test higher roughness values than R_a=1.57μm in order to assess the occurrence of the aforementioned condition. On the other side, the study of the lap shear bond strength founds more meaningful results when the higher joint thickness stack is considered.

In fact, as will be better shown from the failure mode analysis in section 4.4, the 1.3 mm thickness aluminum adherends joints, subjected to tension, undergo severe rotations of the specimens which derive from the following factors:

- Eccentricity of the load path transfer due to the single lap joint geometry as explained in section 2.3.2.
- Increase of peel stresses at ends of the overlap area which develops large stress concentration zones.

Thus it should be noticed that, being the investigation target of the project the assessment of the lap shear bonded joints performance, a more suitable analysis has to be to be carried out for a mixed stress state condition of the joint which minimizes the effects of the peel stresses.

As far as 2.1mm adherends thickness joints are concerned, Figure 4-3 shows the existence of a critical value of surface roughness R_a=0.81µm for which the highest value of joints failure load is reached.

An estimate of the average percentage increase of failure load of 2.1 thick specimens with respect to 1.3 mm thick ones is 41.54%. The value is calculated averaging the percentages of the difference between the two stack thickness failure loads values for the four surface roughness values tested.

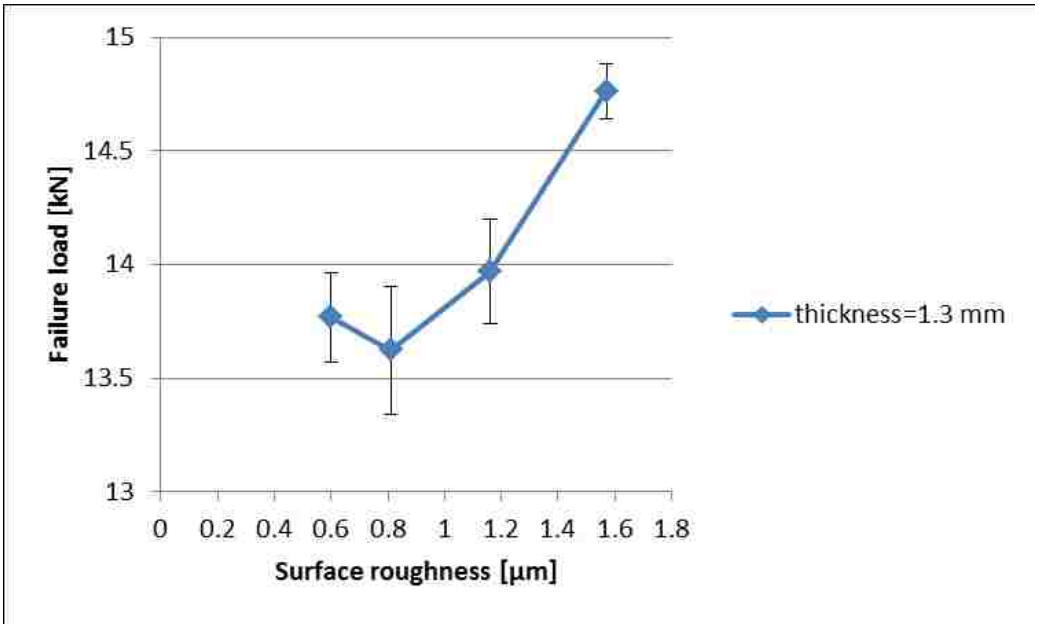

Figure 4-2: Average failure load evolution over surface roughness for 1.3 mm adherend thickness

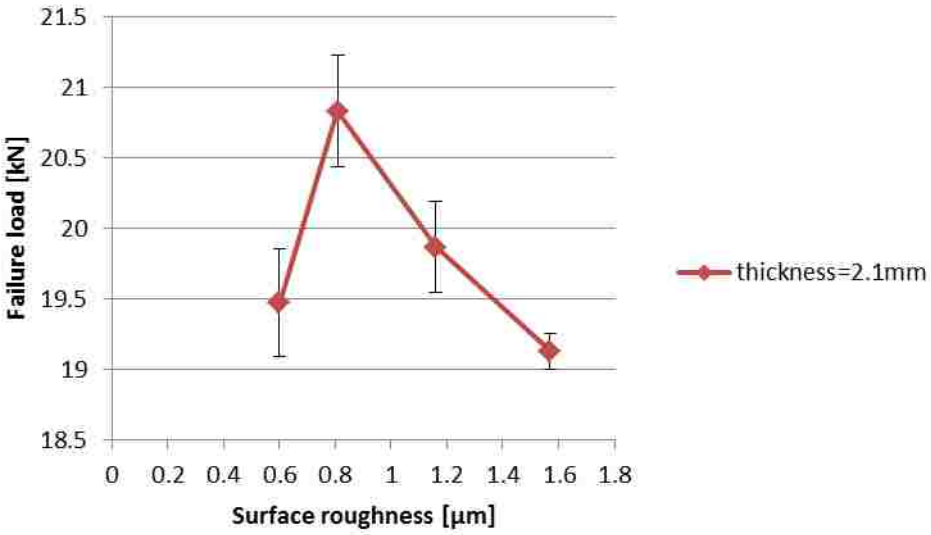

Figure 4-3: Average failure load evolution over surface roughness for 2.1 mm adherend thickness

In Figure 4-4, a 3D diagram allows to get a better understanding of the combined effect of both adherend thickness and surface roughness on the average joint failure loads. In particular the best condition is achieved for surface roughness equal to 0.81µm and aluminum substrate thickness equal to 2.1mm.

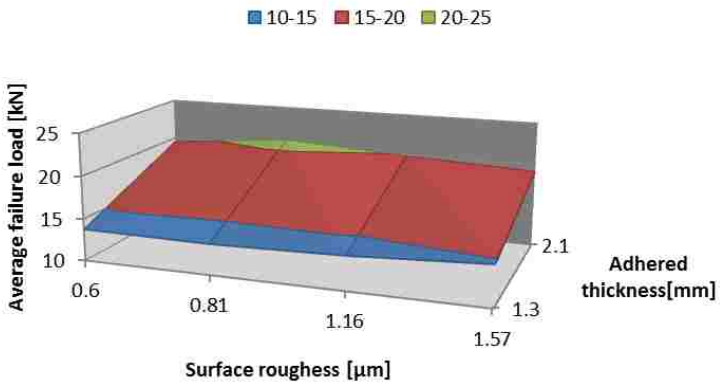

Figure 4-4: 3D plot of average failure load as function of both adherend thickness and surface roughness

Table 19: Average failure load for the two joint stack thickness t_1,t_2 and for the four surface roughness values considered

Surface roughness [μm]	t_1=1.3mm		t_2=2.1 mm	
	Average Failure load[kN]	C.O.V[%]	Average Failure load[kN]	C.O.V[%]
0.6	13.76836	2.841864	19.47202	2.537287
0.81	13.6219	3.355677	20.82946	1.542008
1.16	13.96811	1.646608	19.86599	1.616793
1.57	14.76256	0.812867	19.13038	0.658638

4.1.2. Single lap joint displacement and energy at failure

This section deals with the analysis related to the characteristic failure point for the load displacement curves analyzed in section 4.1.1. In particular two parameters: elongation and energy at failure are computed.

For sake of clarity, it should be remembered that the elongation reported in load-displacement curves, measured by means of the tensile machine as explained in section 3.4, does not consider the pure adhesive elongation. As a matter of fact, the measured elongation takes in account both the adherends and the adhesive. Moreover, the cross-heads displacement is actually measured and some slippage phenomena which can occur between the grips holding the specimens and the specimens itself are not taken in account.

Similar considerations apply for the computed energy at failure. In fact, in order to compute the energy absorbed during the deformation of the single lap joints the procedure adopted has considered as input parameter the elongation reported in the tensile machine tests.

In particular, a linear trapezoidal method was used in order to calculate the area under the load displacement according to

$$Energy = \int Load * Displacement \qquad \textbf{(4.1)}$$

In Figure 4-5 and Figure 4-6, the average displacement at failure for the 4 surface roughness values considered and the two stack thickness values tested are reported. By looking at the failure load graphs mentioned in section 4.1.1, it can been clearly noticed a close agreement between the experimental point locations of both average failure loads and average displacement at failure over the surface roughness. The similarity of the trends occurs for both the two adherend thickness considered. As an example, for 1.3mm aluminum, the highest average failure load (which occurs at Ra=1.57µm) is related to the highest average displacement value (which occurs again at Ra=1.57µm).

Moreover, it should be mentioned that a higher variability of the displacements with respect to the failure load values was detected as indicated from the larger standard deviations.

We must say that the increment of the stack thickness has a beneficial impact on the load at the adhesive yielding peak (failure load). On the other side, at final failure, the 2.1mm thick single lap joints showed a reduced elongation in average -54.1% with respect to the 1.3mm thick joints.

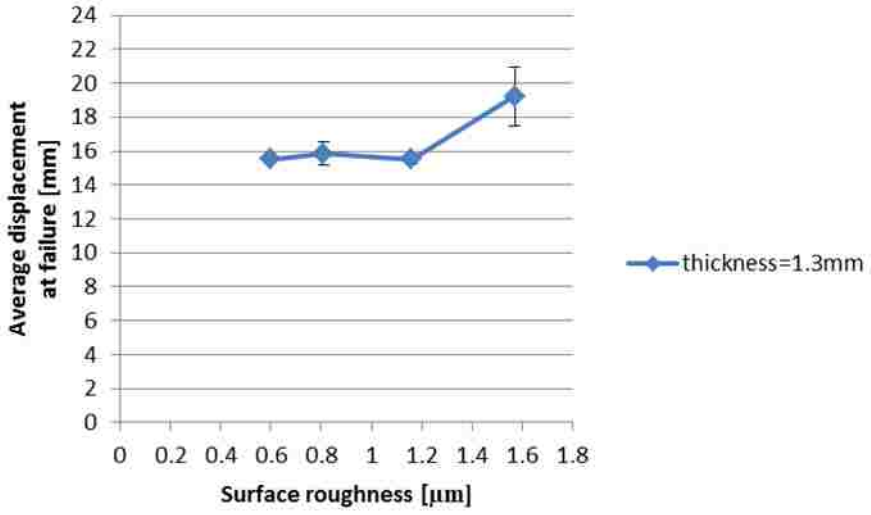

Figure 4-5: Average displacement at failure evolution over surface roughness for 1.3 mm adherend thickness

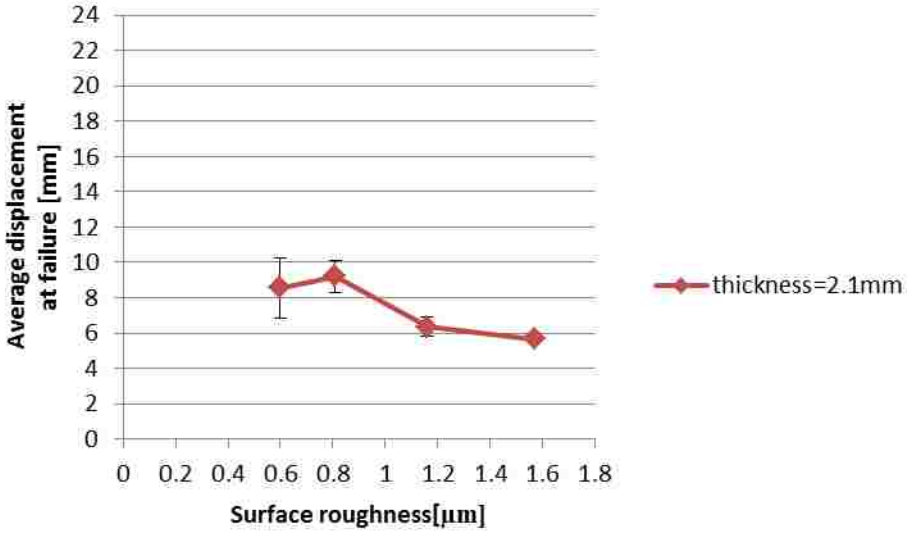

Figure 4-6: Average displacement at failure evolution over surface roughness for 2.1 mm adherend thickness

The energy absorbed during the deformation of the SLJ is illustrated as function of the surface roughness values for the two stack thickness values tested in Figure 4-7 and Figure 4-8. From the calculation of the energy accomplished with an EXCEL® spreadsheet the following conclusion can be drawn:

- The combined variability of failure load and displacement at failure lead to considerable differences between the samples energy computed values for each test condition.
- Although the thicker specimens have shown higher failure loads, the absorbed energy decreased in average of -43.96% with respect to the thinner specimens.
- It should be again pointed out that both elongation and energy at failure are substantially influenced by the severe adherends deformations which remarkably affect the lower joints stack thickness. On the other side, the analysis performed is a good estimate of the adhesive bonds performance.

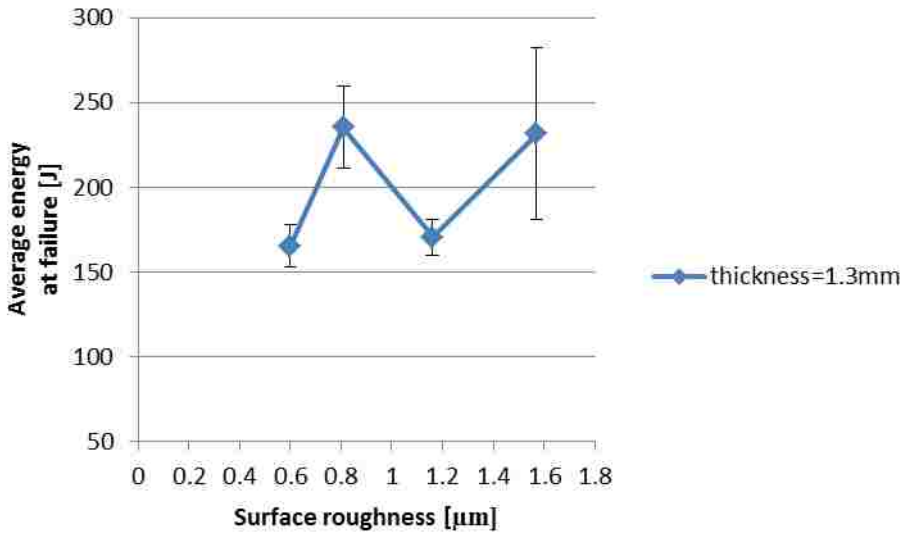

Figure 4-7: Average energy at failure evolution over surface roughness for 1.3 mm adherend thickness

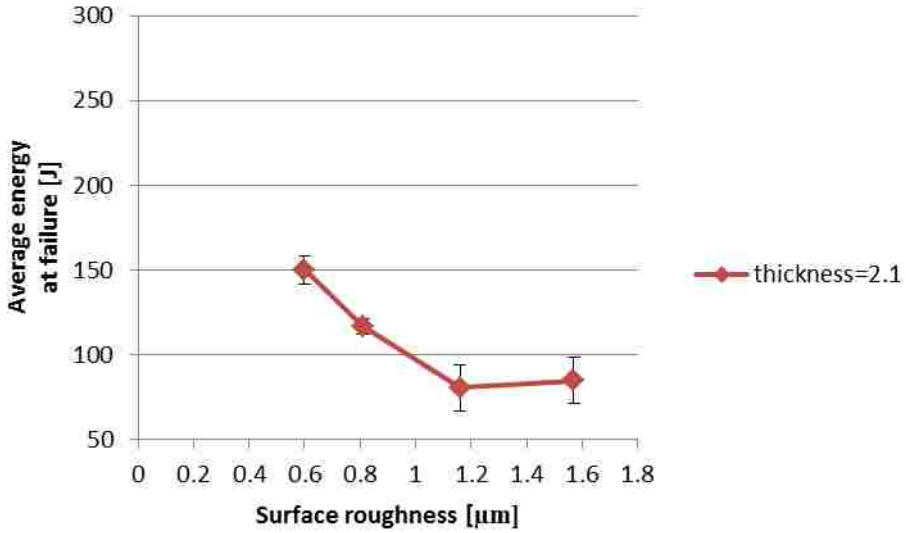

Figure 4-8: Average energy at failure evolution over surface roughness for 2.1 mm adherend thickness

For sake of clarity, the obtained average failure loads, average displacements and average energies at failure are reported for the four surface roughness values and the two stack thickness values considered in Table 19, Table 20 and Table 21. In addition, in the aforementioned tables, an indicator of the measurements variability for the three samples tested for each test condition is provided as the coefficient of variance (C.O.V). The latter has been obtained as the ratio between the average mean value and its corresponded standard deviation for each test condition.

Table 20: Average elongation at failure for the two joint stack thickness t_1, t_2 and for the four surface roughness values considered

Surface roughness [µm]	t_1=1.3mm		t_2=2.1 mm	
	Average disp. At failure [mm]	C.O.V[%]	Average Disp. At failure[mm]	C.O.V[%]
0.6	15.52664	1.305975	8.557129	40.05946
0.81	15.84048	8.689219	9.207324	19.98556
1.16	15.50063	3.481039	6.352661	17.59907
1.57	19.21965	17.95038	5.648828	2.230551

Table 21: Average energy at failure for the two joint stack thickness t_1, t_2 and for the four surface roughness values considered

Surface roughness [µm]	t_1=1.3mm		t_2=2.1 mm	
	Average en. At failure [mm]	C.O.V[%]	Average en At failure[mm]	C.O.V[%]
0.6	165.4048	15.24644	150.0626	11.27628
0.81	235.3805	20.44802	116.805	7.872479
1.16	170.6598	12.42256	80.60064	33.90973
1.57	231.5154	43.62617	84.66975	31.92367

4.2. Effect of adhesive thickness

In this section, the aim is to investigate the adhesive thickness which is another relevant geometrical factor regarding the structural adhesive joints service performance. Moreover, the adhesive thickness has a considerable impact on manufacturing production costs and storage issues considering the low adhesives shelf life values. According to literature, the effect of the adhesive thickness on the single lap bonded joints strength is controversial [48], therefore experimental investigation is a preferable tool for this kind of analysis.

In this section, the outcomes deriving from the design of experiments planned in Table 10 of section 3.1 are presented and discussed. The range of adhesive thickness tested was chosen to be below T_a=0.8mm. In fact, being the recommended adhesive manufacturer values in the range 0.6mm < T_a <1.8mm, the aforementioned test design

was planned in order to assess the possibility to select lower adhesive thickness values towards a production cost reduction taking in account lap shear bond joint strength requirements. As already explained in section 3.3, four values of adhesive thickness were realized by means of glass beads of different constant diameters mixed with the adhesive. A similar procedure to the one discussed in 4.1 was adopted to perform both the lap-shear tests and the subsequent data processing. Therefore, for each adhesive thickness value, the average failure load is computed from 3 tested samples and error bars are shown indicating the standard deviation of the 3 measurements. Figure 4-9 illustrates the evolution of average failure load [kN] over the adhesive thickness [mm].

The other manufacturing specimen parameters adopted are:

- Thickness adherend =1.3 mm
- Surface roughness = 0.81 µm

A similar plot was generated considering a thicker aluminum substrate stack. In fact, as can be seen in Figure 4-10, adhesive thickness values analyzed are the same of Figure 4-9. Surface roughness was kept equal to 0.81 µm while the adherend thickness tested was 2.1mm. Hence, the effect of both adhesive thickness and adherend thickness on the adhesion process is taken in account.

Summarizing, Figure 4-11 reports the effect of the both aforementioned factors on the single lap joint failure load.

4.2.1. Single lap joint failure load

As can be seen from both Figure 4-9 and Figure 4-10 , the two stack thickness considered reach the highest failure loads for T_a=0.25mm. Moreover, the increase of adhesive thickness beyond this point leads to considerable failure load reduction.

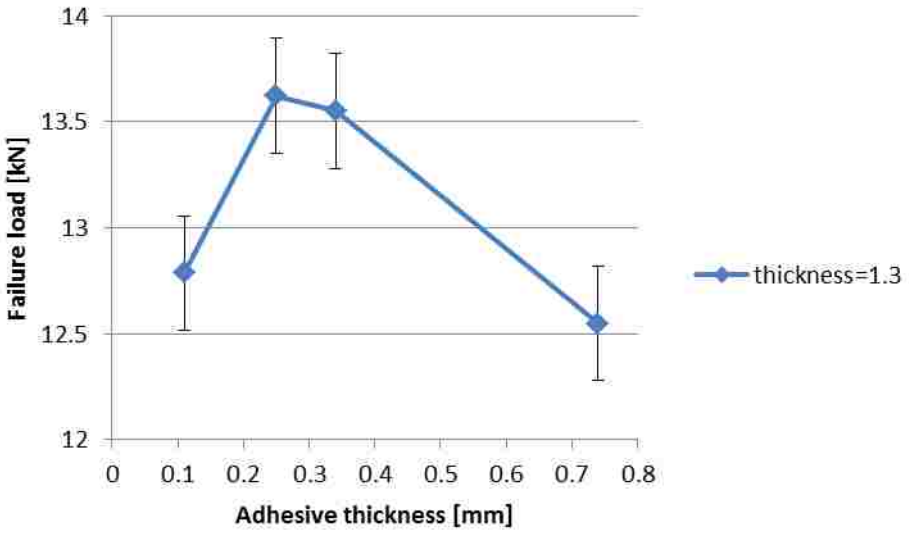

Figure 4-9: Average failure load evolution over adhesive thickness for 1.3 mm adherend thickness

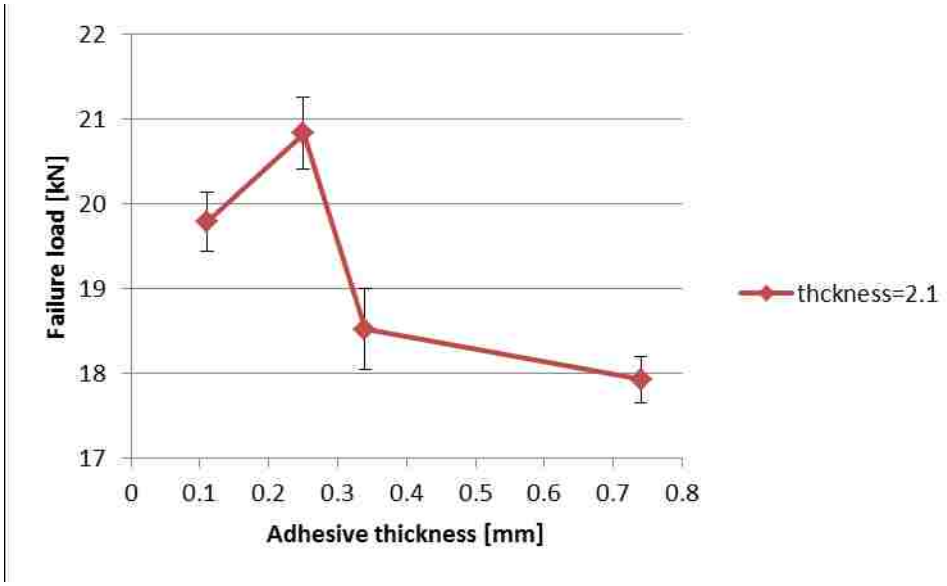

Figure 4-10: Average failure load evolution over adhesive thickness for 2.1 mm adherend thickness

Hence, in disagreement with the classic elastic theory which predicts increase of the strength with the adhesive thickness, the experiments showed an opposite trend.
This discrepancy between theory and experiments can be addressed by the following factors related to the thicker bondine:

- Higher probability of defects and microvoids existence

- Increase of interfacial stresses(both peel and shear stresses).Therefore, supposing failure close to the adhesive/adherend interface, high interfacial stresses lead to joint strength loss [48] [49].
- Rapid occurrence of adhesive plastic spreading along the overlap area
- Increase of the bending moment applied to the aluminum adherends as consequence of increase of eccentricity between the applied loads characteristic of the single lap joint geometry under tension as mentioned in section 2.3.2.

As far as adherend thickness in concerned, according to what pointed out in section 4.1.1, the effect is to increase the failure loads magnitude when thicker specimens are considered. In particular an average percentage increase of failure load of 48.46% was found. On the other side, the failure loads trend over adhesive thickness is not greatly influenced by the adherend thickness factor.

In Figure 4-11 a 3D diagram provides a better understanding of the combined effect of both adherend thickness and adhesive thickness on the average joint failure loads. In particular the best condition is achieved for adhesive thickness equal to 0.25mm and aluminum substrate thickness equal to 2.1mm.

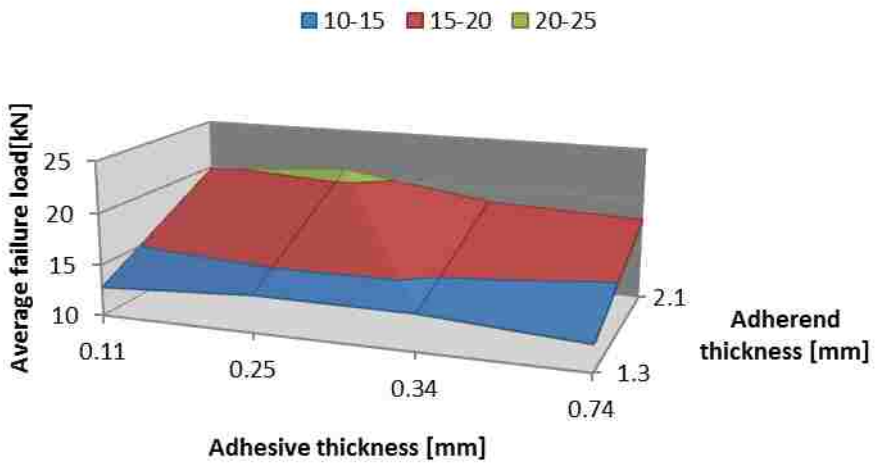

Figure 4-11: 3D plot of average failure load as function of both adherend thickness and adhesive thickness

Table 22: Average failure load for the two joint stack thickness t_1, t_2 and for the four adhesive thickness values considered

Adhesive thickness[mm]	t_1=1.3mm		$t_{2=}$2.1 mm	
	Average Failure load[kN]	C.O.V[%]	Average Failure load[KN]	C.O.V[%]
0.11	12.786	2.346316	19.78434	3.487607
0.25	13.6219	3.711351	20.82946	4.128767
0.34	13.55	4.870849	18.52213	5.182988
0.74	12.54786	2.028418	17.9253	1.741388

4.2.2. Single lap joint elongation and energy at failure

In Figure 4-12 and Figure 4-13 the average displacement at failure for the 4 adhesive thickness values considered and the two stack thickness tested are reported. As for the surface roughness effect, the achieved adhesive bonded joints elongation at failures follow fairly similarly the failure load trend over adhesive thickness mentioned in section 4.2.1. This happens for both the two adherends thickness (1.3mm and 2.1 mm). In particular, it can to be noticed a substantial high variability when considering the elongation at failure for Ta=0.74mm of the l.3 mm aluminum specimens.

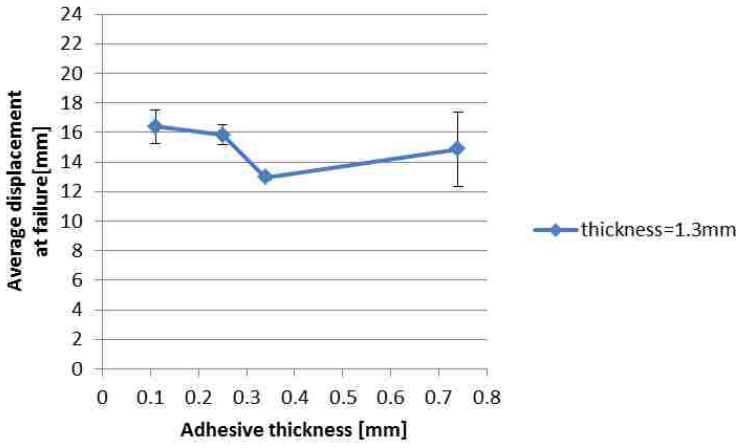

Figure 4-12: Average displacement at failure evolution over adhesive thickness for 1.3 mm adherend thickness

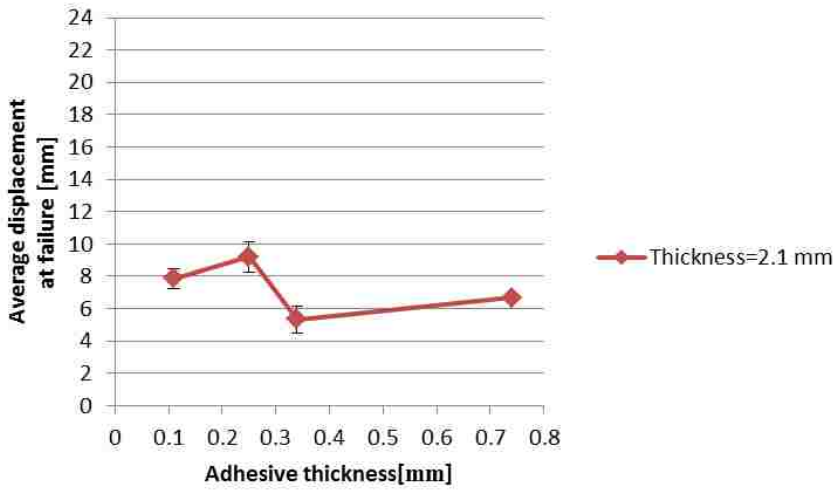

Figure 4-13: Average displacement at failure evolution over adhesive thickness for 2.1 mm adherend thickness

The energy absorbed during the deformation of the SLJ is illustrated as function of the adhesive thickness values for the two stack thickness tested in Figure 4-14 and Figure 4-15. As far as the adherend thickness is concerned, the experiments revealed that thinner specimens undergo larger deformation and energy absorption at failure with respect to the thicker ones. As a matter of fact, the computed average percentage increase for the aforementioned parameters between the two stack thickness joints are respectively 111.6% and 99.66%.

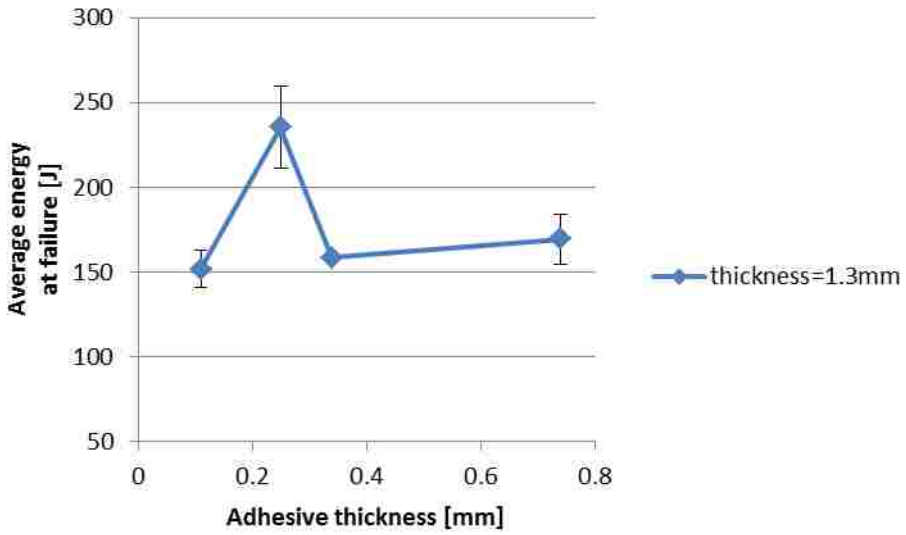

Figure 4-14: Average energy at failure evolution over surface roughness for 1.3 mm adherend thickness

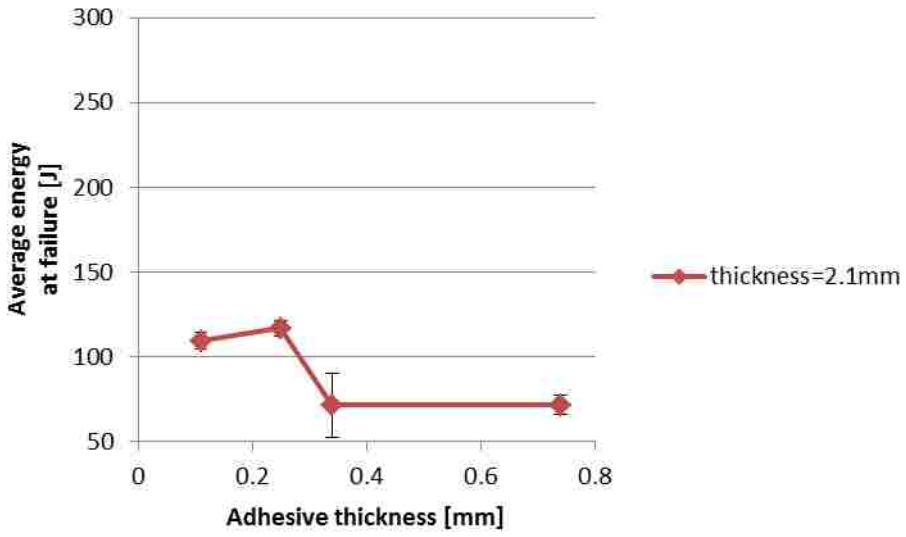

Figure 4-15: Average energy at failure evolution over surface roughness for 2.1 mm adherend thickness

For sake of clarity, the obtained average failure loads, average displacements and average energies at failure are reported for the four adhesive thickness and the two stack thickness values considered in Table 22, Table 23, and Table 24. In addition, in the aforementioned tables, an indicator of the measurements variability for the three samples tested for each test condition is provided as the coefficient of variance (C.O.V).

Table 23: Average elongation at failure for the two joint stack thickness t_1, t_2 and for the four adhesive thickness values considered

Adhesive thickness[mm]	t_1=1.3mm		t_2=2.1 mm	
	Average displ. at failure[mm]	C.O.V[%]	Average displ. at failure[mm]	C.O.V[%]
0.11	16.39653	13.73946	7.85918	15.51717
0.25	15.84048	8.689219	9.207324	19.98556
0.34	12.97319	2.659331	5.324024	31.70316
0.74	14.87728	33.80573	6.69585	5.164273

Table 24: Average energy at failure for the two joint stack thickness t_1, t_2 and for the four adhesive thickness values considered

Adhesive thickness[mm]	t_1=1.3mm		$t_{2=}$2.1 mm	
	Average en. at failure[J]	C.O.V[%]	Average en. at failure[J]	C.O.V[%]
0.11	151.7984	14.3086	109.2596	8.746528
0.25	235.3805	20.44802	116.805	7.872479
0.34	158.4208	2.177571	71.6168	52.77811
0.74	169.3012	17.43649	71.4418	15.93412

4.3. Effect of test speed and temperature

This section is dedicated to the results obtained from the lap shear tensile tests performed at both different temperatures and test speeds as planned in Table 12 of section 3.1. It should be mentioned that the structural adhesive joints involved in the automotive industry have to withstand large variation in temperature and strain rate. In fact, as far as automotive applications are concerned, the temperature typically ranges between -40ºC to 50ºC. In this project, due to the equipment availability only temperature conditions above room temperature have been tested.

Furthermore, considering the impact of both test speed and temperature on the visco-elastic behavior of the polymer-based adhesive, the two aforementioned factors were combined. In Figure 4-16, we can clearly see that, for both the two considered test speeds, the failure load decreases with the increase of temperature. In particular, when considering test speed equal to 5mm/min, the average failure load decrease from room temperature (RT) up to temperature equal to 50ºC was -5.66%. Similarly, when considering test speed equal to 0.1 mm/min, the average failure load decrease was -3.40%. On the other side, for each test temperature, the failure load decreases with the decrease of test speed. In particular, averaging for all the temperature values considered, the average failure load decrease with the variation of test speed from 5 mm/min to 0.1 mm/min was -7.35%.

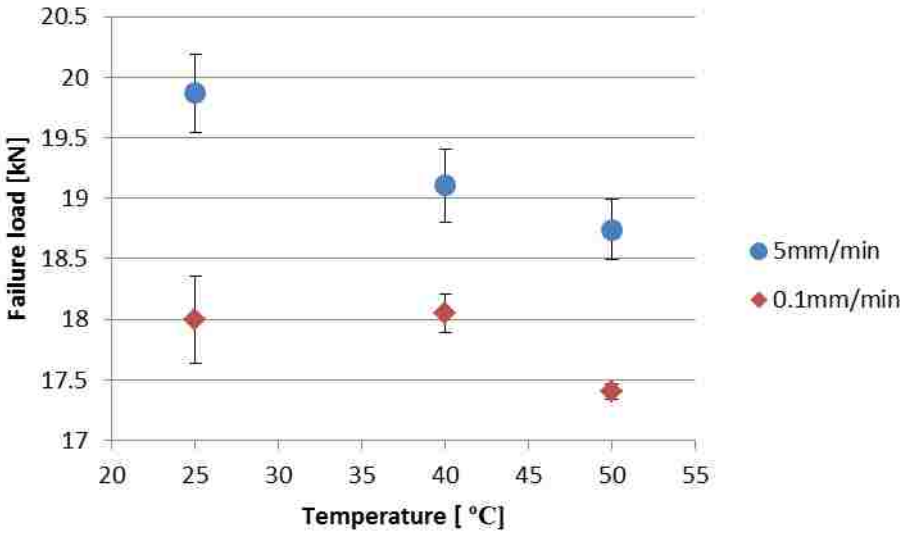

Figure 4-16: Average failure load evolution over temperature(T= RT, 40°C, 50°C) and test speed, the adhesive thickness is Ta=0.25mm, and the surface roughness obtained by manual abrasion through 120 mesh sandpaper.

An explanation of the obtained results can be found by looking on the right of Figure 4-17. The graph shows that, with the increase of temperature, two factors determine the final lap shear strength of the joints:

- the adhesive softens increasing its ductility which allows a better stress distribution along the overlap area
- the adhesive bulk strength decreases

Combining these two factors, the loss of strength in the adhesive single lap joints with the temperature is less remarkable with respect to the loss of the bulk adhesive tensile strength [50] [51]. Moreover, as can be seen in Figure 4-17 (on the left) the increase of temperature beyond a value called Tg (glass transition temperature) lead to substantial changes in the adhesive coefficient of thermal expansion(CTE) and joint strength [52]. Therefore, in order to have reliable structural adhesive joint within their operating environment, is important that the specific Tg of each adhesive is not exceeded. As far as the DowBetamate1620US one-component heat-cured epoxy is concerned, it should be mentioned that the information about its Tg was not provided by the adhesive manufacturer. On the other side according to literature, similar epoxies, as the one considered in this project, feature Tg values in the range of 60°C-

90ºC.This results to be reasonable since, as already mentioned, from the tests conducted up to 50 ºC no substantial losses in lap shear strength were found.

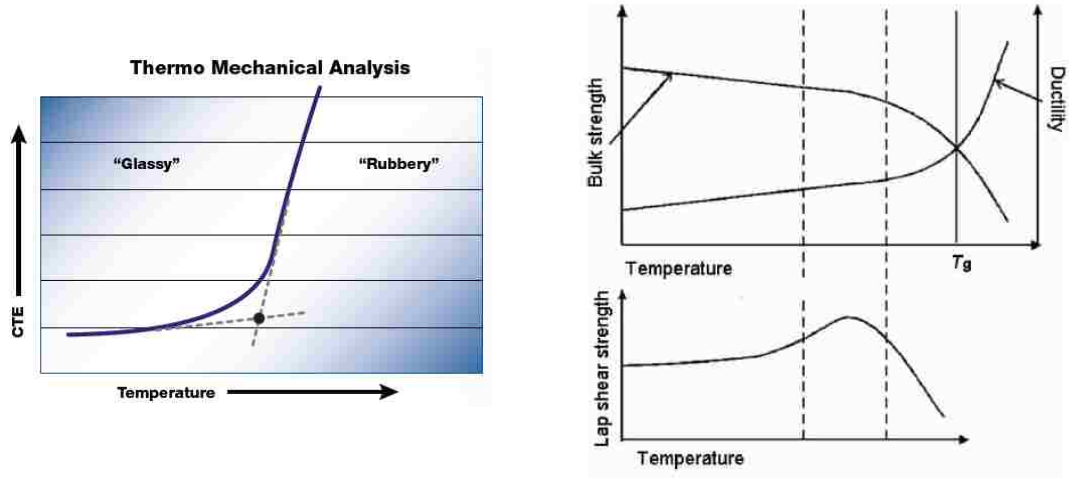

Figure 4-17: CTE evolution over temperature for an epoxy adhesive (left) ; Lap shear strength behavior as function of ductility and bulk strength (right) [51] [52]

Finally, again considering the Figure 4-17 on the bottom right, in this project the highest value of failure load was established for the room temperature test (T=25 ºC). Therefore, we can say that the room temperature is the one providing the best combination of strength-ductility for the adhesive considered. Again, further investigation at temperatures lower than RT, could be give a better understanding of the lap shear bond strength behavior as function of temperature.

Figure 4-18 shows the failure load evolution over the test speeds which in turns is related to the strain-rate. A wide range of test speeds was selected in order to construct a graph able to predict the lap shear strength failure load variation with the test speed. In fact, according to Figure 4-18, by means of a data compiler the following trend equation was found to be the best fit for the experimental data:

$$F_s = Ae^{B\,x} \qquad \textbf{(4.2)}$$

Where A= 18.69, and B=0.0024. It should be noticed that the horizontal coordinate of the graph is in logarithmic scale. The test parameters adopted have been stated in section 3.1. Therefore, the trend found is valid for a specific combination of surface roughness, adhesive thickness, test temperature and adherend thickness. Similar curves can be plotted by testing different combinations of the aforementioned

variables. Similarly to what seen in Figure 4-16, the joint failure load increases with the test speed. This trend has to refer to the viscoelastic adhesive behavior. In fact, on the other side, at low speeds and therefore high loading times considerable creep deformation of the epoxy is developed which decreases the joint failure load.

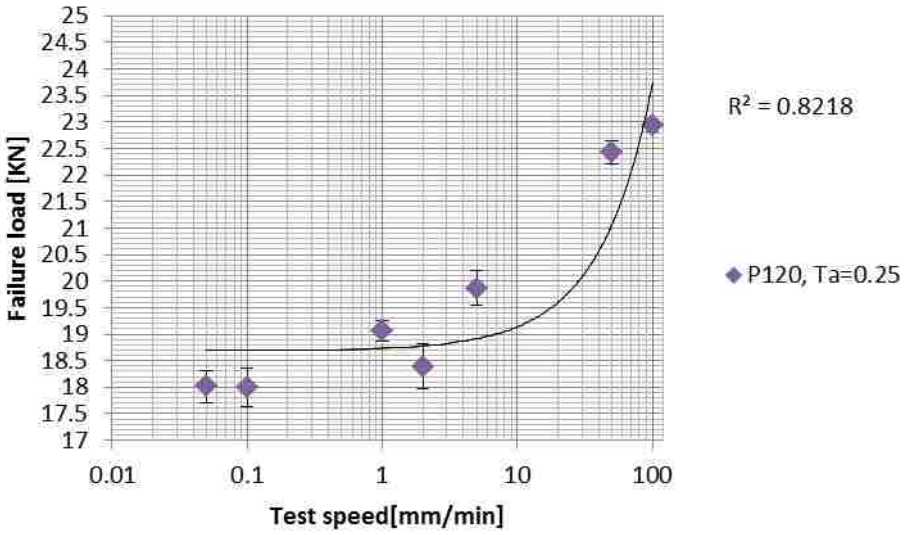

Figure 4-18: Average failure load evolution over test speed (v= 0.05mm/min, 0.1mm/min , 1mm/min, 2mm/min, 5mm/min, 50mm/min, 100mm/min), the adhesive thickness Ta is 0.25mm and the surface roguhness obtained by manual abrasion through 120 mesh sandpaper

4.4. Failure mode analysis

This section deals with the failure mode analysis carried out in order to investigate the previous results obtained from the tensile tests and understand what kind of fracture occurred. For sake of clarity, the procedure adopted to analyze the fractured surfaces in terms of percentage of cohesive/adhesive failure will be described in the following. As an example, the description is given for just one batch of samples treated with manual abrasion using the 60 mesh sandpapers. Nevertheless, the fracture analysis procedures for all the specimens tested are not reported since they are redundant.

In particular, the failure mode analysis was carried out for the following investigated factors:

- Effect of surface roughness and adherend thickness
- Effect of temperature and test speed

Adhesive thickness was not investigated by failure mode analysis but kept equal to 0.25mm for the following cases.

According to Figure 4-19 a) the joint failure mode can be defined neither pure cohesive failure, inside the adhesive, nor apparent adhesive failure at the adhesive/adherend interface.

In fact, all tested joint specimens mainly failed in a mixed interfacial/cohesive failure in the adhesive. Therefore, in order to assess the mixed-mode state of failure, the areas indicated by arrows in Figure 4-19 were examined with stereoscopic microscope under 40X magnification.

The two arrows indicate respectively a portion of the overlap area close to the glue , left on the adherend (red arrow), and another region close to the substrate material (blue arrow). It should be noticed that the area indicated by the red arrow visually shows high percentage of cohesive failure with respect to the area indicated by the blue arrow.

As a consequence, in order to have a uniform estimate for the total area considered, 3 stereoscopic images were captured for each of the two aforementioned regions.

Then, the percentages of cohesive and adhesive failures were computed and averaged within the tree images. Finally, the obtained outcomes derived from two areas were averaged again.

Figure 4-19 b) shows the images captured from the stereoscopic microscope that were first converted to grey-scale, using the image analysis software ImageTool. Then, manually tresholding was used in order to separate the two colors. Finally the conversion to binary image shown in Figure 4-19 c) provides an easy distinction, within a certain error, between the cohesive failure area (identified with the white color) and the adhesive failure area (identified with the black color).

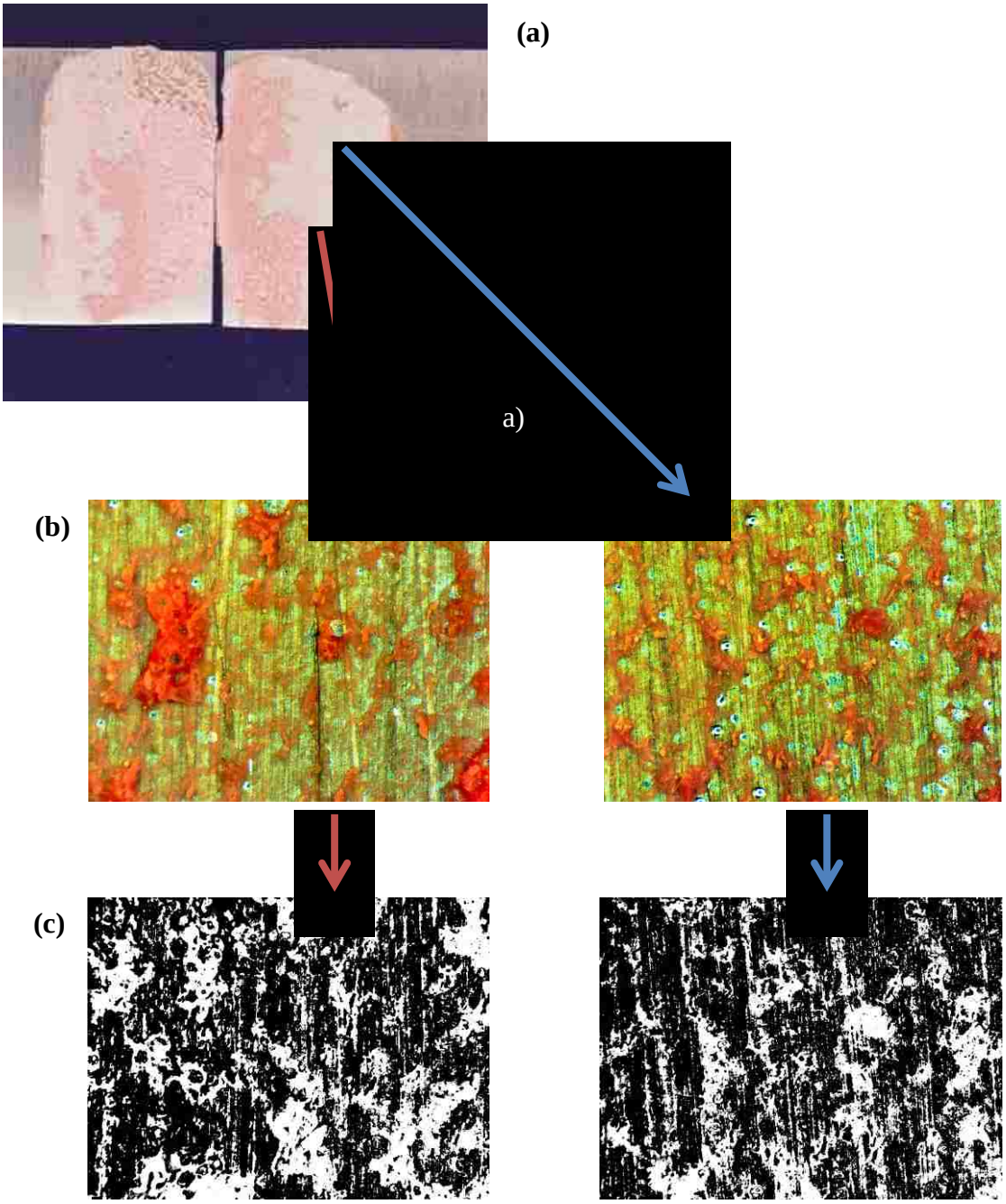

Figure 4-19: Procedure adopted to compute the percentage of adhesive/cohesive failure in the mixed mode failure region of the fracture, a) refers to the fractured specimens treated with p60 mesh sandpaper, b) refers to microscopic images captured in a region close to glue (red arrow) and close to metal (blue arrow), c) refers to the binary images obtained through the software imageTool

4.4.1. Effect of surface roughness and adherend thickness

The first control factor considered in the failure mode analysis is the failure load over the surface roughness. With regards to 1.3 mm aluminum alloy adherends, the failure modes of the specimens were just evaluated visually.

Figure 4-20 a), b), c) clearly show that for the substrate materials, treated with higher mesh sandpapers sizes (p120, p240, p320) ,the facing surfaces fractured in a slanting direction-obliquely. Thus, it is in agreement with the average failure loads for the 3 different surface roughness values considered that, as mentioned in section 4.1.1, revealed similar values. The shown kind of fracture can be addressed by the severe rotations of the 1.3 mm alloy adherends specimens which resemble the shape of the fractured surface. Nevertheless, the substrate with the highest roughness (R_a=1.57μm) results to fail in a different way as shown in Figure 4-20 d). In the latter case, the failure seems to be highly cohesive. Therefore, a seen in 4.1.1, for R_a=1.57μm a beneficial impact of the surface roughness on the failure load has been provided. For sake of clarity, it should be noticed that more pink regions in the fractured specimens overlap areas are related to substantial delamination of the glue on the adherends which shown low adhesion properties.

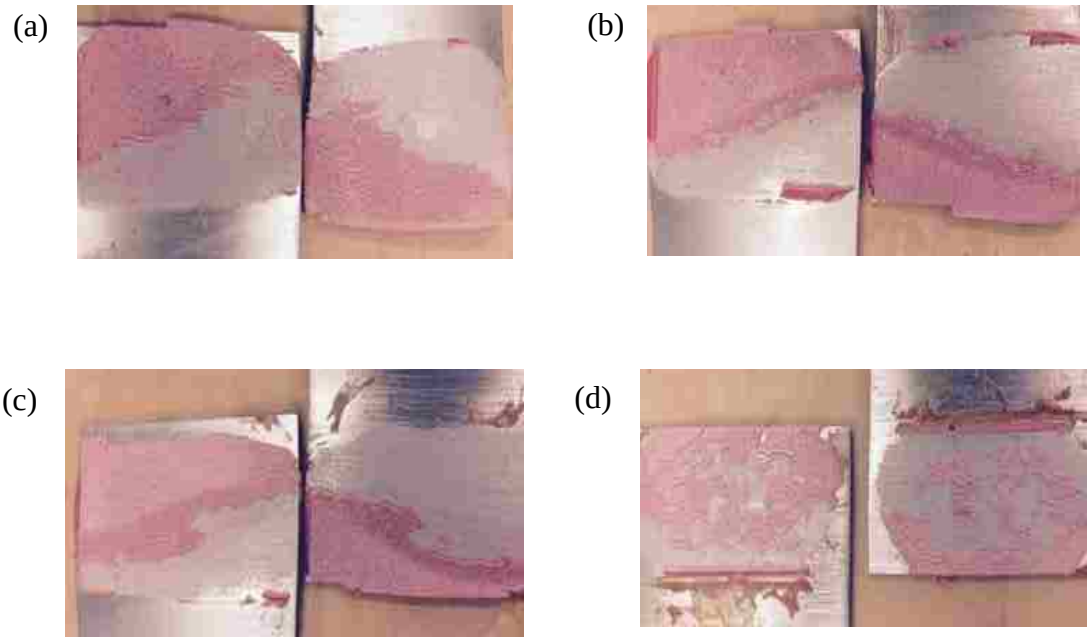

Figure 4-20: Fractured specimen for 1.3mm adherend thickness treated with manual abrasion with mesh different mesh sandpapers sizes, respectively: a) p320, b) p240, c) p120, d) p60

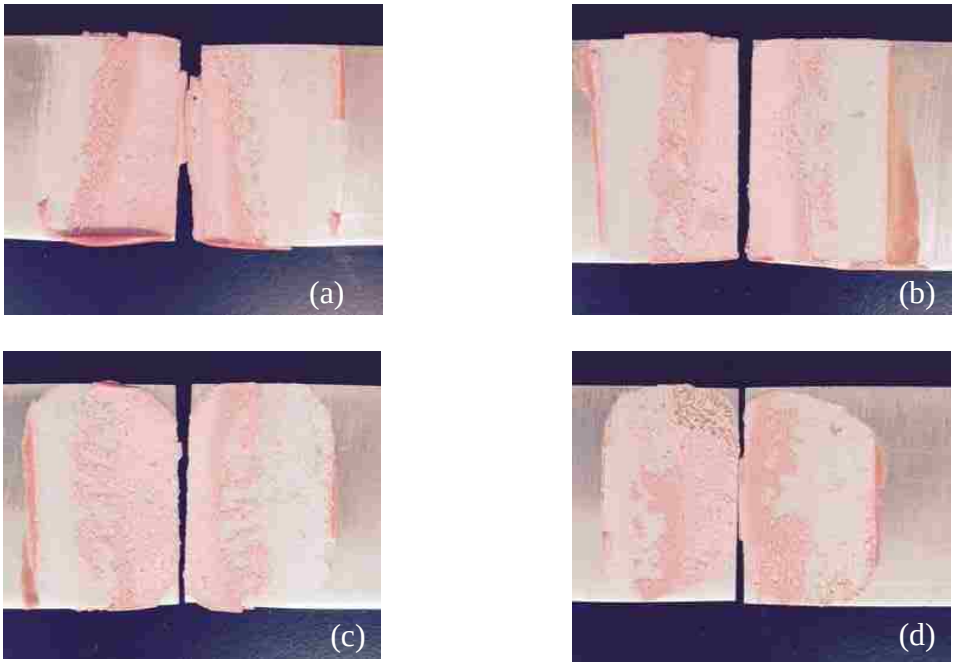

Figure 4-21: Fractured specimen for 2.1 mm adherend thickness treated with manual abrasion with mesh different mesh sandpapers sizes, respectively: a) p320, b) p240, c) p120, d) p60

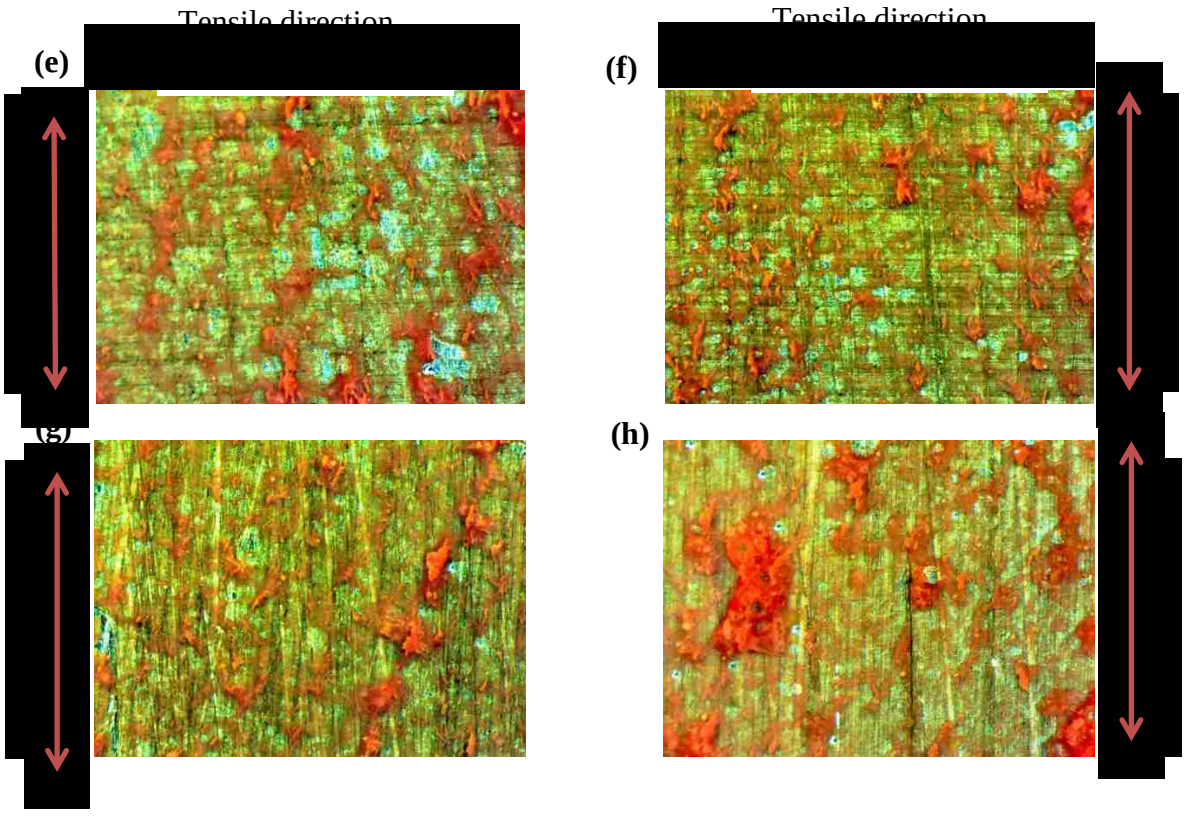

Figure 4-22: As an illustration of the procedure adopted to compute the percentage of adhesive/cohesive failure, images (e), (f), (g) and (h) derive from the regions close to the glue of images (a),(b),(c) and(d). The tensile direction of the load applied to the aluminum adherends and their grinding direction is also reported

Figure 4-21 illustrates the fractured specimens with regards to 2.1 mm adherends, while their relative captured microscope images are reported in Figure 4-22.

It can be shown, from the above figures, that the specimens fractured in a direction perpendicular to the tensile load applied to the aluminum alloys adherends. Therefore, despite of what depicted in Figure 4-20, the effect of the peel stresses on the overlap edges is less remarkable. In fact, for the thicker specimens, the failures mainly initiate at the center of the overlap area where, as explained in section 2.3.2, the shear stresses are predominant. For sake of clarity, as far as the stereoscopic images shown in Figure 4-22 are concerned, both the direction of manual grinding and tensile loading of the aluminum adherends are highlighted. The same reference directions, albeit not reported, apply for the stereoscopic images of Figure 4-26 and Figure 4-24.

Finally, according to the procedure described for Figure 4-19, the percentage of cohesive/adhesives failure loads related to thicker specimens at different roughness values are reported in Table 25. It should be mentioned that being the results coming out from this procedure an estimate, the values of standard deviations are not reported.

Thus, in comparison with the failure loads trend illustrated in Figure 4-3 , it can be noticed that the highest failure loads are obtained when considering R_a=0.8, R_a=0.6 which revealed the highest estimated percentage of cohesive failures.

We can conclude that high percentages of cohesive failure, for this test condition, are related to a good adhesion process.

Table 25: Estimate of percentages of adhesive/cohesive failure mode regarding the mixed mode failure region of the fractured specimens for different surface roguhness.

Adherend thickness=2.1mm	Mixed failure mode	
Surface roughness [µm]	% cohesive failure	% adhesive failure
0.6	~ 53	~ 47
0.81	~ 64	~ 36
1.16	~ 55	~ 45
1.57	~ 56	~ 44

4.4.2. Effect of test speed and temperature

This section refer to the failure mode analysis conducted in order to have a better understanding of the tensile tests outcomes shown in section 4.3.

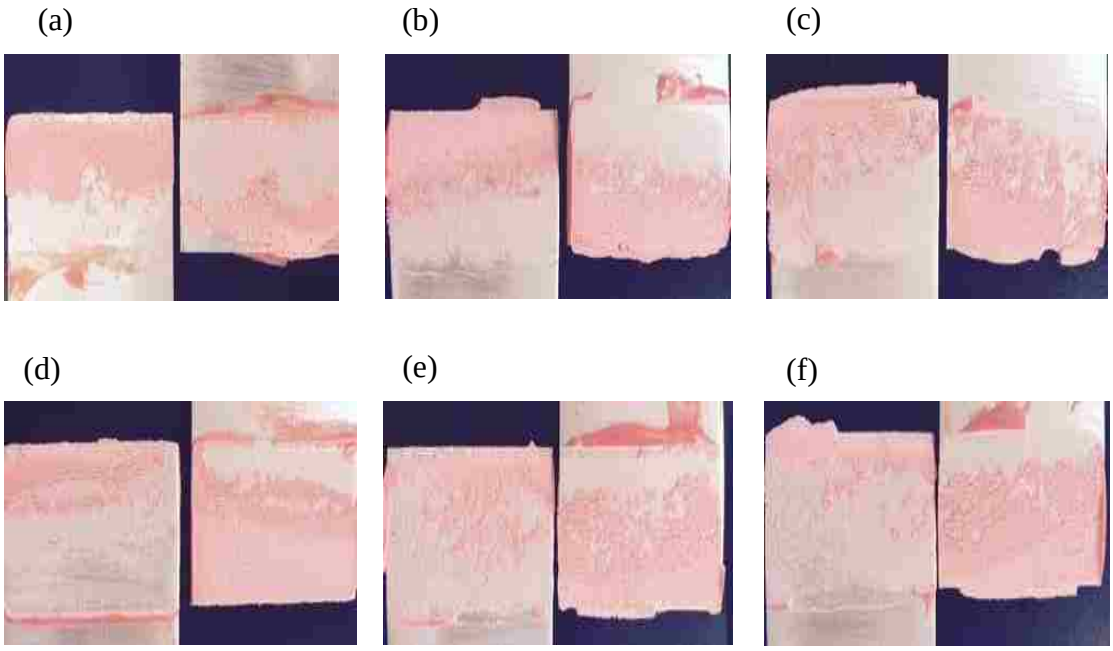

Figure 4-23: Fractured specimen for 2.1mm adherend thicknes, Ta=0.25mm surface roughness by p240 sand paper for different test speed and temperature; a) T=25°C, v= 5mm/min, b) T=40°C, v= 5mm/min, c) T=50°C ,v=5mm/min, d) T=25°C, v=0.1mm/min, e) T=40°C, v=0.1mm/min, f) T=50°C, v=0.1mm/min

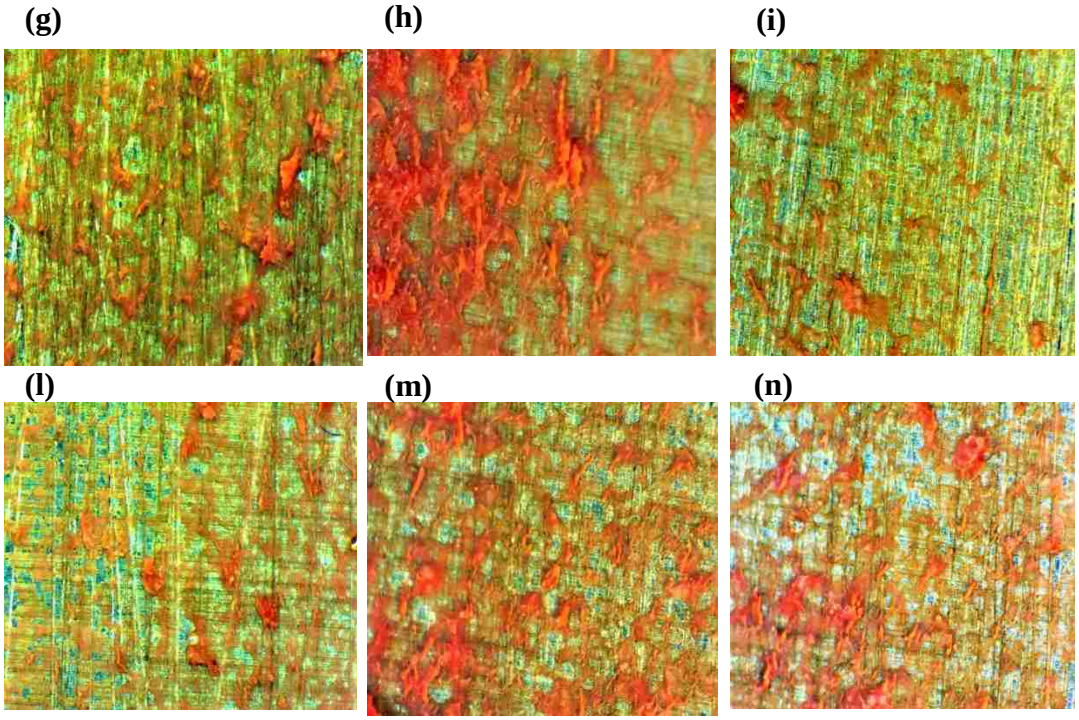

Figure 4-24: Stereoscopic images (g), (h), (i),(l),(m)and (n) derive from the regions close to the glue of images (a),(b),(c),(d),(e)and(f). Tensile and grinding direction though not reported refer to same of Figure 4-22

With regards to combined effect temperature-test speed, Figure 4-23 shows the fractured specimens analyzed. Furthermore, their relative captured microscope images are reported in Figure 4-24.
As can be noticed from the figures above, for both the two test speeds, by increasing the temperature (going from left to right) the following factors can be highlighted:

- The specimen fractured surfaces become rougher; this is an indicator of considerable adhesive deformation which is a sign of increasing glue ductility.
- Increase of cohesive percentage of failure; in fact, the adhesion of the glue to the surface remains still good whereas a lowering of the adhesive strength has occurred. Failure initiates from the shear of the glue itself.

According to the procedure described for Figure 4-19, the percentage of cohesive/adhesives failure loads related to thicker specimens for different combinations of temperature and test speed values are reported in Table 26.

Table 26: Estimate of percentages of adhesive/cohesive failure mode regarding the mixed mode failure region of the fractured specimens for different temperatures and test speeds.

Adherend thickness=2.1mm		Mixed mode failure	
Temperature [ºC]	Test speed [mm/min]	% cohesive failure	% adhesive failure
25	5	~57	~43
40	5	~69	~31
50	5	~67	~33
25	0.1	~49	~51
40	0.1	~55	~45
50	0.1	~62	~38

The last failure mode analysis refers to the tests realized at different test speeds. Figure 4-25 shows the fractured specimens surfaces, while their relative captured microscope images are reported in Figure 4-26. It should be mentioned that the analysis after the rupture of the joints was carried out not for all tests speeds analyzed in 4.3. In fact considering similar failure loads obtained between the following pairs of test speeds: 0.05mm/ min-0.1mm/ min, 1mm /min-2mm/min and 50mm/min-100

mm/min; only the latter test speed of each pair has been considered for this further analysis.

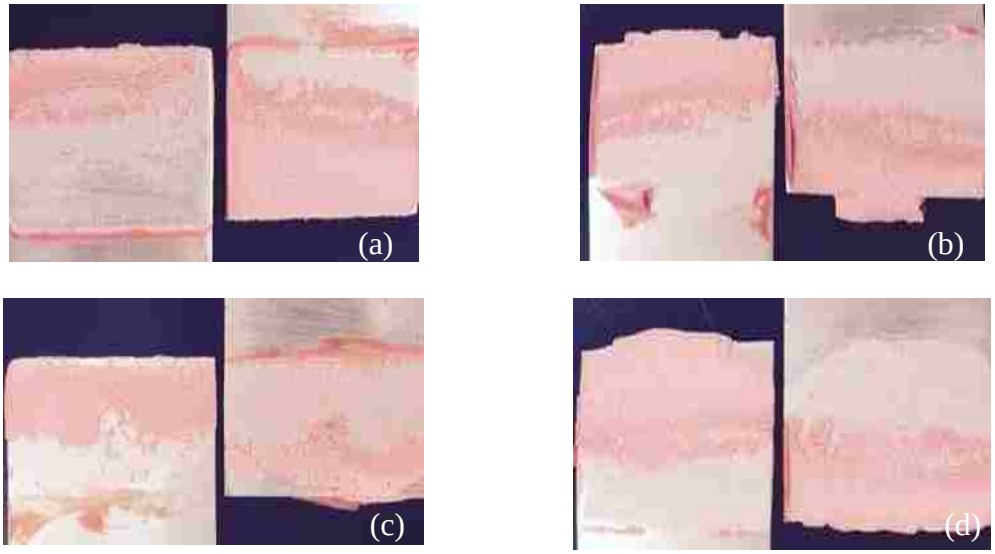

Figure 4-25: Fractured specimen for 2.1mm adherend thicknes, adhesive thickness=0.25mm, surface roughness obtained though p240 sand paper for different test speed values; (a) v=0.1 mm/min b) v=2mm/min c) v=5mm/min d) v=100mm/min

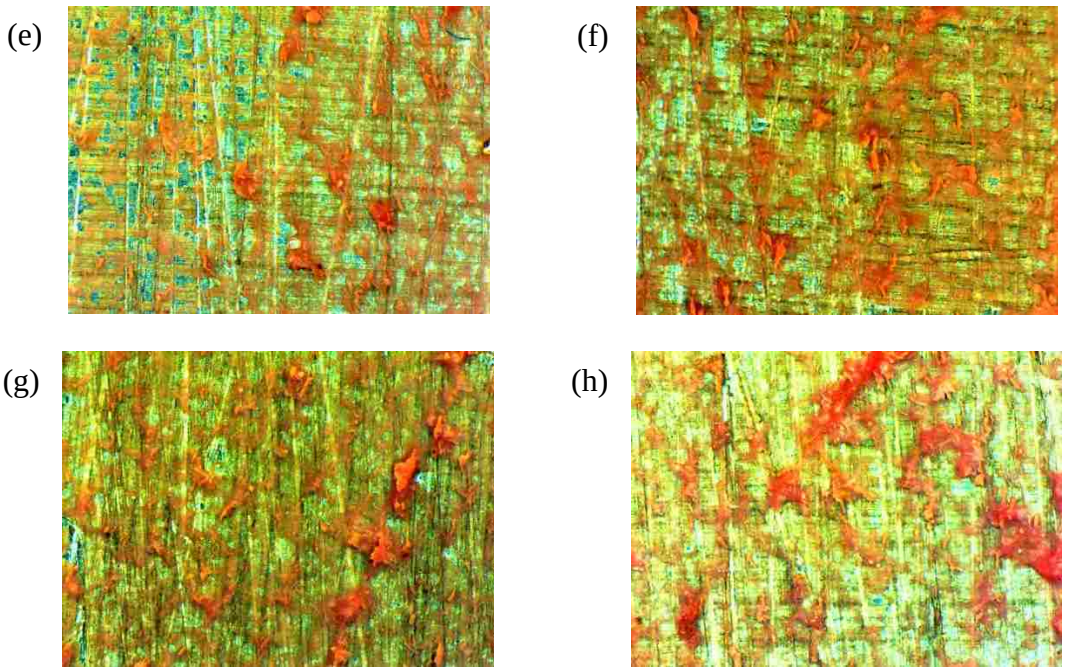

Figure 4-26: Stereoscopic images (e), (f), (g) and (h) derive from the regions close to the glue of images (a),(b),(c) and (d); tensile and grinding direction though not reported refer to same of Figure 4-22

From the qualitative observation of the fractured surfaces and from the computation made to define the percentage of cohesive/adhesive failure, the following conclusions can be drawn:

- At lower speeds, the decrease of failure load stated in 4.3, can be explained with the increase of apparent adhesive failure mode. This is indicated by the fact that, as shown by the microscopic images related to low-speed tests (Figure 4-26 (e)), the surface scratches from sandpapers treatment (grinding direction) result evident.
- Furthermore, again at low speeds, the glue has enough time for develop its creep deformation. Then, it produce a sliding of the fractured surfaces one against each other as can be seen from the scratches along the tensile directions (Figure 4-26 (e)).
- At high speeds, instead, the lower adhesive creep deformation allows less mismatch at interface between the adherends and the glue.

Finally, the percentage of cohesive/adhesives failure loads related to thicker specimens for different combinations test speed values are reported in Table 27.

Table 27: Estimate of percentages of adhesive/cohesive failure mode regarding the mixed mode failure region of the fractured specimens for different test speed.

Adherend thickness=2.1mm	Mixed mode failure	
Test speed [mm/min]	% cohesive failure	% adhesive failure
0.1	~37	~63
2	~44	~56
5	~48	~52
100	~46	~54

5. CONCLUSIONS AND RECOMMENDATIONS

5.1.Conclusions

This thesis investigated the static strength of aluminum alloy adhesively bonded structural joints.

The epoxy based adhesive used for the research is a structural adhesive used for bonding in vehicle body structures. In particular, it is usually applied as a swirl bead or a streaming bead to seal sandwiched metals construction with regards to hem flanges for closures. An experimental campaign was carried out in order to assess the influence of geometrical and test condition factors on the strength of the single lap bonded joints, with the aim of optimizing shear strength for the test variable values selected.

In particular, the factors analyzed are:

- Aluminum adherends surface roughness
- Aluminum adherends thickness
- Adhesive thickness
- Test speed and temperature

A failure mode analysis was eventually conducted in order to either verify or discover the nature of the fracture. From the results of the tensile tests and failure mode analysis the following conclusions can be drawn:

1. Surface preparation affects the lap shear strength. In particular, for 2.1mm adherend thickness, a critical value of surface roughness was found to be equal to 0.81μm. With regards to 1.3 mm adherend thickness, due to severe rotations of the specimens during testing, no meaningful results in terms of shear strength can be stated within the surface roughness values considered. On the other side, the test revealed that the highest lap bonded strength is obtained for surface roughness equal to 1.57 μm. The failure mode analysis revealed an increase of percentage of cohesive failure for the fractured surfaces treated by means of the 60 grit size sand paper. It shows that the adhesion between adherends and the glue is improved thanks to benefits provided by the surface roughness. In fact, higher percentage of cohesive failure means lower number of cracks initiation at the interface adherends/adhesive.

2. Increase of adherend thickness from 1.3 to 2.1mm was found to increase the joint lap shear strength. In fact, with increase of stack thickness both peel and shear stress concentration at the ends of the overlap area are reduced.

   Conversely, the increase of adherend thickness negatively affects the energy absorption. Instead, for 1.3 mm adherends thickness, higher plastic deformations of the plates promoted high energy absorption.

   These results were proved for both the tests concerning the surface roughness and adhesive thickness influence on the lap shear strength.
3. The lap shear strength attains the highest value for adhesive thickness equal to 0.25mm. Beyond this value, the lap shear strength decreases with the increase of the adhesive thickness.
4. The lap shear strength was found to be highly test speed dependent. In particular, the lap bonded joint failure load increases exponentially with the test speed. An exponential trend and specific equation coefficients are obtained by considering specific values for the other influencing variables.

   The fractured surfaces show an increase of percentage of adhesion failure for the test conducted at lower test speed. In fact, the considerable creep deformation developed by the glue in this case, produces substantial mismatch at the adherends/adhesive interface.
5. With regards to the tests conducted at different temperatures (25ºC (RT), 40ºC, 50ºC), the lap shear failure load decreases with the increase of temperature. Therefore, The RT was found to be the best compromise between ductility and adhesive bulk strength requirements. The decrease of bonded joint strength with the increase of temperature is explained with the increase of cohesive percentage of failure. In fact, due to the adhesive strength worsening, failure initiate mainly from the shear of the glue itself.
6. The test conducted at different temperatures (25ºC (RT), 40ºC, 50ºC) and strain rates (0.1mm/min, 5mm/min) revealed that the bonded joint failure load increases when it is subjected to either high test speeds or lower temperatures. Moreover, at low temperatures, the failure load is subjected to high test speed sensitivity.

5.2. Recommendations

Considering the results obtained, further tests in a wide range of surface roughness and test temperatures (temperatures lower than zero) are suggested.

The work conducted in this project refers to static loading conditions. Therefore, a fatigue analysis of adhesive bonded joints and a study of its dependence upon factors such as surface preparation and joint geometry would be beneficial. Moreover, looking towards a multi-material design environment, testing of materials such as composites or mixing steels and aluminum adherends with carbon fibre reinforced plastics CFRp is suggested. Then, the acquired experimental results could be valuable tool for a subsequent FEM analysis and adhesive bonding model validation.

With regards to the failure mode analysis, in order to study the micrography of the fractured specimens, a SEM analysis is recommended.

Finally, other further interesting tests could be the peel and impact tests to verify the properties of adhesive bonds for crashworthiness applications.

6. APPENDIX A

6.1. Load vs .displacement curves

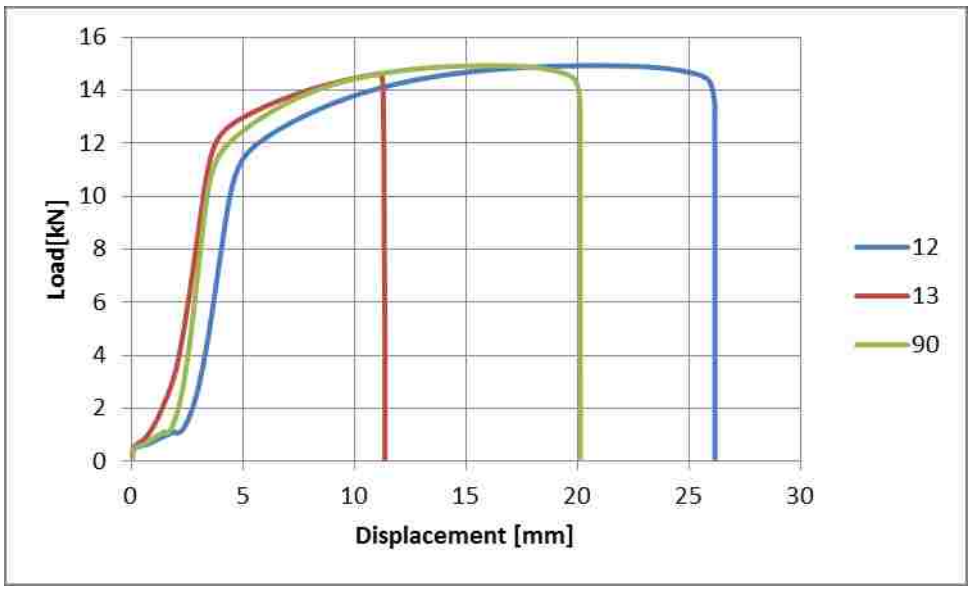

Figure 6-1: Load-displacement curves for 1.3 mm adherend thickness single lap-joint, 0.25 mm adhesive thickness and surface roughness obtained by manual abrasion with mesh p60 sandpaper size, test speed v=5 mm/min

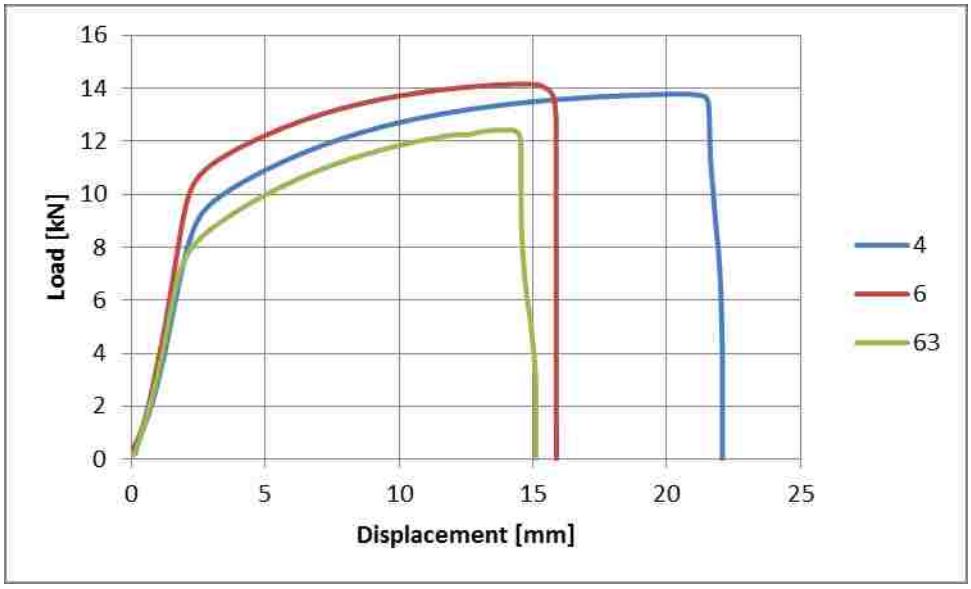

Figure 6-2: Load-Displacement curves for 1.3 mm adherend thickness single lap-joint, 0.25 mm adhesive thickness and surface roughness obtained by manual abrasion with mesh p120 sandpaper size, test speed v=5 mm/min

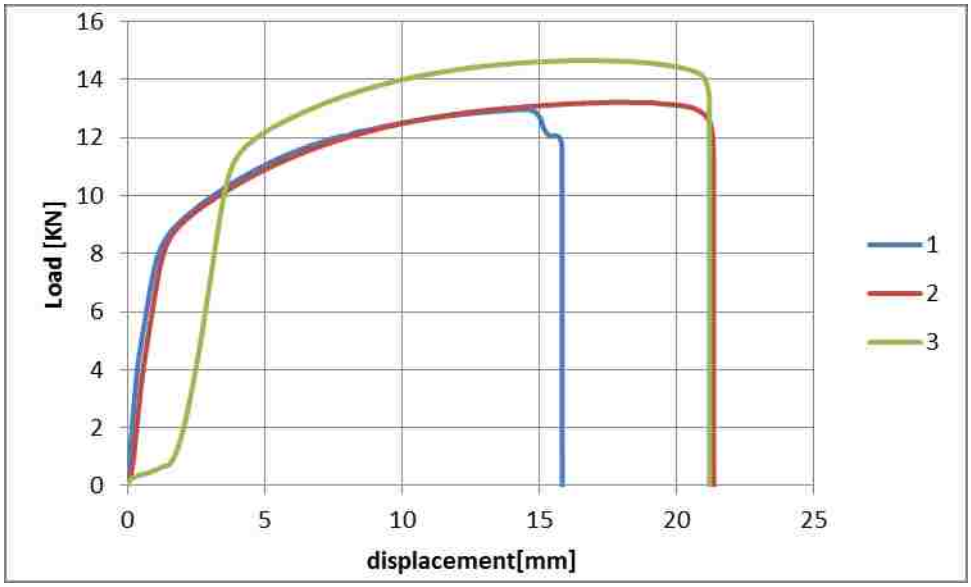

Figure 6-3: Load-displacement curves for 1.3 mm adherend thickness single lap-joint, 0.25 mm adhesive thickness and surface roughness obtained by manual abrasion with mesh p240 sandpaper size, test speed v=5 mm/min

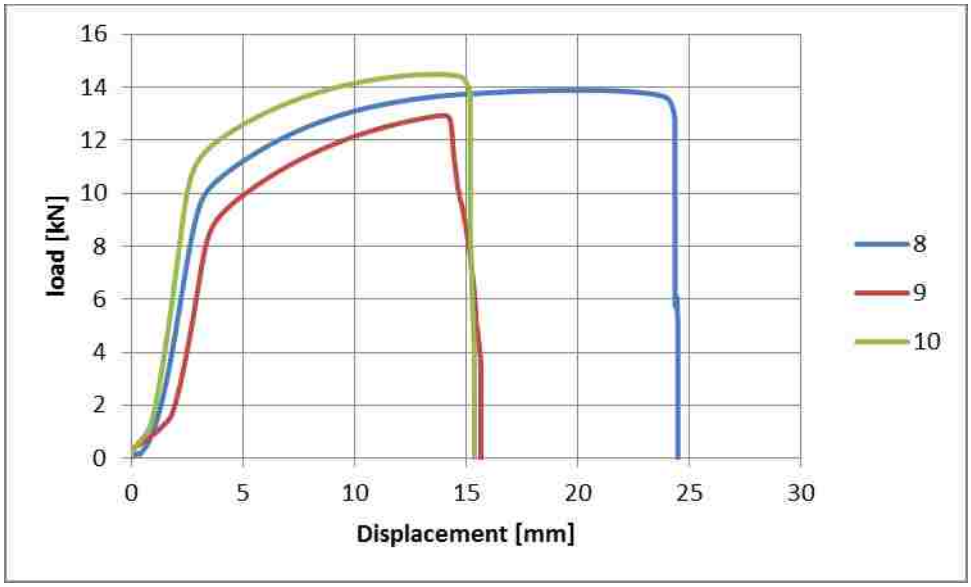

Figure 6-4: Load-displacement curves for 1.3 mm adherend thickness single lap-joint, 0.25 mm adhesive thickness and surface roughness obtained by manual abrasion with mesh p2320 sandpaper size, test speed v=5 mm/min

Figure 6-5: Load-displacement curves for 2.1 mm adherend thickness single lap-joint, 0.25 mm adhesive thickness and surface roughness obtained by manual abrasion with mesh p60 sandpaper size, test speed v=5 mm/min

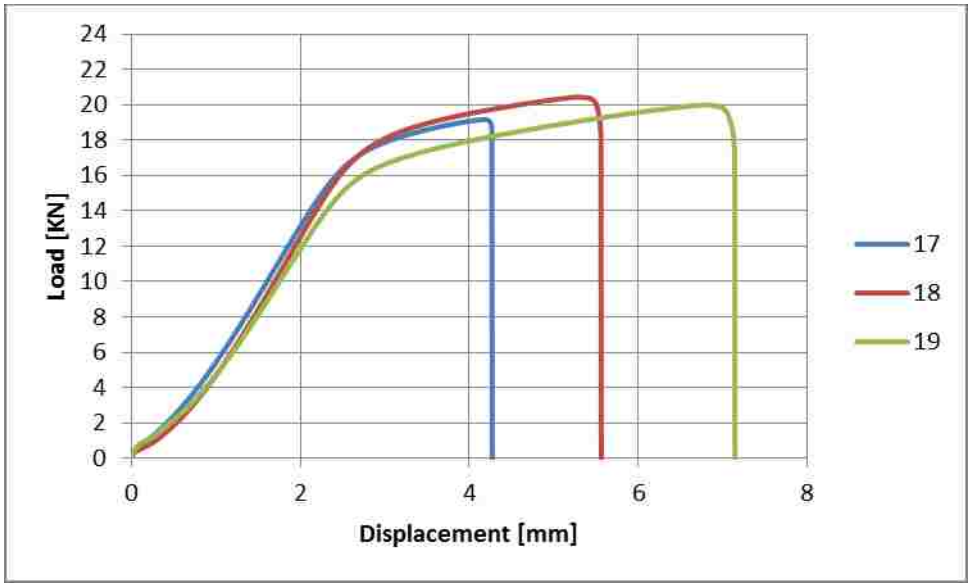

Figure 6-6: Load-displacement curves for 2.1 mm adherend thickness single lap-joint, 0.25 mm adhesive thickness and surface roughness obtained by manual abrasion with mesh p120 sandpaper size, test speed v=5 mm/min

Figure 6-7: Load-displacement curves for 2.1 mm adherend thickness single lap-joint, 0.25 mm adhesive thickness and surface roughness obtained by manual abrasion with mesh p240 sandpaper size, test speed v=5 mm/min

Figure 6-8: Load-displacement curves for 2.1 mm adherend thickness single lap-joint, 0.25 mm adhesive thickness and surface roughness obtained by manual abrasion with mesh p320 sandpaper size, test speed v=5 mm/min

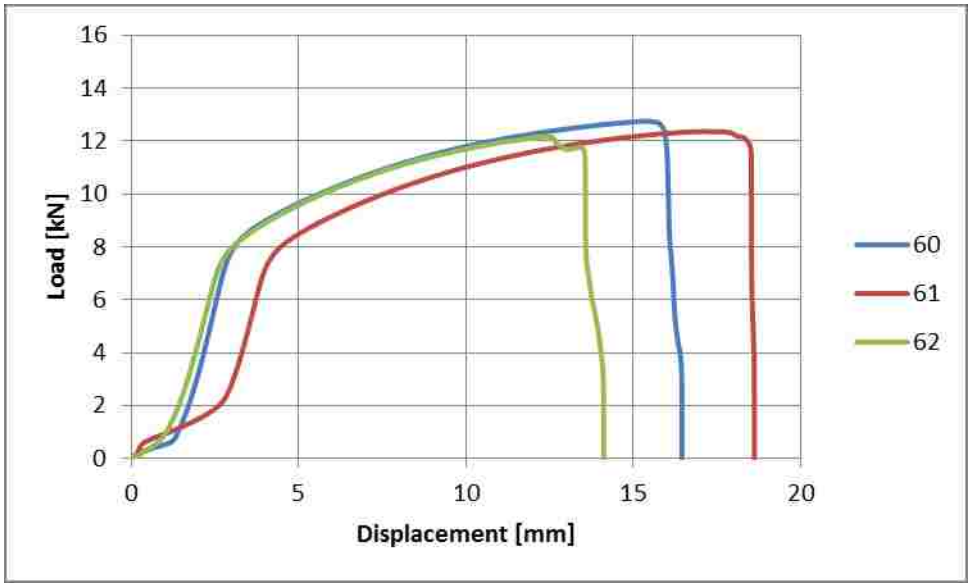

Figure 6-9: Load-displacement curves for 1.3 mm adherend thickness, surface roughness obtained by manual abrasion with mesh p240 sandpaper size, 0.11 mm adhesive thickness, test speed v=5 mm/min

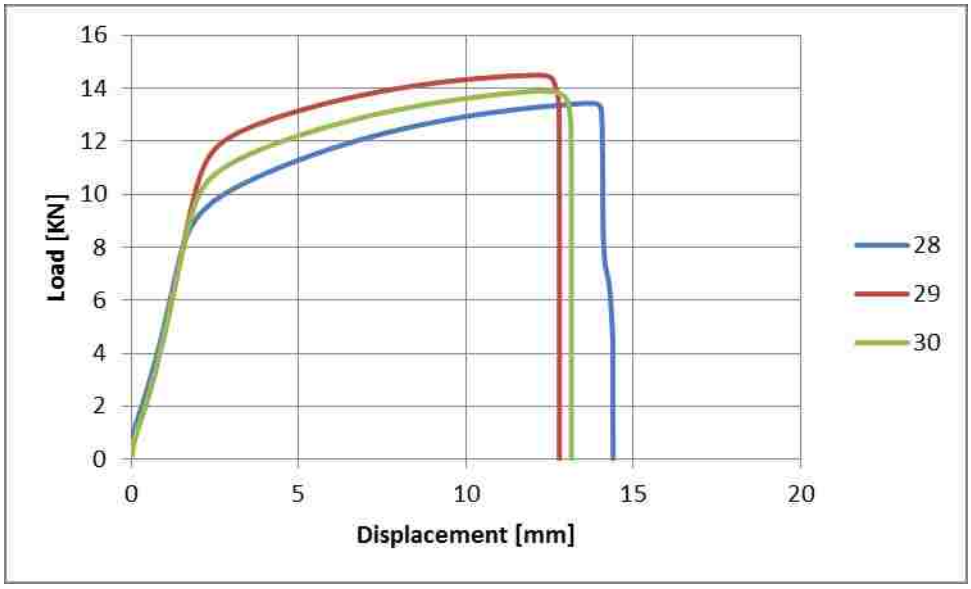

Figure 6-10: Load-displacement curves for 1.3 mm adherend thickness, surface roughness obtained by manual abrasion with mesh p240 sandpaper size, 0.34 mm adhesive thickness, test speed v=5 mm/min

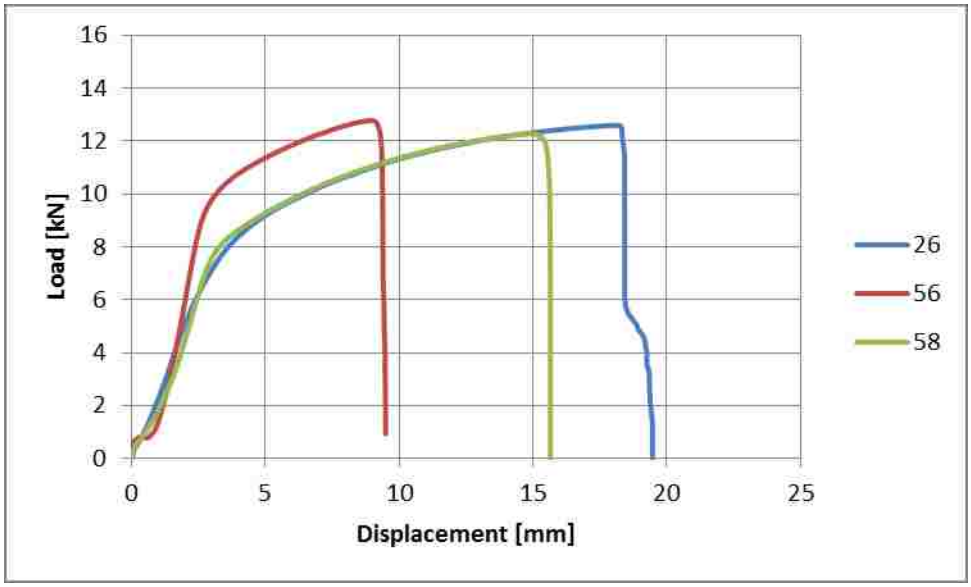

Figure 6-11: Load-Displacement curves for 1.3 mm adherend thickness, surface roughness obtained by manual abrasion with mesh p240 sandpaper size, 0.74 mm adhesive thickness, test speed v=5 mm/min

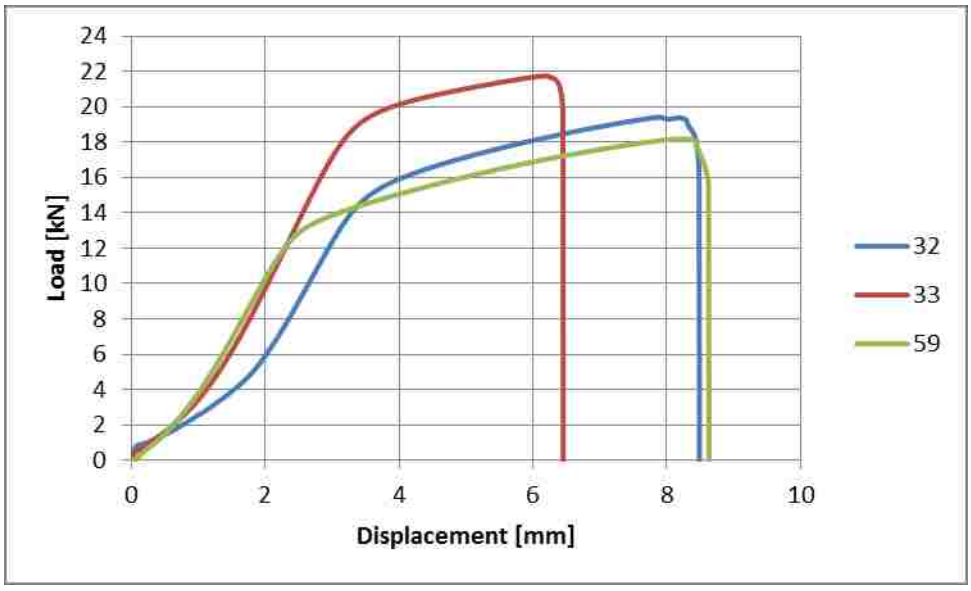

Figure 6-12: Load-displacement curves for 2.1 mm adherend thickness, surface roughness obtained by manual abrasion with mesh p240 sandpaper size, 0.11 mm adhesive thickness, test speed v=5 mm/min

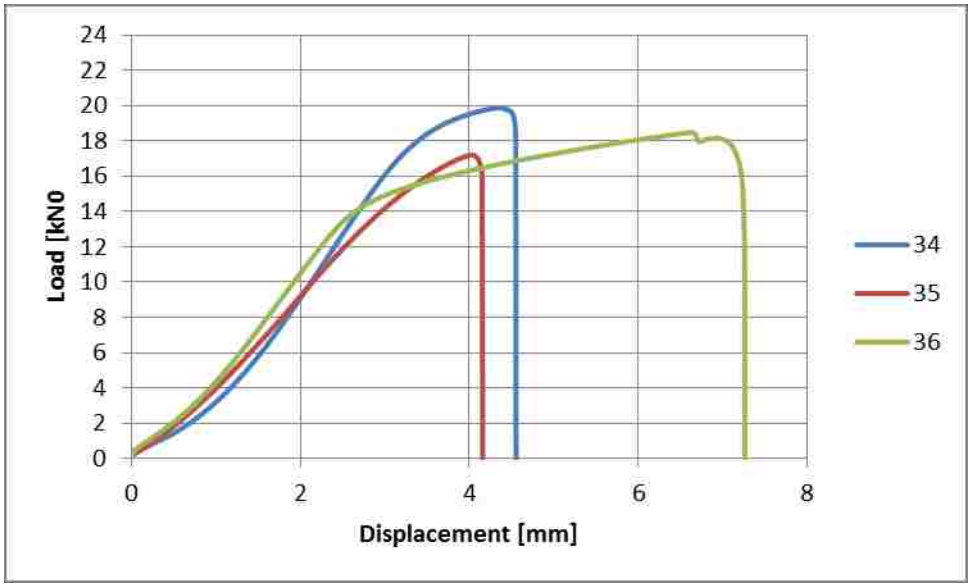

Figure 6-13: Load-displacement curves for 2.1 mm adherend thickness, surface roughness obtained by manual abrasion with mesh p240 sandpaper size, 0.34 mm adhesive thickness, test speed v=5 mm/min

Figure 6-14: Load-displacement curves for 2.1 mm adherend thickness, surface roughness obtained by manual abrasion with mesh p240 sandpaper size, 0.74 mm adhesive thickness, test speed v=5 mm/min

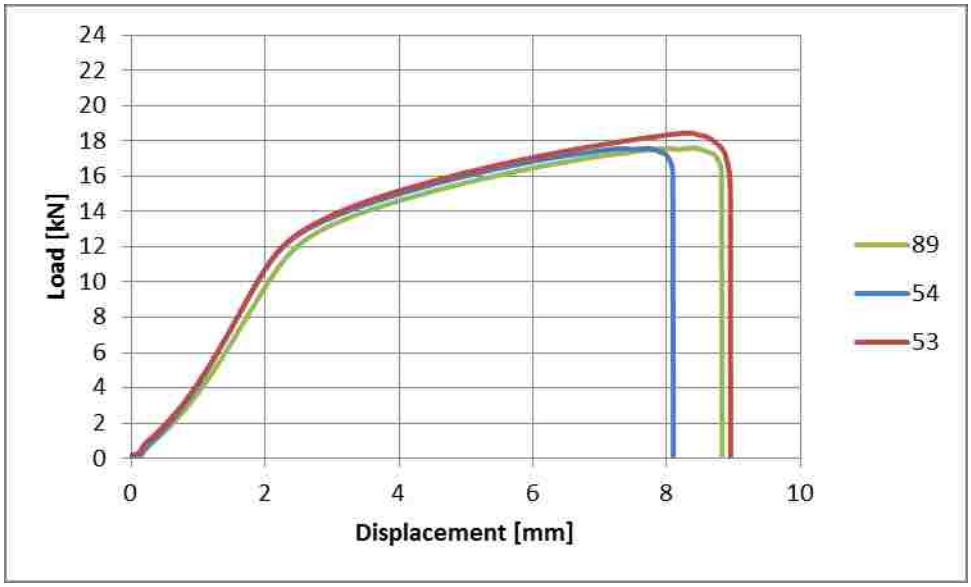

Figure 6-15: Load-displacement curves for 2.1 mm adherend thickness, surface roughness obtained by manual abrasion with mesh p240 sandpaper size, 0.25 mm adhesive thickness, test speed v=0.05mm/min

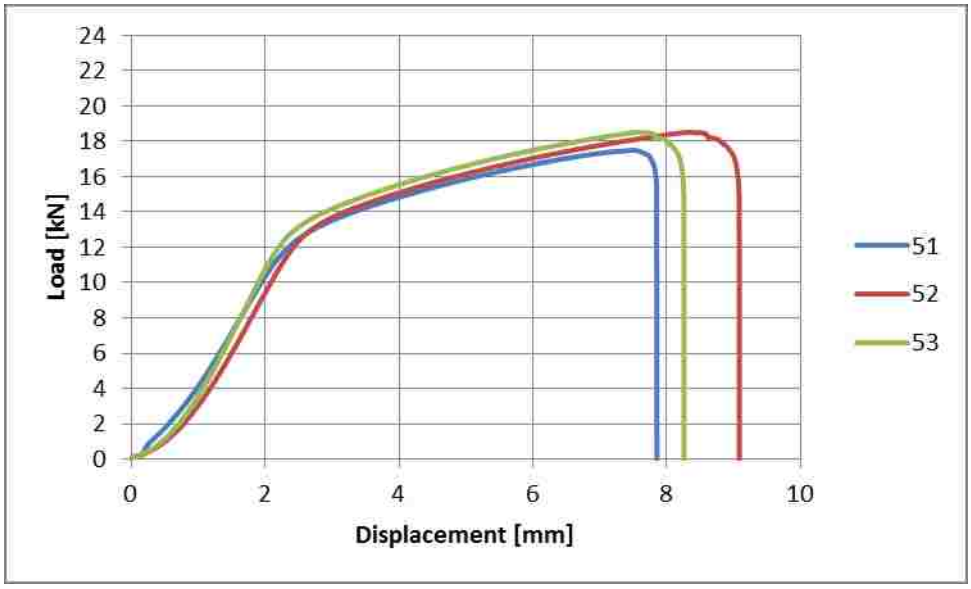

Figure 6-16: Load-displacement curves for 2.1 mm adherend thickness, surface roughness obtained by manual abrasion with mesh p240 sandpaper size, 0.25 mm adhesive thickness, test speed v=0.1mm/min

Figure 6-17: Load-displacement curves for 2.1 mm adherend thickness, surface roughness obtained by manual abrasion with mesh p240 sandpaper size, 0.25 mm adhesive thickness, test speed v=1 mm/min

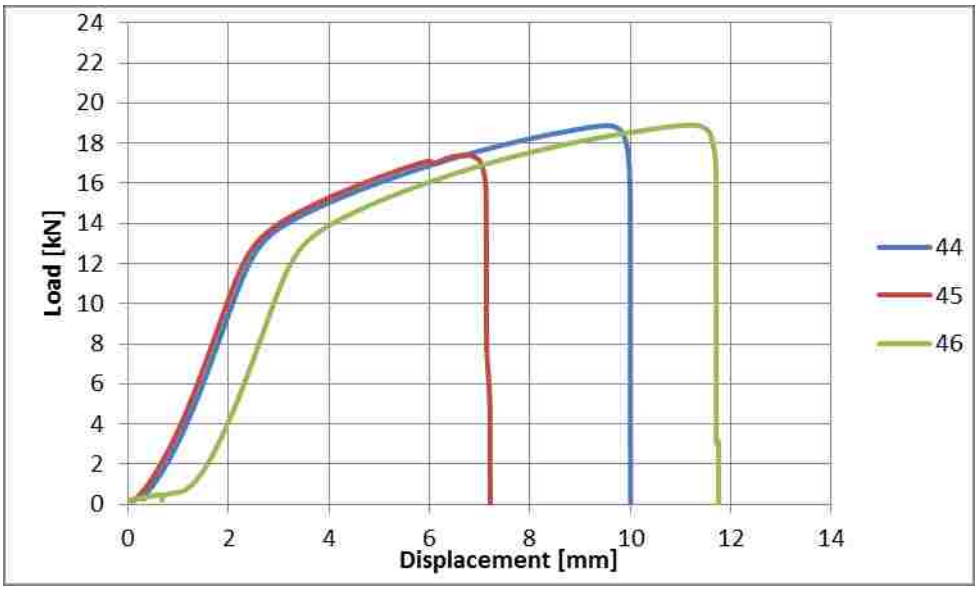

Figure 6-18: Load-displacement curves for 2.1 mm adherend thickness, surface roughness obtained by manual abrasion with mesh p240 sandpaper size, 0.25 mm adhesive thickness, test speed v=2 mm/min

Figure 6-19: Load-displacement curves for 2.1 mm adherend thickness, surface roughness obtained by manual abrasion with mesh p240 sandpaper size, 0.25 mm adhesive thickness, test speed v=50 mm/min

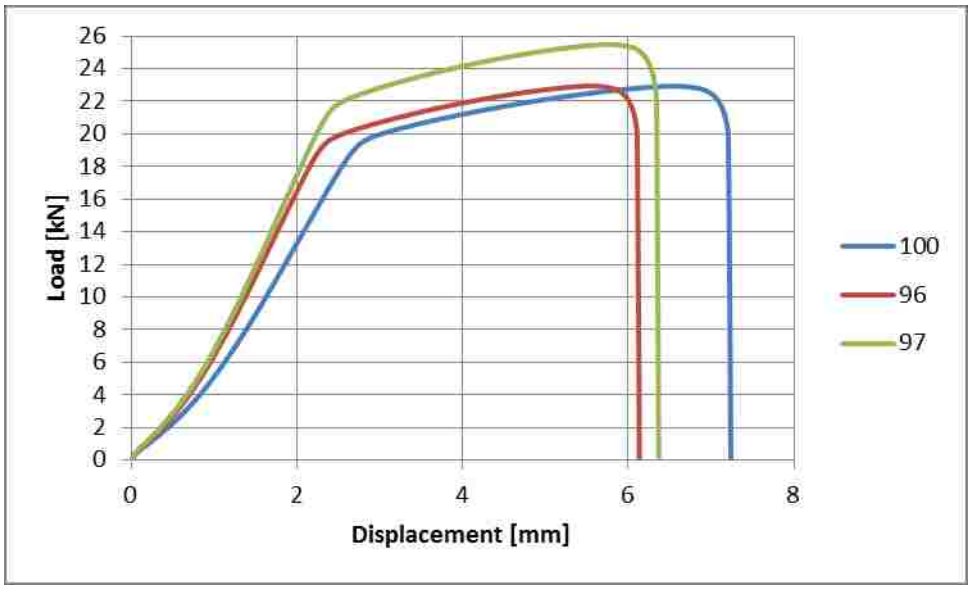

Figure 6-20: Load-displacement curves for 2.1 mm adherend thickness, surface roughness obtained by manual abrasion with mesh p240 sandpaper size, 0.25 mm adhesive thickness, test speed v=100 mm/min

REFERENCES

[1] FEDERAL VEHICLE STANDARDS, [Online]. Available : http://www.c2es.org/federal/executive/vehicle-standards#timeline. [Accessed 13 6 2015].

[2] EPA, [Online]. Available : http://www.epa.gov/climatechange /ghgemissions /gases/co2.htm. [Accessed 12 6 2015].

[3] Wikipedia, "Miles per gallon gasoline equivalent," [Online]. Available: https://en.wikipedia.org/wiki/Miles_per_gallon_gasoline_equivalent. [Accessed 23 06 2015].

[4] M. Johannaber, M. Espig, R. Wohlecker, H. Wallentowitz and J. Leyers, "Determination of Weight Elasticity of Fuel Economy for Conventional ICE Vehicles, Hybrid Vehicles and Fuel Cell Vehicles," FORSCHUNGSGESELLSCHAFT KRAFTFAHRWESEN mbH AACHEN, Aachen, 2007.

[5] A. Ambroziak and M. Korzeniowki, "Using resistance spot welding for joining aluminium elements in automotive industry," *Archives of Civil and Mechanical Engineering,* vol. X, no. 1, 2010.

[6] I. Michaelec and M. Maronek, "Adhesive bonding of Aluminium alloy A5754 b epoxy resins," *Acta Polytechnica* , vol. 53, no. 4, pp. 371-374, 2013.

[7] X. He, I. Pearson and K. Young, "Self-pierce riveting for sheet materials: state of the art," *Journal of Materials Processing Technology*,vol. 10, pp. 27-36, 2008.

[8] L. Bertin, *Tensile Strengtht of Automotive Aluminum Joints Using Resistance Spot Welding,* Master's Thesis: University of Windsor, 2013.

[9] P. Mallik and M. Fu, "Effect of process variables on the static and fatigue properties of self-piercing riveted joint in Aluminum Alloy 5754," Sae World Congress ", pp. 1-15, 2001.

[10] J. Robert and W. Wessler, Joining of materials and structures from pragmatic process to enabling technology, Elsevier, 2004.

[11] Dow Automotive, "Structural Adhesive Bonding:the most innovative joining technique for modern lightweight design, safety and modular concept," SAE International, Switzerland, 2005.

[12] V. M. Cassidy, "Adhesive bonding grows: replaces welds, fasteners," *Modern Metals,* pp. 82-93, 1986.

[13] P. Dvorak, "Building a better adhesive bond," *Fastening & Joining,* pp. 83-86, 6 November 2003.

[14] *"Adhesive bonding", EAA Aluminuium Automotive Manual-Joining,* The Aluminum Automtoive Manual, pp. 1-42,2015

[15] L. F. M. Silva, A. Öchsner and R. Adams, Handbook of Adhesion Technology, Berlin, London: Springer, 2011.

[16] E. M. Petrie, "Adhesive Use in Auto Industry Increases - Just as the Market Tanks, "Omnexus, [Online]. Available : http://www.omnexus4adhesives.com/services/print.aspx?id=1485. [Accessed 05 06 2015].

[17] R. D. Adams, "What are Adhesives and Sealants and How Do They Work?," in *Adhesive Bonding - Science, Technology and Applications*, Woodhead Publishing, pp. 36-46,2005.

[18] Adhesives and Sealant Council, "Adhesive.org," 2014. [Online]. Available: http://www.adhesives.org/adhesives-sealants/science-of-adhesion/adhesion-cohesion. [Accessed 10 05 2015].

[19] A. Butt, A. Chughtai, J. Ahmad and R. Ahmad, "Theory of adhesion and its practical implications," *Journal of Faculty of Engineering & Technology*, pp. 21-45, 2008.

[20] Y. Yuan and T. Lee, "Contact angle and wetting properties," in *Surface Science Tecnhiques*, Springer, pp. 3-34,2013.

[21] J.J.Bikerman, "Final strength of adhint," in *The Science of Adhesive joints*, New york and London, Academic press, pp. 125-134,1961.

[22] S. Ebnesajjad and A. H. Landrock, " Introduction and Adhesion Theories," in *Adhesives Technology Handbook (3rd Edition)*, Elsevier, pp. 5-13,2015

[23] S. Ebnesajjad, "Introduction and Adhesion Theories," in *Adhesives Technology Handbook 2nd Edition*, Norwich, William Andrew, pp. 6-13,2008

[24] A. V. Pocius, "The Relationship of Surface Science and Adhesion Science," in *Adhesion and Adhesives Technology - An Introduction (3rd Edition)*, Hanser Publishers, pp. 145-175,2012.

[25] S. Ebnesajjad, "Introduction," in *Handbook of Adhesives and Surface Preparation - Technology, Applications and Manufacturing*, Elsevier, pp. 6-10,2011.

[26] S.S.Voyutski, Autohesion and Adhesion of High Polymers, Wiley, 1964.

[27] H. J. and Scott.R., The solubility of Non-Electrolytes,3rd.Ed., New york: Reinhold, 1950.

[28] Y. Iyengar and Scott.R, *J.Appl.Polymer Sci.*, vol. 11, p. 2311, 1967.

[29] J. Comyn, Adhesion science, Cambridge: The Royal Society of Chemistry, 1997.

[30] J.Derjaguin and V. Smilga, Adhesion, Fundamentals and Practise, London: McLaren and Son, 1969.

[31] M. J.Dean, Handbook of Aluminum Bonding Technology and Data, New York: Taylor & Francis Group, 1981.

[32] A.M. Pereira, J. Ferreira, F. Antunes and P. Bartolo, "Analysis of manufacutring parameters on the shear strength of aluminium adhesive single-lap joints,"

Journal of Materials Processing Technology, vol. 21, pp. 610-617, 2010.

[33] L. F. da Silva, G. Critchlow and M. figuelredo, "Parametric Study of Adhesively Bonded Sinlge Lap Joints by the Taguchi Method," *Journal of Adhesion Science and Technology,* pp. 1477-1494, 2008.

[34] K. Uehara and M. Sakurai, "Bonding strength of adhesives and surface roughness of joined parts," *Journal of Materials Processing Technology,* pp. 178-181, 2002.

[35] C. Borsellino, G. Di Bella and V. Ruisi, "Adhesive joining of aluminium AA6082: The effects of resin and surface treatment," *International Journal of Adhesion & Adhesives,* vol. 29, pp. 36-44, 2009.

[36] A.Spiaggiari and E. Dragoni, "Effect of mechanical surface treatment on the static strength of adhesive lap joints," *The Journal of Adhesion,* vol. 89, p. 677–696, 2013.

[37] S. G.Prolongo, G. Rosario and A. Urena, "Study of the effect of substrate roughness on adhesive joints by SEM image analysis," *Journal of Adhesion Science and Technology,* vol. XX, no. 5, p. 457–470, 2006.

[38] "Adhesive Design Toolkit," [Online]. Available: http:// www.adhesive stoolkit .com /Toolkits/DesignGuidance/JointTypes.xtp. [Accessed 20 06 2015].

[39] A. Stoic, M. Lucic and J. Kopac, "Investigation of aluminum single lap adhesively bonded joints," in *11th Interational Scientific Conference on Contemporany Achievements in Mechanics, Manufacturing and Material Science*, Gliwice, 2005.

[40] A. De Morais, A. Pereira, J. Teixeira and N. Cavaleiro, "Strength of epoxy adhesive-bonded stainless-steel joints," *International Journal of Adhesion and Adhesives,* vol. 27, no. 8, pp. 679-686, 2007.

[41] L. F. da Silva, R. Carbas, G. Critchlow, M. Figueiredo and k. Brown, "Effect ofmaterial ,geometry, surface treatment and environment on thes shear strength of single lap joints," *InternationalJournalofAdhesion&Adhesives,* vol. 29, p. 621–632, 2009.

[42] K. GÜLTEKIN, S. AKPINAR and A. ÖZEL, "The Effect of Moment and Flexural Rigidity of Adherend on the Strength of Adhesively bonded single lap joints," *The Journal of Adhesion,* vol. 91, p. 637–650, 2015.

[43] Smart adhesives, "Surface Prep Guide for Adhesives," [Online]. Available: http://www.adhesive.com/instructions_detail_surfaceprep__adhesives_application.html. [Accessed 10 5 2014].

[44] R.G.King, surface treatment and finishing of alluminum, Oxford: Pergamon Press, 1988.

[45] C. Yan, J. Mao, S. Nassar, X. Wu and A. Kazemi, "Experimental and numerical investigation of the effect of key joint variables on the static and fatigue performance of bonded metallic single-lap joint," *Journal of Adhesion Science and Technology,* vol. 28, no. 20, pp. 2069-2099, 2014.

[46] L. F. da Silva, B. Blackman, R. D. Adams and D. A. Dillard , "Manufacture of quality specimens," in *Testing Adhesive Joints, Best Practices*, Wiley-VCH, 2012, pp. 15-26.

[47] R. Campilho, A. Pinto, M. Banea and L. da Silva, "Optimization study of hybrid spot-welded/bonded single-lap joints," *International Journal of Adhesion & Adhesives*, vol. 37, pp. 86-95, 2012.

[48] J. M. Arenas, J. J. Narbon and C. Alia, "Optimum adhesive thickness in structural adhesive joints using statistical techniques based on Weibull distribution," *International Journal of Adhesion & Adhesives*, vol. 30, pp. 160-165, 2010.

[49] L. F. M. da Silva, T. N. S. S. Rodrigues, M. A. V. Figueiredo, M. F. S. F. de Moura and J. A. G. Chousal, "Effect of Adhesive Type and Thickness on the Lap Shear Strength," *The Journal of Adhesion,* p. 1091–1115, 2006.

[50] M. Banea and L. da Silva , "Characterization of aluminium single-lap joints for high temperature applications," *Material Science Forum*, Vols. 730-732, pp. 721-726, 2013.

[51] M. Banea and L. da Silva, "The effect of temperature on the mechanical properties of adhesives for the automotive industry," *Materials: Design and Applications*, vol. 224, pp. 51-62, 2010.

[52] "Tg-Glass transition temperature for epoxies," Epoxy Technology, [Online]. Available: http://www.epotek.com/site/files/Techtips/pdfs/tip23.pdf. [Accessed 23 06 2015].

VITA AUCTORIS

NAME:	Francesco Vincenzo Amoruso
PLACE OF BIRTH:	Arezzo, Italy
YEAR OF BIRTH:	1992
EDUCATION:	Politecnico di Torino, B.Sc. in Automotive Engineering, Torino, Italy, 2013
	Politecnico di Torino, M.A.Sc. in Automotive Engineering, Torino, Italy, 2015
	University of Windsor, International M.A.Sc. in Mechanical Engineering, Windsor, Canada, 2015